Microstructure and mechanical properties of Ti6Al4V (ELI) parts produced by DMLS

MORAKANE GLORIA MOLETSANE

Dissertation Submitted in Fulfilment of the Requirements for the Degree

MASTER OF ENGINEERING: MECHANICAL ENGINEERING
in the

Department of Mechanical and Mechatronics Engineering

Faculty of Engineering & Information Technology

at the

Central University of Technology, Free State

BLOEMFONTEIN

Supervisor: Prof. Ihar Yadroitsau, D. Eng.

Co-supervisor: Dr. Ina Yadroitsava, Ph. D.

Declaration of independent work

I, Morakane Gloria Moletsane, identity number [redacted] and student number [redacted], do hereby declare that this research project submitted to the Central University of Technology, Free State for the MASTER of ENGINEERING: MECHANICAL ENGINEERING, is my own independent work; and complies with the code of Academic integrity, as well as other relevant policies, procedures, rules and regulations of the Central University of Technology, Free State; and has not been submitted previously to any institution by myself or any other person in fulfilment of the requirements for the attainment of any qualification.

SIGNATURE OF STUDENT  25 November 2016

Acknowledgements

The author is grateful to many individuals and departments who helped in this dissertation and to whom I would like to express appreciation. I am grateful for my supervisors Prof. Ihar Yadroitsau (Igor Yadroitsev) and Dr. Ina Yadroitsava, they have guided me and relentlessly push me to make this work a success.

I would like to thank the South African Research Chairs Initiative of the Department of Science and Technology and National Research Foundation of South Africa and the Collaborative Program in Additive Manufacturing sincerely for their financial support, which made it possible this work. This work is based also on the research cooperation with Department of Engineering and Physics in Karlstad University, Sweden (Prof. P. Krakhmalev); Institute of Metal Physics from Urals Branch of the Academy of Sciences, Russia (Prof. N. Kazantseva) and CT Scanner Facility from Stellenbosch University, South Africa (Dr. A. Du Plessis). Mechanical testing has been performed in mechanical testing laboratory in CSIR and in CRPM laboratory at CUT. Author is grateful to Chris McDuling from CSIR for teaching me in mechanical testing. The work also benefited from the cooperation between the Central University of Technology, Free State and Nelson Mandela Metropolitan University. Author would like to acknowledge Director of eNtsa NMMU Prof. D.Hattingh, S. Grewar and R. Brown for performing the XRD measurements.

Special mention needs to be made for the following people without whom this project would not have been possible:

- I would like to thank the faculty of engineering at CUT, the Dean Prof. A. Ngowi, the Head of department in mechanical engineering and mechatronics Mr. N. Du Toit and the support of all my colleagues.
- I wish thank to everyone at CRPM who has helped with the project and supported me in many ways: Prof. W. du Preez, Dr. J.G. van der Walt, G. Booysen, J. Els and I. van Zyl.
- I want to thank Prof. J.F.R. Lues and Dr. Malebo Ntsoaki from Department of Life Sciences, Faculty of Health and Environmental Sciences in CUT for giving us the opportunity to work with the SEM.
- I would like to thank my father R.J. Lenono for his love and support and all my siblings for encouragement through the study.
- I also thank God and my CRC family through their love and support.

ABSTRACT

Direct Metal Laser Sintering (DMLS) is an Additive Manufacturing (AM) technology where powder is melted by the laser beam track-by-track, layer-by layer to produce complex components. The advantage of DMLS is manufacturing functional parts, tools and also medical implants with complex shape and about 100% density. Microstructure and mechanical properties of as-built DMLS objects depend on not only material properties, but also process-parameters such as laser power density, scanning speed, powder layer thickness, scanning strategy, preheating and building strategies, etc.

Titanium (Ti) alloys have superior qualities compared to other biomaterials: they are strong, lightweight, high corrosion resistant, non-toxic, biocompatible, long-lasting, and non-ferromagnetic, it has osseointegration capabilities. Ti6Al4V is one of the most widely used α-β Ti alloy containing 6 wt% Aluminium and 4 wt% Vanadium. Ti6Al4V (ELI) alloy is a higher-purity ("Extra-Low Interstitial") version of Ti6Al4V, with lower specified limits of iron and the interstitial elements C and O. Ti6Al4V (ELI) has an excellent combination of strength and toughness along with excellent corrosion resistance.

High cooling rates at DMLS result in a formation of the α´ martensitic phase in Ti6Al4V alloy. As built Ti6Al4V DMLS parts have higher yield strength and lower ductility in comparison with cast material used for implants. Literature review revealed high variations in mechanical properties of DMLS Ti6Al4V under different process-parameters and building strategies. The main aim of the study was to analyse the microstructure and mechanical properties of DMLS Ti6Al4V (ELI) samples and comparison with the appropriate quality standard for the conventional alloy for biomedical applications. EOSINT M280 machine was used to produce samples for defect analysis, microstructural and mechanical studies. In this work DMLS Ti6Al4V (ELI) specimens with different building strategy, surface qualities and shapes were investigated.

The low level of porosity in DMLS samples was observed by CT scans and the material had >99.9 % density.

XRD measurements of residual stresses in as-built DMLS specimens attached to the substrate were performed and high tensile stresses in wide range of 220–800 MPa were measured. The direction of the maximal principal stress coincided with the direction of the laser scanning. It was found that second principal stress which is perpendicular to the scanning direction, correlates with surface roughness.

Defect analysis by CT scans in pre-strained samples was used to detect the crack formation mechanism during tensile loading of as-built and heat-treated samples. The material in all the

experiments showed a moderate ductile behaviour through necking formation, pores coalescence and cup and cone fracture. Vertical and horizontal samples showed similar mechanical properties.

The results of this study show that if the DMLS process parameters are properly selected, the properties of DMLS Ti6Al4V (ELI) fully meet the requirements of the standards, and the only post-processing that is required is stress-relieving. After the stress-relief of Ti6Al4V (ELI) at 650°C for 3 hours in Ar argon atmosphere, no beta phase was detected by TEM, EBSD, and XRD, very small (500 nm) globular grains of alpha phase were found. The stress-relieved DMLS samples had good tensile properties that correspond to ASTM standard (F1108-14) for biomedical applications.

It also was shown that mini-samples are effective for the determination of the basic mechanical properties of DMLS material.

Key words: DMLS, Ti6Al4V, Microstructure, Mechanical Properties, Residual Stress

Contents

List of tables

List of figures

Glossary

3D-CAD	Three Dimensional-Computer Aided Drawing
AM	Additive Manufacturing
ASTM	American Society for Testing and Materials
BCC	Body Centred Cubic
CRPM	Centre for Rapid Prototyping and Manufacturing
CSIR	Council for Scientific and Industrial Research
CUT, FS	Central University of Technology, Free State
DMLS	Direct Metal Laser Sintering
EBM	Electron Beam Melting
ELI	Extra Low Interstitial
FEA	Finite Element Analysis
HCP	Hexagonal Close-Packed
HIP	Hot Isostatic Pressing
HV	Vickers Hardness
SEM	Scanning Electron Microscope
SLM	Selective Laser Melting
XRD	X-Ray Diffraction

Chapter 1. INTRODUCTION

1.1. Background

Development of a new processes like Direct Laser Metal Sintering (DMLS) and new biocompatible materials has resulted in significant progress in design, efficiency and reduction in production time of implants and prostheses. Components, produced by DMLS, have to comply with the international standards required for biomedical applications. Mechanical properties of the samples produced through the DMLS depend on process parameters, scanning strategy and build direction. Due to very fine and special microstructure the DMLS object should be heat-treated differently from conventional parts. Thus the development of appropriate heat treatment to improve the mechanical properties of the DMLS objects for biomedical applications without compromising their functionality is an important task. The relationships between process, microstructure and mechanical properties of DMLS samples have to be determined.

1.2. The Aim of the Project

The aims of the study are:

- To study Ti alloys and their properties, features of DMLS process, and to analyse properties of DMLS Ti6Al4V at different scanning strategies, process-parameters and heat treatments.
- To determine tensile properties, microstructure and porosity of Ti6Al4V (ELI) components, produced by DMLS with EOSINT M280 machine at fixed process parameters and to compare them with accepted standards for biomedical applications.
- To estimate direction and values of residual stress of Ti6Al4V (ELI) multi-layered samples produced at fixed process-parameters and to find correlation between numbers of powder layers, morphology of the layers and residual stresses.
- To analyse the influence of building strategy on microstructure, tensile properties and fractures of vertical and horizontal DMLS specimens from Ti6Al4V (ELI) powder.
- To compare mechanical properties of standard (ASTM E8 / E8M-16a) and mini-tensile specimens and to show applicability of mini-tensile tests for the express analysis of DMLS process.

1.3. Research Methodology

The methodology for the study is summarized in the following schematic diagram (Fig. 1.2.1).

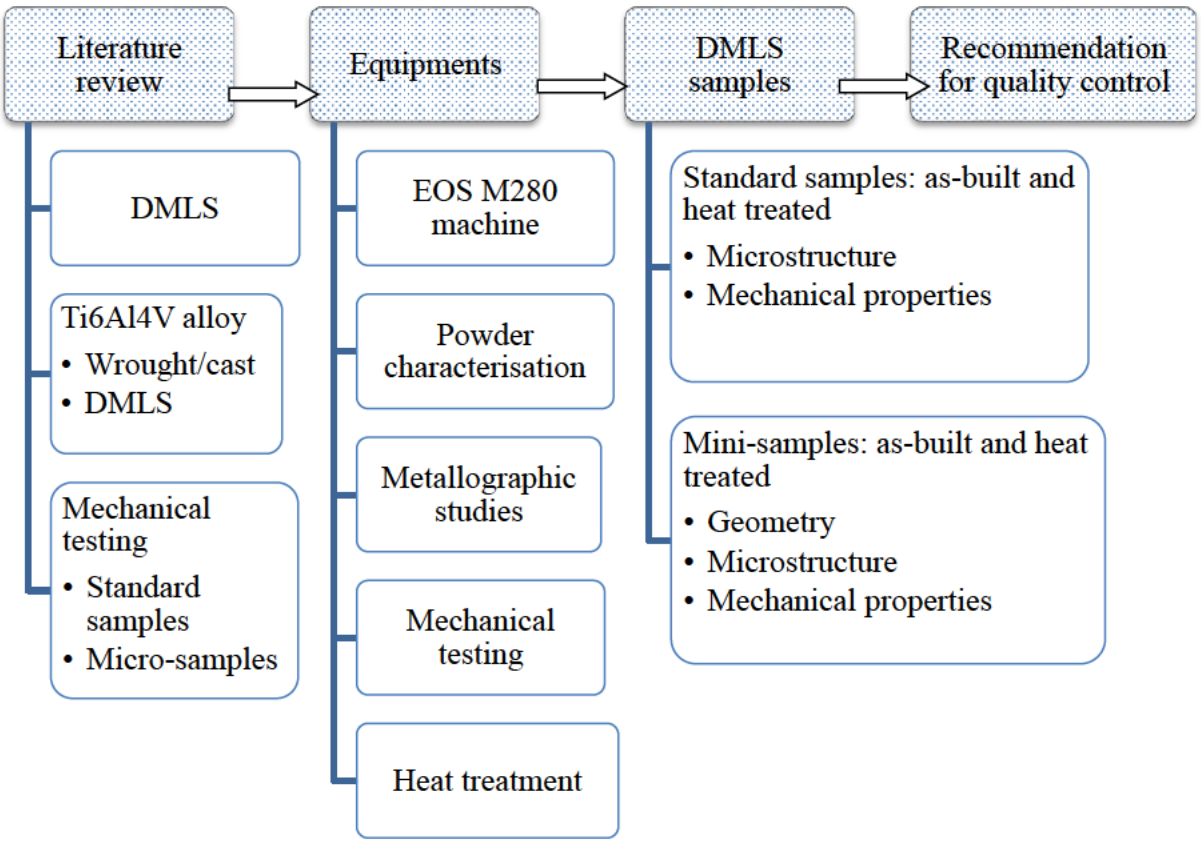

Fig. 1.2.1. Research methodology of the study.

1.4. Expected Contributions

To reduce the cost of the specimens for mechanical testing, micro DMLS samples can be applied. The as-built and polished surface of the samples can influence the results of the mechanical testing. These peculiarities will be established in the process of the present study and the most appropriate options for the geometric characteristics and surface quality of the samples will be chosen to monitor the quality control of the DMLS objects produced in CRPM.

1.5. An Overview of the Dissertation

Thesis presented as introduction, general literature review, material and methods and collection of research already-published conference papers. The overview of this research is elaborated as follows:

- The first chapter introduces the research, the aim, the scope and the methodology of the thesis.

- The second chapter presents literature review that has been done according to the research plan: DMLS process, mechanical testing of materials, titanium alloys and their properties.
- The third chapter is about materials and methods used for the research. Powder characterisation, it's processing and heat treatment of TiAl6V4 (ELI) samples, shapes of the samples, mechanical testing, CT scans, surface tests and metallographic methods are described there.
- The fourth chapter presented the results and discussion of the experiments both mechanical and microstructural for TiAl6V4 (ELI) alloy produced at EOSINT M 280 fixed process parameters.
- The fifth chapter is the conclusions and future work based on the research done in according to the theme of the dissertation.

1.6. Publications and presentations to date

- Moletsane, M.G., Krakhmalev, P., Kazantseva, N., Du Plessis, A., Yadroitsava, I. and Yadroitsev, I., 2016. Tensile properties and microstructure of direct metal laser-sintered TI6AL4V (ELI) alloy. *South African Journal of Industrial Engineering*, 27(3), pp.110-121.
  Presented by M.G. Moletsane at the 17th annual international conference of the Rapid Product Development Association of South Africa (RAPDASA), held from 2-4 November 2016 in Vanderbijlpark, South Africa.

- Moletsane, M.G., Krakhmalev, P., Yadroitsava, I. and Yadroitsev, I., 2016. Tensile properties and microstructure of standard vertical and horizontal DMLS Ti6Al4V (ELI) samples *INTERIM CUT*, 15(1), pp.133-140.
  Presented by M.G. Moletsane at 19th Annual Research seminar, Faculty of Mechanical Engineering and Informational Technology, held from 26 October 2016 in Free State University, Bloemfontein.

- I. Yadroitsev, I. van Zyl, M.G. Moletsane, I. Yadroitsava. Direct Metal Laser Sintering of Ti6Al4V (ELI) Powder, *Proc. International Conference on Competitive Manufacturing*, 27-29 January 2016, Stellenbosch - Western Cape, South Africa.
  Presented by I. van Zyl

- van Zyl, I., Moletsane, M., Krakhmalev, P., Yadroitsava, I. and Yadroitsev, I., 2016. Validation of miniaturised tensile testing on DMLS TI6AL4V (ELI) specimens. *South African Journal of Industrial Engineering*, 27(3), pp.192-200
  Presented by I. van Zyl at the 17th annual international conference of the Rapid Product Development Association of South Africa (RAPDASA), held from 2-4 November 2016 in Vanderbijlpark, South Africa.

CHAPTER 2. LITERATURE REVIEW

This chapter focuses on the published literature on the process of DMLS using Ti6Al4V alloy for implants. The influence of process parameters through DMLS process and its effects on mechanical and microstructure of Ti6Al4V.

2.1. Direct Metal Laser Sintering

ASTM standard F2792-12a defines Additive manufacturing (AM) as a "*process of joining materials to make objects from 3D model data, usually layer upon layer, as opposed to subtractive manufacturing methodologies. Synonyms: additive fabrication, additive processes, additive techniques, additive layer manufacturing, layer manufacturing, and freeform fabrication*". Initially AM technologies were used to make models and prototypes. Now AM is used to create prototypes and also functional parts because the method reduces the time for manufacturing: modifications and corrections can be made easily. The main advantage of AM is ability to create functional parts with complex design directly from 3D model data.

There are several different categories and processes of AM available; different AM technologies use appropriate methods and materials (Fig. 2.1.1). AM systems can be categorized on the basis of used material: liquid-based (Stereolithography, Aerosol Jet Deposition), solid-based (Laminated Object Manufacturing, LOM) and powder-based (Direct Metal Laser Sintering, DMLS; Electron Beam Melting, EBM; Direct Metal Deposition, DMD).

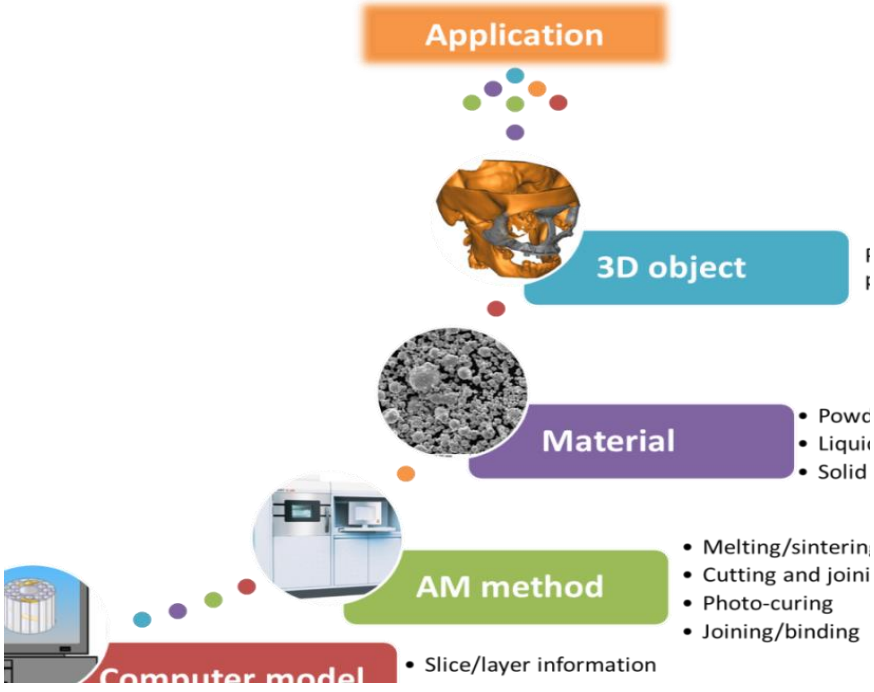

Fig. 2.1.1. Additive manufacturing process.

2.1.1. Background of DMLS process

Direct metal laser sintering (DMLS) is *"a powder bed fusion process used to make metal parts directly from metal powders without intermediate "green" or "brown" parts; term denotes metal-based laser sintering systems from EOS GmbH - Electro Optical Systems. Synonym: direct metal laser melting"* (ASTM Standard F2792-12a, 2012). Other synonyms are: Laser Powder Bed Fusion, Selective Laser Melting, LaserCusing.

DMLS is widely used in aerospace, automotive, electronic, chemical and biomedical, as well as other high-tech areas. DMLS is advantageous in comparison with the other methods for manufacturing parts with complex geometry and sophisticated inner structure. One of the features is able to produce objects with functional work surfaces during manufacturing process. It is to impart some particular texturing or smoothness; to create some periodic structures or periodic porosity. Also significant benefit is the ability to manufacture multi-material objects; objects with graded composition and light weight structures. DMLS is a kind of AM where metal powder is fused/solidified track-by-track, layer-by-layer to form 3D part on the building platform (Fig. 2.1.2).

The process begins when the engineer designs the 3D part with a CAD software. The .stl file is sent into the special software, 3D model is divided into 2D cross sections (layers) and after is loaded to DMLS machine.

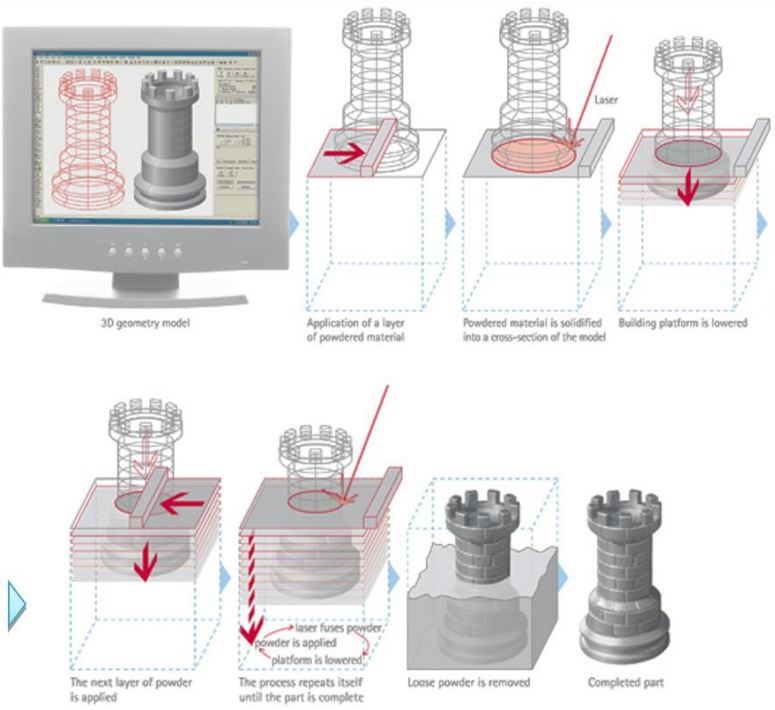

Fig. 2.1.2. General functional principle of DMLS (EOS Gmbh, 2015).

The building process starts with the dispenser being raised on layer thickness; a re-coater (roller, blade or brush) moves across the dispenser and deposits a layer of powder onto the building platform (Figs. 2.1.2-2.1.3). Moving by scanner, laser beam exposures track-by-track powder layer hatching the cross-section of the part. Then a new powder layer is delivered by re-coater on the solidified layer and cycles are repeated until the 3D part is completed.

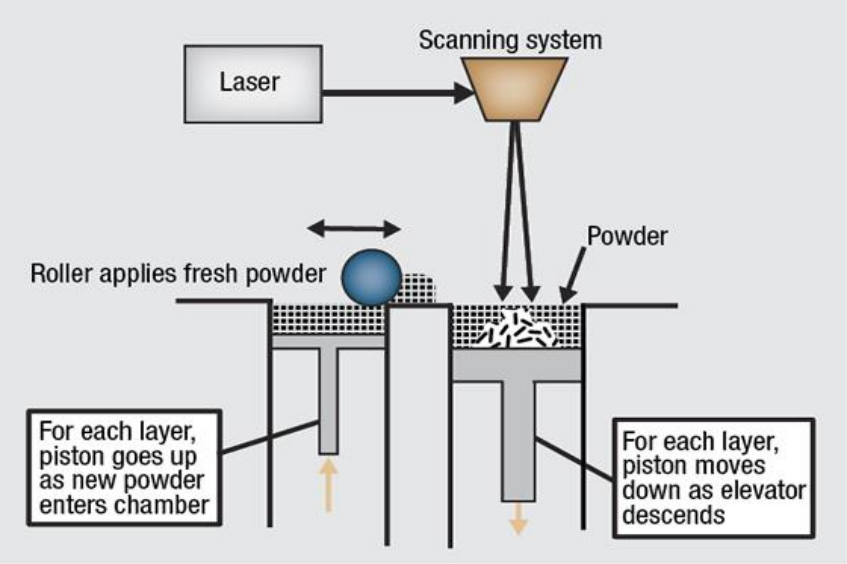

Fig. 2.1.3. The laser sintering process (Micro-manufacturing, 2014).

Since laser beam at DMLS has small spot size (about 10-150 μm), a very small molten pool is formed and a large temperature gradient exists. The quality and properties of single tracks and single layers influence the properties of a part produced by DMLS. During DMLS, non-optimal process parameters can cause balling effect or instability of single tracks, which is a severe barrier to a uniform deposition of the powder on the previously processed layer and tends to produce porosity induced by poor interlayer bonding (Gu, 2014). An excess in power input can lead to keyhole mode during DMLS and pores occur in 3D DMLS samples (Yadroitsava *et al.*, 2015). The tracks instability depends of laser power, scanning speed, powder layer thickness, substrate material, physical properties and granulomorphometry of the powder used. Experiments done by Yadroitsev (2009) showed a correlation between process parameters and the quality of single track formation. By comparing different laser powers, scanning speeds and layer thickness, optimal process parameters were investigated for 316L stainless steel single tracks. Powder was delivered on the substrate to vary from 0-400 μm. Laser power was 25-50 W, scanning speed was varied between 0.04-0.28 m/s. Stable continuous single tracks and unstable zones (not continuous single tracks) were formed (Fig. 2.1.4). The study showed that low scanning speed tends to form distortions and irregularities while excessively high scanning speed tends to form drops (balling

effect). The stability of the single track formation does not only depend on the laser power, scanning speed and layer thickness but also the substrate material, physical properties and morphology of the powder material.

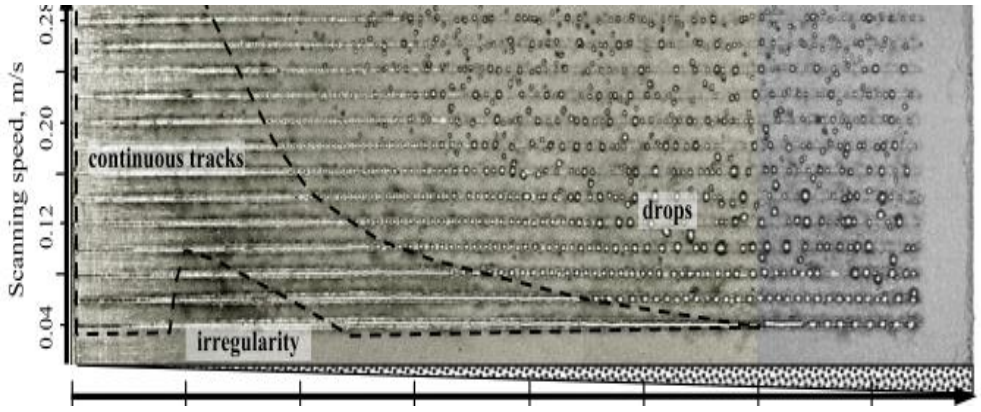

Fig. 2.1.4. Influence of powder layer thickness and scanning speed on stability of DMLS single tracks (Yadroitsev, 2009).

For the one-pass thin walls with gradual increase layer thickness from 40 μm up to 80 μm, thin wall had no pores up to the scanning speed of 0.12 m/s for all the range of layer thickness. For *V*= 0.04-0.06 m/s for all the range of layer thickness, the surface of the wall was rough. Surface imperfections resulted from irregularity and distortions of single vectors due to power. For scanning speed 0.14 m/s and layer thickness 70 μm and higher, small irregular pores appeared. With increase of the scanning speed, pores became regular and large, and they appeared at smaller layer thickness. Pores are elongated and perpendicular to the sintering direction. With increase of scanning speed and layer thickness pores became more oriented (Fig. 2.1.5). For the smaller layer thickness the surface of the wall is smoother as a result of fine structure of the sintered tracks: the height of the track was smaller and the re-melted depth into underlying track was bigger (Yadroitsev & Smurov, 2011).

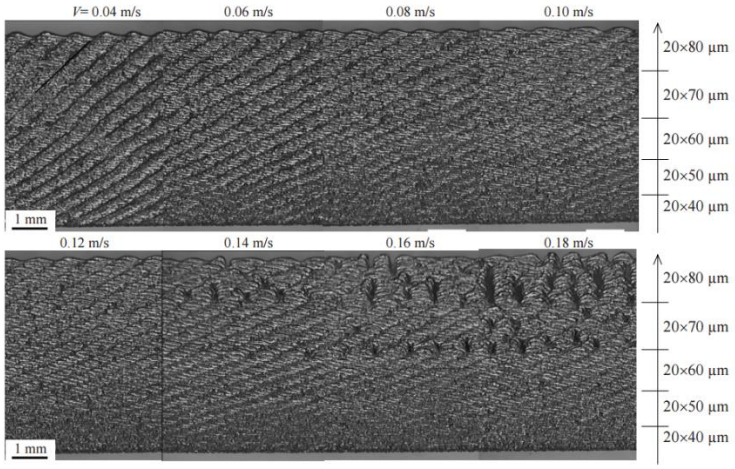

Fig. 2.1.5. Laser sintered thin walls from SS grade 316L powder (Yadroitsev & Smurov, 2011).

The influence of the scanning strategy and hatch spacing on layer morphology is demonstrated on the Fig. 2.1.6. In the experiment the laser power and the scanning speed are fixed with the material of Stainless Steel grade 904L powder (Yadroitsev, 2009; Yadroitsev & Smurov, 2011). The variation of the hatch spacing from 60, 120 and 240 μm shows that when hatch spacing increases more of the power is not sintered. At 240 μm hatch distance shows that a lot of powder is not sintered compared to the 60 μm. Thus choosing of hatch distance must be optimal to avoid pore formation in 3D object.

60 μm 120 μm 240 μm

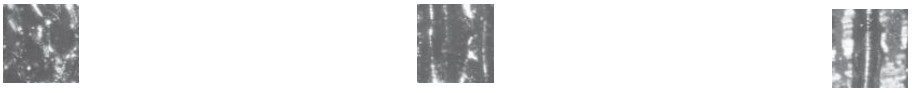

Fig. 2.1.6. Surfaces of the first layer from SS grade 904L powder obtained at different hatch distances (60, 120 and 240 μm) (Yadroitsev & Smurov, 2011).

To manufacture DMLS part, different scanning strategies can be used (Fig. 2.1.7). Scanning strategy can influence also on the microstructure of DMLS objects: changing the scan direction at each layer can have an effect of the prior β grain growth direction but the origin of the relationship is empirical and not well understood (Thijs *et al.*, 2010). Kruth *et al.*, 2012 showed that island scanning can be used to reduce the residual stresses.

(a) (b) (c) (d) (e)

Fig. 2.1.7. Different scan patterns: a) one direction b) double scanning each layer c) alternating scanning d) the direction of scanning rotated of certain angle between consecutive layer, island strategy e) (Manfredi *et al.*, 2014; Qiu *et al.*, 2013).

Process scheme of DMLS involves machine-based, material-based and process-based input parameters (Fig. 2.1.8). Microstructure and mechanical properties of as-built DMLS objects depend on not only material, but also process-parameters (Klocke *et al.*, 2003; Yadroitsev, 2009).

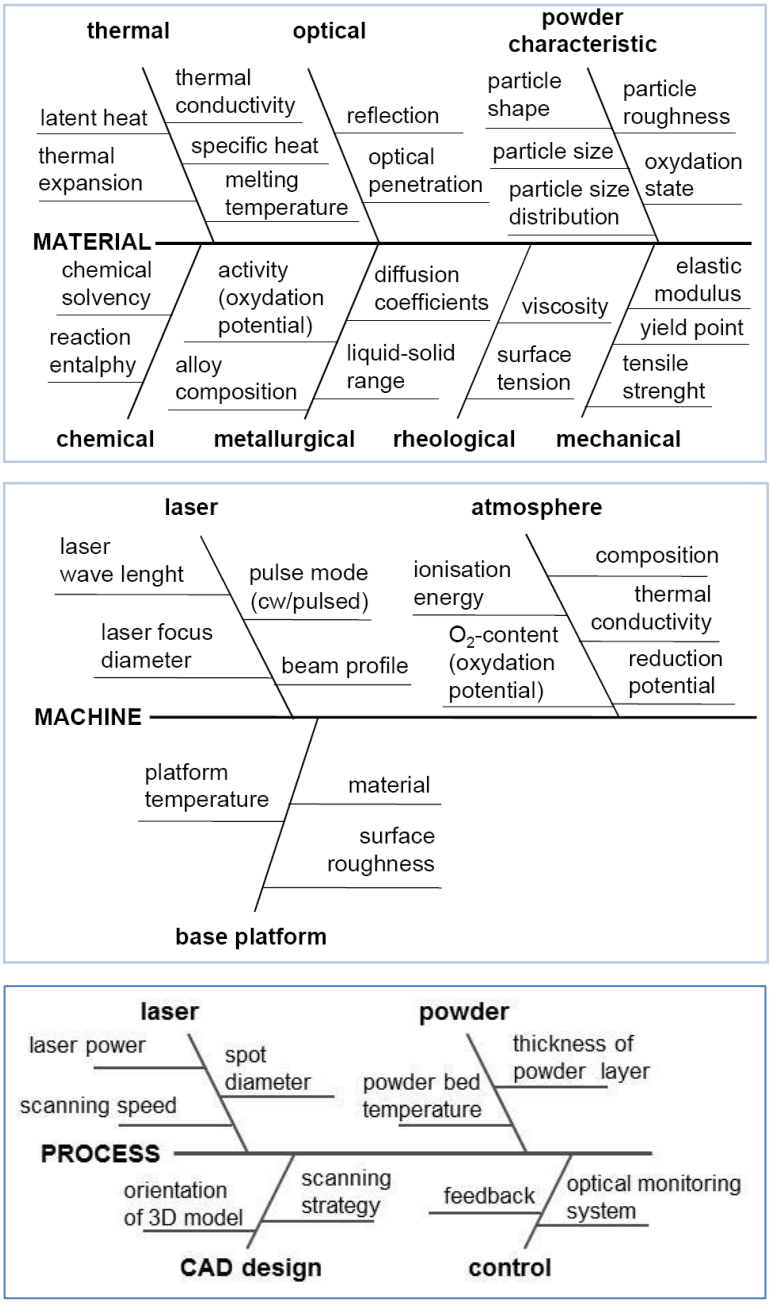

Fig. 2.1.8. Factors influencing on DMLS process (Klocke *et al.*, 2003).

Yadroitsev *et al.* (2015) suggested a system of hierarchical approach to identify optimal process parameters of DMLS. As example of the approach, AISI 420 stainless steel was used. It was shown that to produce continuous and stable single track, optimum laser power, laser spot size and scanning speed for different powder layer thicknesses must be used. The powder layer thickness has to be chosen in respect to the particle size of the employed powder. The geometric characteristics of the tracks affect the choice of subsequent scanning strategies and hatch distances. Choosing a scanning strategy defines the layer's morphology which in turn affects the subsequent layer thickness, regularity and continuity. The high quality of the synthesized single layer should

guarantee that the thickness of the next deposited powder layer does not vary greatly preventing further irregularity and balling effect. Numerical simulation of the temperature fields and analysis of pores' shapes could provide comprehensive information to determine the optimal process parameters for manufacturing non-porous 3D DMLS objects (Yadroitsev *et al.*, 2015).

Porosity in DMLS samples

In order to receive good mechanical properties, maximum density should be achieved. Optimal power density, scan speed, layer thickness, scanning strategy and other process-parameters must be optimal to produce non-porous DMLS parts.

Slotwinski *et al.* (2014) checked how hatch spacing influences on the porosity. A total of sixteen CoCr disks with nominal diameters of 40 mm and thicknesses of 10 mm were produced using an EOS M270. It was shown that increasing hatch spacing would increase the porosity level (Table 2.1.1).

Table 2.1.1. Build parameters and preliminary measured porosity values

Sample	Hatch Speed (mm/s)	Hatch spacing (mm)	Porosity by weight (%)	Porosity by micrograph (%)
1	800	0.1	0	0.07
2	1600	0.1	1.37	0.5
3	3200	0.1	18.12	12.22
4	800	0.2	2.07	0.29
5	800	0.4	10.19	14.38
6	3200	0.4	72.00	72.4

Yasa *et al.* (2010) concluded that the increases in scan speed and layer thickness will increase porosity due to lower energy input (Fig. 2.1.9). Maraging steel 300 powder was processed by Concept Laser M3 Linear machine with laser power of 105 W. It was found that to achieve high density, there is a certain entry for the energy density. Below that level the density decreases with decreasing energy density. Above the entry, the density is not affected by increasing energy densities in the tested range. The effect of the scan speed on the relative density was important especially at high scan speed.

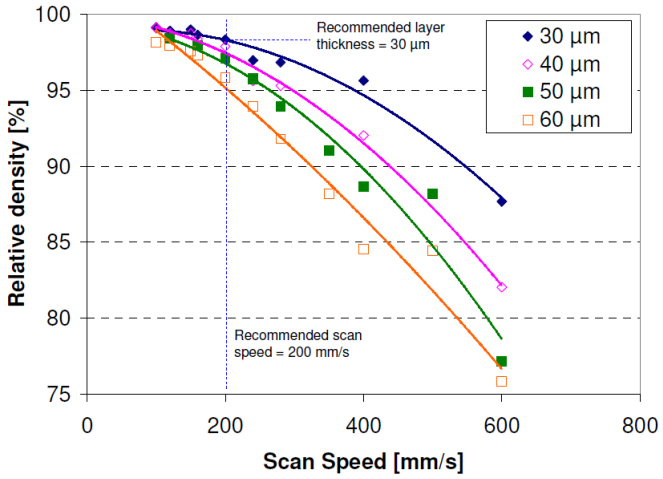

Fig. 2.1.9. Relative density *versus* scan speed for CL50WS for different layer thickness values (Yasa *et al.*, 2010).

Residual stress in DMLS samples

Residual stress can be defined as stress that remain in a component or material after processing and manufacturing in the absence of external force or thermal gradient (Löhe *et al.*, 2003). Residual stress can be defined as macro residual stresses also referred as Type I that develop in the body of a component on a scale larger than the grain size of the material. Micro residual stresses, which result from differences within the microstructure of a material, can be classified as Type II or III (Fig. 2.1.10). Micro residual stresses as referred Type II develop at the grain- size level while Type III are generated at the atomic level.

Residual stresses are either tensile or compressive in nature. Residual stresses are beneficial when they operate in the plane of the applied load and are opposite in sense (Kandil *et al.*, 2001; Paranjpe, 2014). Tensile residual stresses in the surface of a component are generally undesirable because they are often the major cause of fatigue failure, quench cracking and stress.

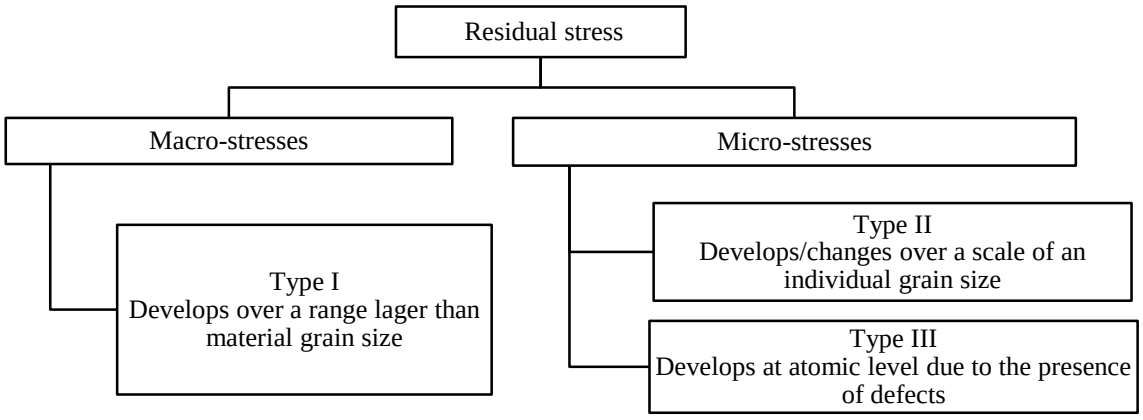

Fig. 2.1.10. Classification of residual stresses (Paranjpe, 2014).

As a result of the locally concentrated energy input by laser beam and thermal cycling during DMLS (Fig. 2.1.11), the temperature gradient mechanism and the related plastification lead to residual stresses and part deformations. A shrinkage or the reduction in volume due to rapid cooling or solidification though limited in the DMLS process none the less leads to strain (Fig. 2.1.12). Already solidified layers constrain the physical shrinkage of the top layer, leading to residual stress within the component (Knowles *et al.*, 2012; Vrancken *et al.*, 2012). These stresses can exceed the yield strength of the material and have been reported to initiate deformation and premature fracture of the component.

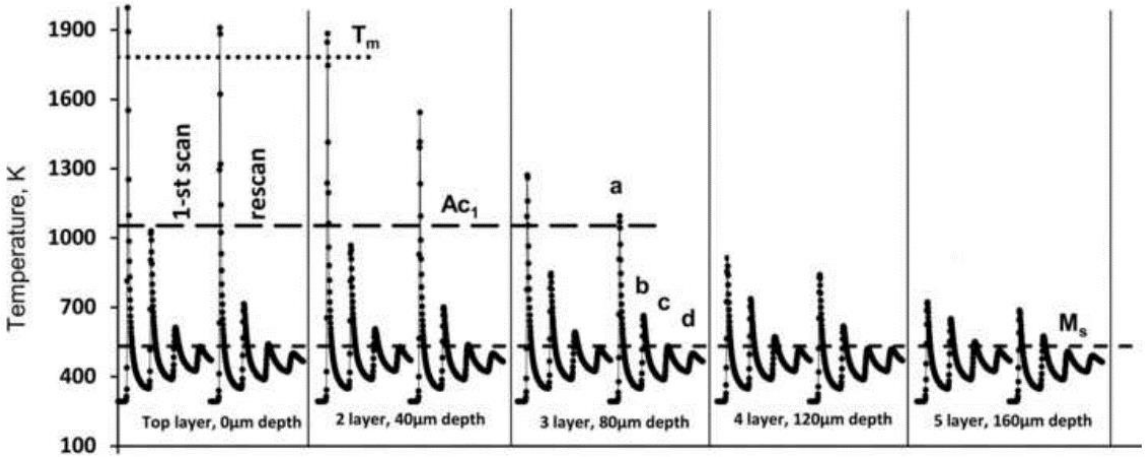

Fig. 2.1.11. Thermal cycling at different depths during laser melting of AISI 420 steel (Krakhmalev *et al.*, 2015).

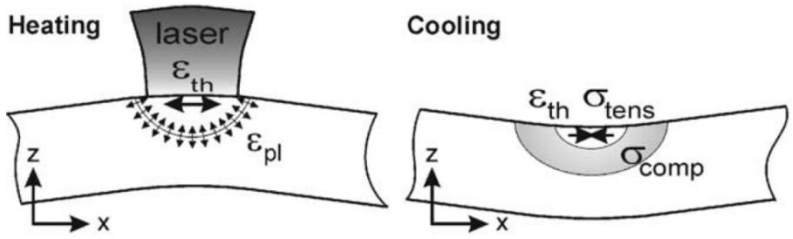

Fig. 2.1.12. Schematic showing heating and cooling phenomena of laser passes (Mercelis & Kruth, 2006).

There are different ways to manage residual stress in additive manufacturing. Kruth *et al.* (2010) showed that the island scanning reduces the residual stresses, but changing the island size does not contribute any further improvement. Alkahari *et al.* (2012) found that preheating of the substrate relieved the tensile residual stress more effectively than post heating at the top layer by the laser beam. Yadroitsev & Yadroitsava (2015) also postulated that during DMLS, heat treatment is seen as the main way to reduce residual stresses in DMLS parts.

2.1.2. Mechanical properties of DMLS objects

Track-by-track, layer-by-layer nature of DMLS can lead to anisotropy of mechanical properties of as-built DMLS objects. In the Table 2.1.2 the comparison of the mechanical properties of DMLS specimens according to their build orientation is presented. It was found that DMLS Maraging Steel MS1 has slightly high properties in the horizontal compared to the vertical direction. EOS Titanium Ti6Al4V samples built in vertical direction had higher yield strength and elongation at break compared to horizontal direction (Frey *et al.*, 2009). Mier & Harbeland (2008) studied mechanical properties of 316L stainless steel DMLS specimens. It was found that when the build orientation angle is less than the obtuse angle, the strength characteristics decrease (Fig. 2.1.13). It is seen that when the angle is less than the obtuse angle between processing direction and the direction of the load the more strength characteristics decrease. The horizontal test piece (b and c in Fig. 2.1.13) had the high tensile strength.

Table 2.1.2. Comparison of mechanical properties of horizontal and vertical specimens in EOS Maraging Steel MS1 and EOS Titanium Ti6Al4V (Frey *et al.*, 2009)

		EOS Maraging Steel MS1		EOS Titanium Ti6Al4V	
		horizontal	vertical	horizontal	vertical
Young ‘s modulus	[GPa]	172	160	112	111
Yield strength	[MPa]	1085	1076	1043	1088
Ultimate tensile strength	[MPa]	1188	1140	1248	1201
Elongation at break	[%]	13.3	10.0	8.5	10.6

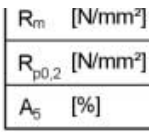

Fig. 2.1.13. Tensile tests characteristics of specimens of steel powder 316L produced with thickness of 50 µm, but different orientations as well as of conventionally fabricated reference material. Tensile strength R_m, technical elastic limit $R_{p0,2}$ and elongation after fracture A_5 (Mier & Harbeland, 2008).

Yadroitsev *et al.* (2009) demonstrated the influence of the building direction on properties of DMLS Inconel 625 parts. The samples of Inconel 625 (–16 µm) powder were built on the substrate at angles of 0^0, 90^0 and 45^0. The rectangular samples 50 mm × 20 mm × 4 mm were fabricated by two-zones technique, with laser power 50 W, layer thickness of 50 µm, scanning

speed of 0.13 m/s. The results from tensile testing showed higher yield strength and ultimate strength for DMLS samples compared to the wrought but the ductility was inferior. For building direction the vertical and horizontal showed almost similar ultimate strength. It was found that the Young's modulus of the "horizontal" samples was by 1.5 times higher than that for the "vertical" samples and it was close to that of wrought Inconel 625 (Table 2.1.4). It has been suggested that vertical samples showed lower modulus of elasticity which might be caused by amount of thermal stress accumulated during the heating/cooling cycles because of many layers compared to horizontal samples.

Table 2.1.3. Comparison of mechanical properties of horizontal and vertical specimens in DMLS Inconel 625 samples (Yadroitsev *et al.*, 2009)

Type	Ultimate tensile strength, MPa	Yield strength (0.2% offset, MPa	Elongation
Horizontal samples	1030±50	800±20	8-10
Vertical samples	1070±60	720±30	8-10
Wrought Inconel 625	940	430-520	40

Table 2.1.4. Young's modulus values (GPa) for different manufacturing strategies of the samples from Inconel 625 powder (Yadroitsev & Smurov, 2010)

Strategy	0^0	90^0	45^0
Horizontal samples	206.34	206.88	199.49
Vertical	132.21	140.22	149.55

The study done by Shifeng *et al.* (2014) also showed how building direction affects the mechanical properties of DMLS stainless steel 316L. The building direction was defined as an acute angle between the longitudinal axis of a given sample and the vertical axis (Fig. 2.1.14). The parameters were set as follows: fiber laser power of 180 W, scanning speed of 0.9 m/s, powder layer thickness of 20 μm, hatch distance of 60 μm. The average value of UTS for horizontal positions was 624 MPa and for vertical 669 MPa. The vertical samples were 6.8% stronger. The average elongation of vertical samples was higher by 68.5% compared to horizontal samples (49.6% vertical, 15.6% horizontal). These results suggest that the mechanical properties of the DMLS parts built along the vertical direction were higher than those built in the horizontal direction. This indicates anisotropic behaviour of mechanical properties. The sample built in the direction of 0° (the longitudinal axis is parallel with the *x*-axis) showed the worst elongation and the lowest strength. Another sample built along a 45° angle had the best combination of strength and ductility, while the sample built at 60° had maximum elongation (Shifeng *et al.*, 2014).

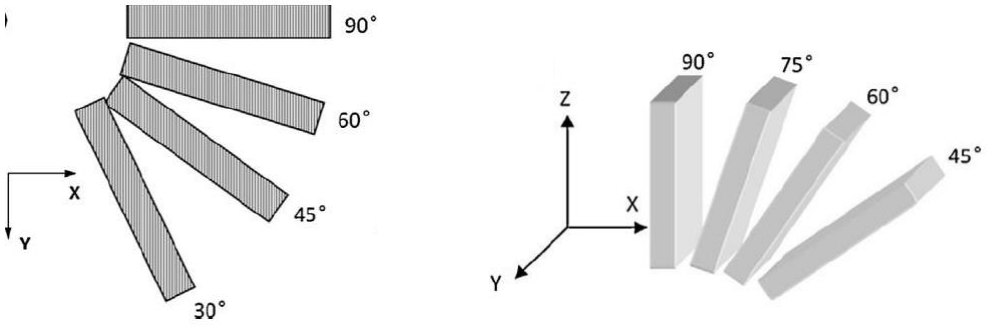

Fig. 2.1.14. Manufacturing strategy of the tensile samples: a) horizontal; b) vertical (Shifeng *et al.*, 2014).

AlSiMg specimens were prepared by DMLS with the EOSINT M270 by Manfredi *et al.* (2014) also to investigate the influence of different building directions on mechanical properties. DMLS specimens showed very high values of yield strength, with an enhancement of about 43% for samples built in the *xy*-plane and 36% for samples along the *z* axis (Table 2.1.5). For the ultimate tensile strength the values are higher in both cases. The elongation at break shows the higher value on the *xy*-plane compared to other building direction.

Table 2.1.5. Tensile properties of AlSi10Mg specimens produced according to the standard ASTM E8M along different orientations, compared to the conventional casting alloy (Manfredi *et al.*, 2014)

Material	Orientation	Yield Strength	Ultimate Tensile Strength	Elongation at break (%)	Young's Modulus, GPa
AlSiMg after DMLS	*xy*-plane	243 ± 7	330 ± 3	6.2 ± 0.3	73±1
	z axis	231 ± 3	329 ± 2	4.1 ± 0.2	72±1
A360.2 alloy	-	170	317	5	

Analysis of fractographs of DMLS tensile samples, which was done Yadroitsev (2009), shows combination of brittle and ductile fractures (Fig. 2.1.15). Some characteristics of brittle fracture are: there is no gross, permanent deformation of the material; the surface of the brittle fracture tends to be perpendicular to the principal tensile stress although other components of stress can be factors; characteristic crack advance markings frequently point to where the fracture originated; in metals, transgranular and intergranular cleavage are important. Vertical sample with scanning direction 0° has monolithic «zebra-like» structure with smooth and rough strips. Transversal destruction accompanied by spalling of some parts of material is observed (Fig. 2.1.16).

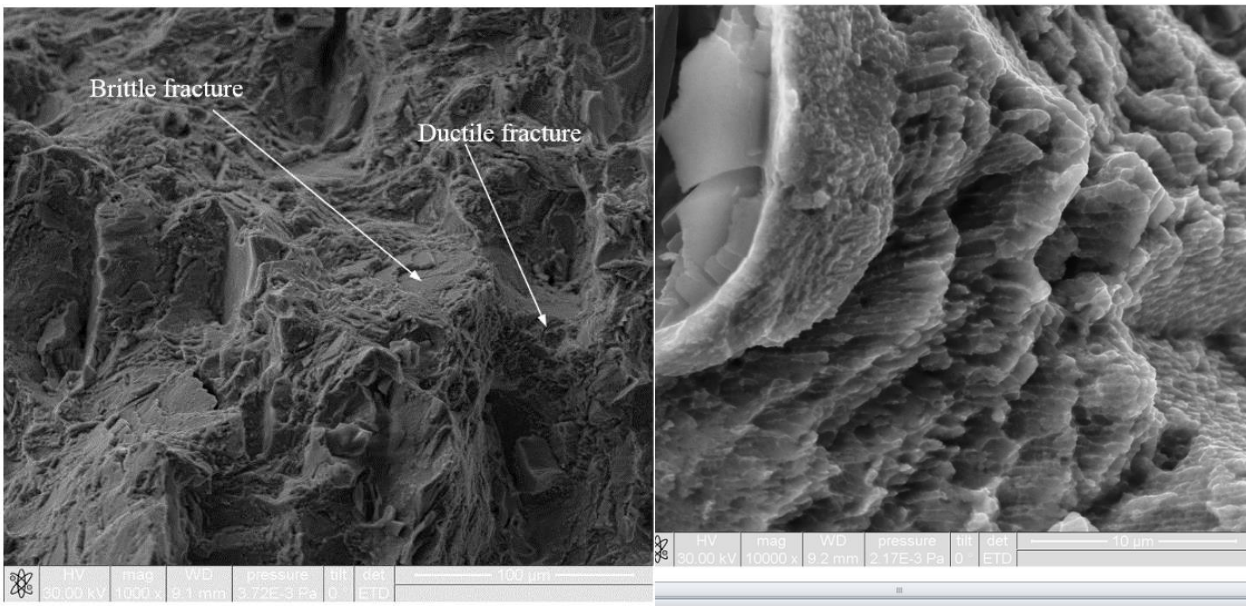

Fig. 2.1.15. SEM photos of destruction for monolithic area of the horizontal DMLS Inconel 625 sample (Yadroitsev, 2009).

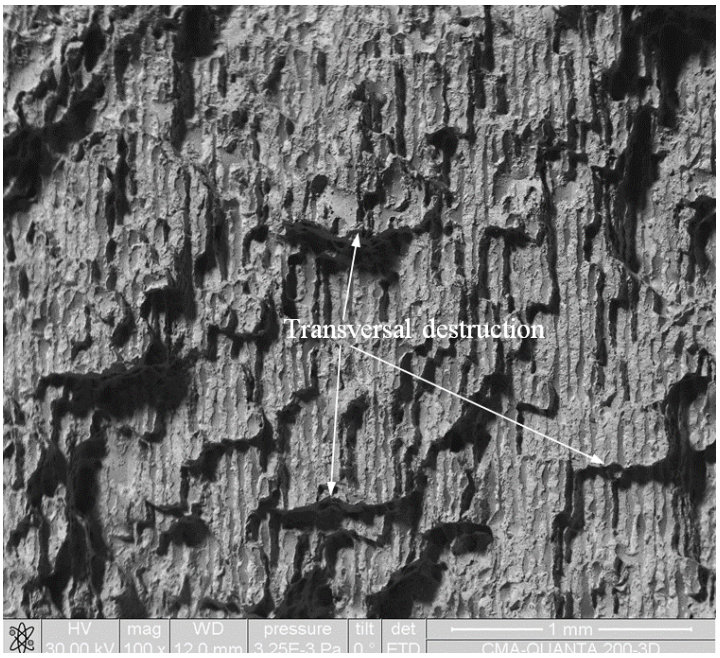

Fig. 2.1.16. SEM photos of destruction for monolithic area of the vertical DMLS Inconel 625 sample (Yadroitsev, 2009).

It was also noted that samples manufactured by DMLS had a greater elasticity within one layer than between layers. All vertical samples broke at layer contacts. The horizontal ones broke at the plane perpendicular to the laser scanning direction (Yadroitsev, 2009).

2.1.3. Modern DMLS equipment

DMLS systems are used for the production of high quality, complex prototypes as well the end-user products. Some producers elaborate optimal process-parameters for certain powder and the process parameter are programmed by the machine provider. Each machine has different construction volume which determines how big the size of the DMLS object is. Laser power is varied from 50 to 1000 W and laser spot size 10-700 μm (Table 2.1.6). Typical layer thickness is about 20-50 μm. Producers proposed optimal process-parameters for high-grade steels, Co-Cr, Al alloys, Ni-based alloys, Ti alloys and also precious-metal alloys.

Table 2.1.6. Modern DMLS machines *

System	Built volume x/y/z, mm	Laser power, W	Scan. speed/ up to, m/s	Layer thickness, μm	Laser spot size, μm	Powders
EOS GmbH Electro Optical Systems						
EOSINT M280	250x250x325	200/400	7		100-500	Al alloys, Ni alloys, Ti, Ti6Al4V (ELI), Co-Cr alloys, stainless steels
EOS M290	250 x 250 x 325	400	7		100	Al alloys, Ni alloys, Ti, Ti6Al4V (ELI), Co-Cr alloys
EOS M400	400 x 400 x 400	1000	7		90	
PRECIOUS M 080	80 x 95	100	7		< 30	
SLM Solutions GmbH						
125HL	125x125x75	400	10	20-160	60-70/90	Stainless Steel, Tool Steel, Co-Cr, Al and Ti alloys
SLM® 280 HL	280 x 280 x 360	400/1000	15	20-75/100	70 - 120 /700	
SLM® 500 HL	500 x 280 x 365	2 x400	10	20-75	80 - 115	
Concept Laser GmbH						
X line 1000R	630 x 400 x 500	1000	7	30 - 150	100-500	Al and Ti alloys, Ni-based alloy (Inconel 718)
X line 2000R	800 x 400 x 500	2 x 1000				
M2 cusing	250 x 250 x 280	2 x 200 optional 2 x 400	4.5/7	20 - 80	50 - 500	High-grade steels, Al alloys ,Ni-based alloys, Ti alloys, precious-metal alloys
M1 cusing	250 x 250 x 250	200/400	7	20 - 80	50	
Mlab cusing R	50 x 50 x 80 70 x 70 x 80 90 x 90 x 80	100	4.5/7	15 - 50	40	
Mlab cusing	50 x 50 x 80 70 x 70 x 80 90 x 90 x 80	50 / 100	7	15 - 50	40	Stainless steel, Co-Cr alloys, bronze, yellow gold, Ag alloys
3D Systems, Inc.						
ProX™ 100	100 x 100 x 80	50		10 -50		Stainless steels, tool steels, non-ferrous alloys, super alloys and others
ProX™ 200		300		10 -50		
ProX™ 200 Dental	140 x 140 x 100			10 -50		
ProX™ 300	250 x 250 x 300	500				
ProX™ 400	500 x 500 x 500	2 x 500 (1 000)		10 -100		

System	Built volume x/y/z, mm	Laser power, W	Scan. speed/ up to, m/s	Layer thickness, µm	Laser spot size, µm	Powders
ReaLizer GmbH						
SLM 50	500 x 800 x 700	120		20- 50		Co-Cr, Ti alloys, steel alloys
SLM125	125 x 125x 200	100-400		20- 100		
SLM250	300 x250 x250	100-400		20-100		
SLM300	300 x300x300	100 -400		20 -100		
Renishaw plc.						
RenAM 500M	250 × 250 × 350	500				
AM 400	250 × 250× 300	200/400			70	
AM 250	250 × 250 × 300	200/400			100	

*(ConceptLaser, 2012; SLM, 2014; 3D Systems, 2013; EOS, 2015)

Summary

DMLS is an additive manufacturing technology where powder metal is fused by laser track-by-track, layer-by layer to form a 3D part. The process of the part sintering can be influenced by different parameters including machine parameters, process parameters and also powder materials properties. The process-parameters, scanning and building strategy have a great influence on the porosity, residual stress of the component and, finally, on mechanical properties of the DMLS object. It's crucial to select the right modern DMLS equipment used for specific materials that can deliver quality DMLS products when also the right process parameters are implemented.

2.2. Mechanical testing of materials

2.2.1. Tensile tests and standards

The mechanical testing is used for evaluating fundamental properties of engineering materials as well as in developing new materials and checking material quality before design and construction. Mechanical testing of engineering materials subjected to tension, compression, bending or torsion loading. The most common type of test used to measure the mechanical properties of a material is the tension test which widely used to provide basic design information on the strength of materials and is an acceptance test for the specification of materials (Tensile testing, 2004). According to ASTM E8/E8M , test methods cover the tension testing of metallic materials in any form at room temperature of 10 to 38 C unless otherwise, specifically, the methods of determination of yield strength, tensile strength, elongation, and reduction of area. For tensile testing the common used specimen are flat and round specimens (Fig. 2.2.1).

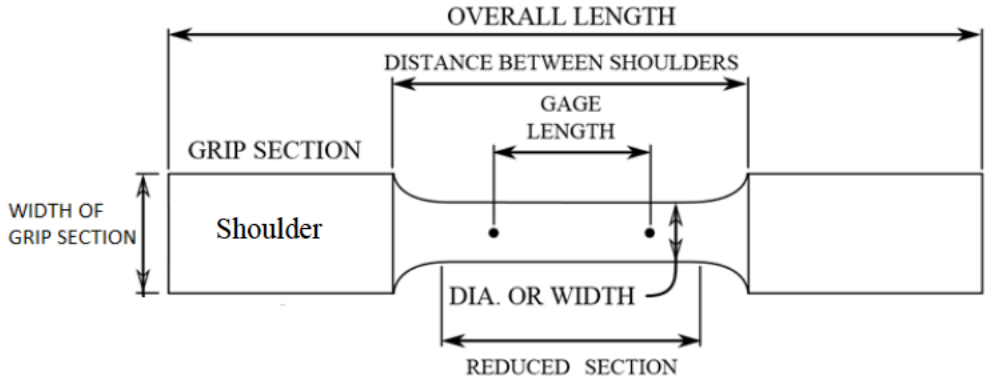

Fig. 2.2.1. The cross section for a typical specimen for tensile testing.

Various types of gripping devices are used to transmit the measured force applied by the testing machine to the test specimens. Gripping devices are used according to the specimen type. Grips have to be able to securely hold the specimen during the test without slippage to ensure accurate results (Fig. 2.2.2).

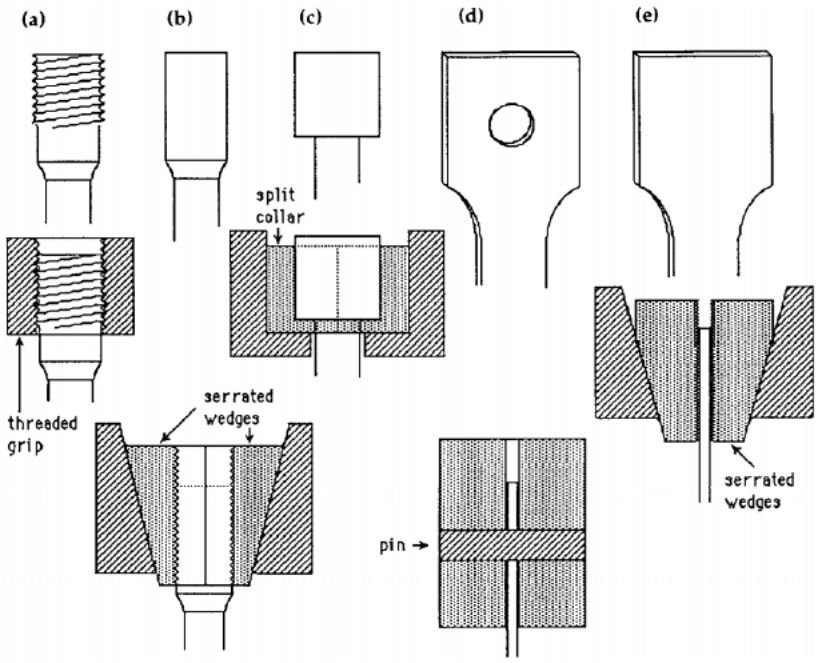

Fig. 2.2.2. Systems for gripping tensile specimens. For round specimens, these include threaded grips (a), serrated wedges (b), and for butt end specimens, split collars constrained by a solid collar (c). Flat specimens may be gripped with pins (d) or serrated wedges (e) (Tensile testing, 2004).

The forces used in determining tensile strength and yield strength shall be within the verified force application range of the testing machine. After testing the specimen the deformation can be encountered showing different changes. Stress-strain diagram contains different stages until the specimen fractures as demonstrated in Fig. 2.2.3.

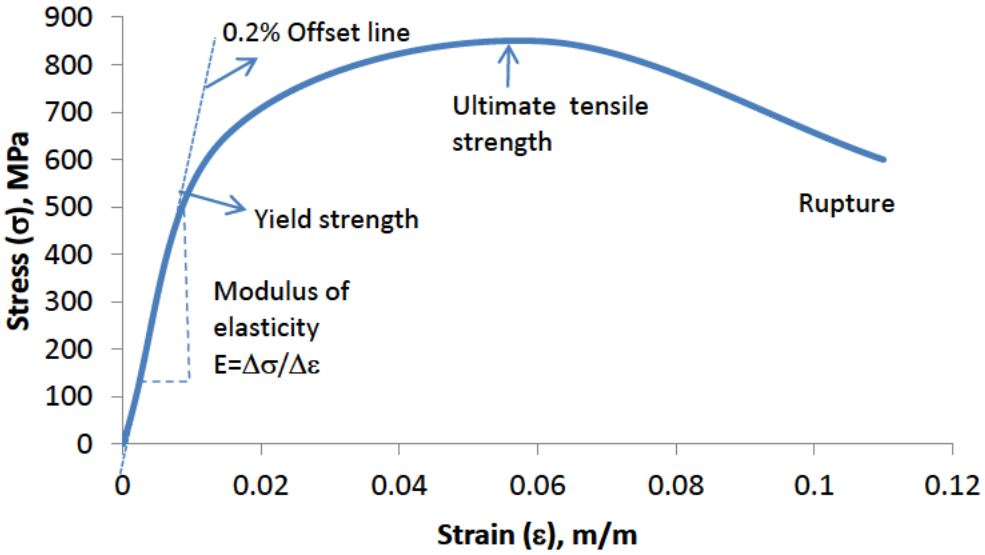

Fig. 2.2.3. Typical stress-strain diagram.

- Elastic Limit. The elastic limit is the limit beyond which the material will no longer go back to its original shape when the load is removed, or it is the maximum stress that may developed such that there is no permanent or residual deformation when the load is entirely removed.
- The 0.2% offset yield strength is the stress value, σ0.2%YS of the intersection of a line (called the offset) constructed parallel to the elastic portion of the curve but offset to the right by a strain of 0.002. It represents the onset of plastic deformation.
- Yield Point. Yield point is the point at which the material will have an appreciable elongation or yielding without any increase in load.
- Ultimate Strength. The maximum ordinate in the stress-strain diagram is the ultimate strength or tensile strength.
- Rupture Strength. Rupture strength is the strength of the material at rupture. This is also known as the breaking strength.

In most case fracture is of the shear or of the separation: the cause of failure is normally affected by the testing temperature, speed of testing, the shape and size of the test piece, and other conditions. The original orientation of the crystal is an important factor in determining the character of the fracture. There are basic two types of fracture of materials that are normally found after mechanical testing: brittle fracture and ductile fracture. The basic types of fracture of material are shown in Fig. 2.2.4. A complete brittle cleavage fracture will show sharp planar facets which reflect light. While ductile fracture presented rough dirty-grey surface this is due to its rough surface, irregular contour where much of the surface is inclined sharply to the average plan of the fracture.

The failure of most ductile materials in the polycrystalline form occurs with a cup and cone fracture and is typically formed during tensile testing deformation process. The fracture begins at the centre of necked region on a plane that is macroscopically normal to the applied tensile –stress axis. In the necked region of a tensile-test specimen, small cavities may form in the metal near the centre of the cross section before a visible crack is found. Ductile fracture also have double cup fracture which can be observed in many face centred cubic metals (Becker & Lampman, 2002). Ductile materials are characterized by their ability to yield at normal temperatures. As the specimen is subjected to an increasing load, its length first increases linearly with the load and at a slow rate (Fig. 2.2.4)

Brittle materials are characterized by the fact that rupture occurs without any noticeable prior change in the rate of elongation (for example, cast iron or glass). Also, the strain at the time

of rupture is much smaller for brittle than for ductile materials; there is no necking or length increasing.

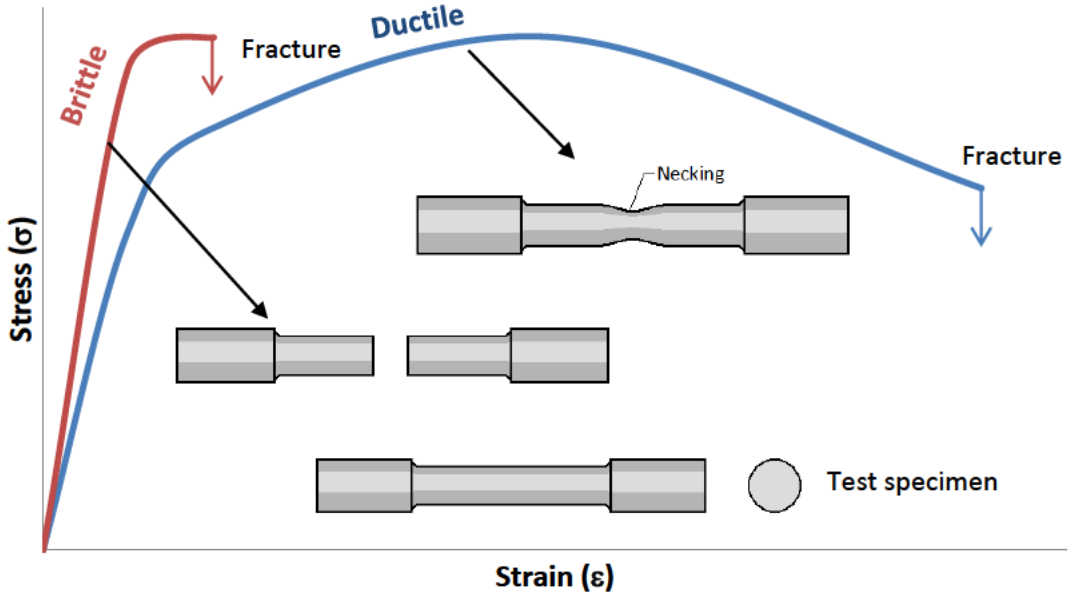

Fig. 2.2.4. The stress-strain graphs demonstrating analysis of fracture and types of fracture.

Standard tensile specimens

Tension test provides information about ductility of materials under uniaxial tensile stresses and can be used in alloy development, quality control and design under certain circumstances. Standard Test Methods for Tension Testing of Metallic Materials E8/E8M (ASTM E8/ E8M-16a, 2016) describes the tension testing of metallic materials in any form at room temperature. Fig. 2.2.5 shows typical dimensions of tensile specimens.

According to ASTM Standard E8, for flat specimens it has standard specifications as follows:

- "*Note 1—The ends of the reduced section shall differ in width by not more than 0.1 mm. There may be a gradual taper in width from the ends to the center, but the width at each end shall be not more than 1 % greater than the width at the center.*
- *Note 2—The dimension T is the thickness of the test specimen as stated in the applicable product specifications.*
- *Note 3—For some materials, a fillet radius R larger than 13 mm may be needed.*
- *Note 4—Holes must be on center line of reduced section within ± 0.05mm.*
- *Note 5—Variations of dimensions C, D, E, F, and L may be used that will permit failure within the gage length*".

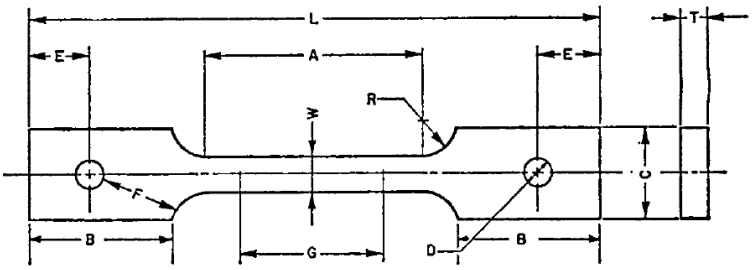

Dimensions, mm [in.]	
G—Gage length	50.0 ± 0.1 [2.000 ± 0.005]
W—Width (Note 1)	12.5 ± 0.2 [0.500 ± 0.010]
T—Thickness, max (Note 2)	16 [0.625]
R—Radius of fillet, min (Note 3)	13 [0.5]
L—Overall length, min	200 [8]
A—Length of reduced section, min	57 [2.25]
B—Length of grip section, min	50 [2]
C—Width of grip section, approximate	50 [2]
D—Diameter of hole for pin, min (Note 4)	13 [0.5]
E—Edge distance from pin, approximate	40 [1.5]
F—Distance from hole to fillet, min	13 [0.5]

(a)

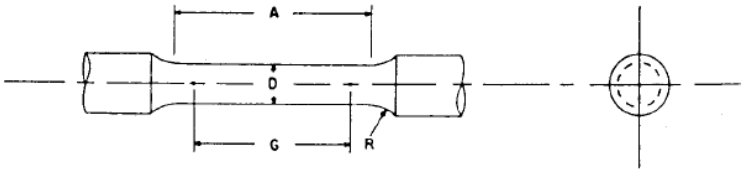

Dimensions, mm [in.]
For Test Specimens with Gage Length Four times the Diameter [E8]

	Standard Specimen	Small-Size Specimens Proportional to Standard			
	Specimen 1	Specimen 2	Specimen 3	Specimen 4	Specimen 5
G—Gage length	50.0 ± 0.1 [2.000 ± 0.005]	36.0 ± 0.1 [1.400 ± 0.005]	24.0 ± 0.1 [1.000 ± 0.005]	16.0 ± 0.1 [0.640 ± 0.005]	10.0 ±0.1 [0.450 ± 0.005]
D—Diameter (Note 1)	12.5 ± 0.2 [0.500 ± 0.010]	9.0 ±0.1 [0.350 ± 0.007]	6.0 ± 0.1 [0.250 ± 0.005]	4.0 ± 0.1 [0.160 ± 0.003]	2.5 ± 0.1 [0.113 ± 0.002]
R—Radius of fillet, min	10 [0.375]	8 [0.25]	6 [0.188]	4 [0.156]	2 [0.094]
A—Length of reduced section, min (Note 2)	56 [2.25]	45 [1.75]	30 [1.25]	20 [0.75]	16 [0.625]

(b)

Fig. 2.2.5. Typical dimensions of tensile specimens: (a) pin-loaded tension test specimen with 50-mm and (b) standard 12.5-mm round tension test specimen and examples of small-size specimens with gage length four times the diameter (ASTM E8 / E8M-16a, 2016).

According to ASTM Standard E8, for round specimens it has standard specifications as follows:

- "*Note 1: the reduced section may have a gradual taper from the ends toward the centre, with the ends not more than 1 % larger in diameter than the centre (controlling dimension).*
- *Note 2: If desired, the length of the reduced section may be increased to accommodate an extensometer of any convenient gage length. Reference marks for the measurement of elongation should, nevertheless, be spaced at the indicated gage length.*
- *Note 3: The gage length and fillets may be as shown, but the ends may be of any form to fit the holders of the testing machine in such a way that the force shall be axial .If the ends are to be*

held in wedge grips it is desirable, if possible, to make the length of the grip section great enough to allow the specimen to extend into the grips a distance equal to two thirds or more of the length of the grips.

- *Note 4: On the round specimens in Fig. above, the gage lengths are equal to four [E8] or five times [E8M] the nominal diameter. In some product specifications other specimens may be provided for, but unless the 4-to-1 [E8] or 5-to-1 [E8M] ratio is maintained within dimensional tolerances, the elongation values may not be comparable with those obtained from the standard test specimen.*
- *Note 5—The use of specimens smaller than 6-mm [0.250-in.] diameter shall be restricted to cases when the material to be tested is of insufficient size to obtain larger specimens or when all parties agree to their use for acceptance testing. Smaller specimens require suitable equipment and greater skill in both machining and testing."*

Micro-specimens

Micro specimens were used Kashaev *et al.* (2013) to investigate the mechanical properties to obtain reliable tensile and fatigue test results for different materials. For micro-tensile specimens, a 5 kN electro-mechanic universal testing machine with a constant transverse main displacement was used. Dimensions of micro-specimens for fatigue and tensile tests are shown in Fig. 2.2.6. All micro-specimens were extracted via electro discharge machining (EDM). The geometry of micro-specimens was designed on the basis of standards DIN EN 2002-001:2006-11, DIN EN ISO 6892-1:2009-12 and DIN 50100.

(a) (b)

Fig. 2.2.6. Dimensions of micro-specimens fatigue test sample (a) and tensile test sample (b) (Kashaev *et al.*, 2013).

The Fig. 2.2.7 shows the mechanical properties for Ti6Al4V standard size and micro specimens. The stress-strain curves obtained for standard and micro-specimens were compared and only minor differences between the strain-stress curves was noticed (Kashaev *et al.*, 2013).

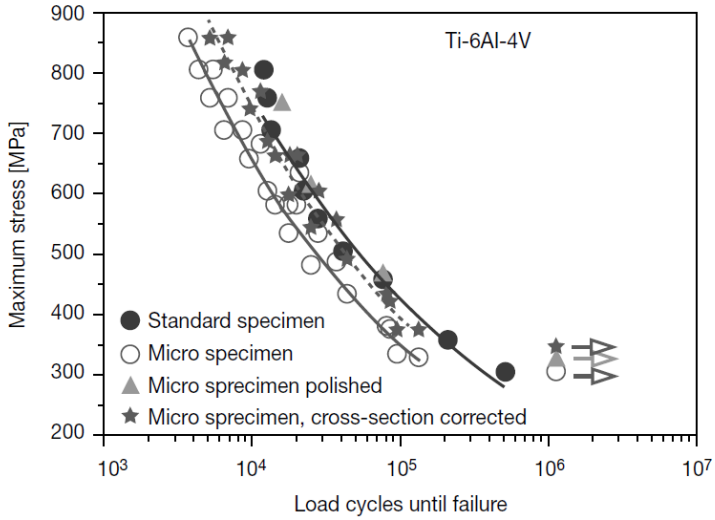

(a)

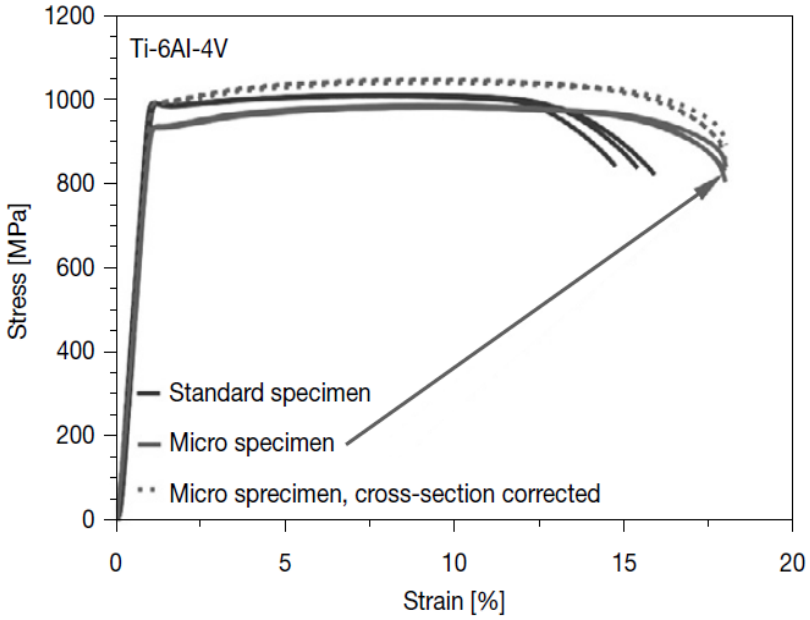

(b)

Fig. 2.2.7. Results of the fatigue tests (a) and stress-strain (b) curves of Ti6Al4V base materials obtained by testing standard and micro-specimens (Kashaev *et al.*, 2013).

The tensile tests were done and the strength of Ti6Al4V don't differ much values when standard or micro specimens. It can be seen that only the differences between the obtained elongations could be attributed to size effects.

Table 2.2.1. The tensile results of Inconel 625, Inconel 718 and Ti6Al4V with standard deviations (Kashaev *et al.*, 2013)

Material	Tensile strength, R_m [MPa]				Yield strength, $R_{P0.2}$ [MPa]				Elongation, A_5 [%]		
	S	SS	MS	MSC	S	SS	MS	MSC	S	SS	MS
Inconel 625	890	896 ± 1	821 ± 2	884 ± 2	450	442 ± 2	409 ± 9	436 ± 7	50.7	55.4 ± 0.7	58.9 ± 0.1
Inconel 718	865	891 ± 2	808 ± 5	871 ± 6	390	417 ± 1	386 ± 6	420 ± 4	50.3	50.8 ± 1.4	56.0 ± 0.2
Ti-6Al-4V	930	1,019 ± 2	992 ± 3	1,052 ± 3	865	998 ± 3	943 ± 2	1,000 ± 2	14.0	15.1 ± 0.5	17.9 ± 0.01

MS: obtained from micro-tensile specimens; MSC: obtained from micro-tensile specimens, the cross-section was corrected for roughness; S: according to the manufacturer's specification; SS: obtained from standard specimens.

It was found that roughness, notches or any impurities can affect the results. Roughness reduces the cross-section and this significantly decrease the load-bearing cross-section. Thus the tensile strength and yield strength of micro-specimens can be reduced. The cross section of micro specimen was corrected considering roughness, and it was found the micro- fatigue specimens have fatigue life the same as the standard specimen.

Study was done by Seguineau *et al.* (2008) for micro-tensile tests of micro-machined metal samples on polymer. The tensile sample's dimensions were: 5 mm total length, 3 mm gage length and 0.5 mm width. The mechanical properties results was concluded to of copper on polymer samples were in agreement to expect results like for the large strains. It was shown that micro-tensile experiments are useful to determine the mechanical response of thin films and coatings.

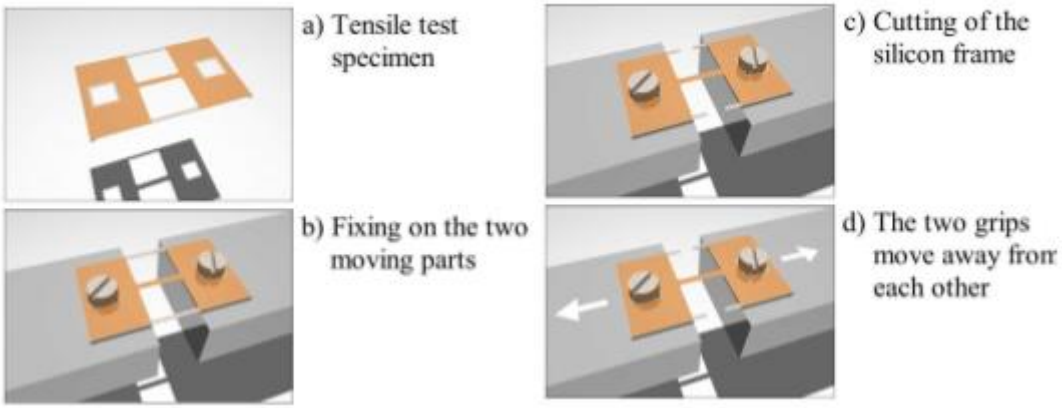

Fig 2.2.8. The artistic view of the specimen Seguineau *et al.* (2008).

The investigation of mechanical properties for micro-tensile test for steel sheets done by Rund *et al.* (2015) the investigated materials were two perlitic-feritic structure materials S355JR and S235JR, third investigated material was austenitic steel 1.4301. Tests were done at room temperature at different loading velocities resulting in initial strain rates ranging from 0.001; 0.1; 1; 10 s^{-1}. The specimen dimension is demonstrated on Fig 2.2.9 (a), there was no significant difference between standard and micro specimens (Fig. 2.2.9 b).

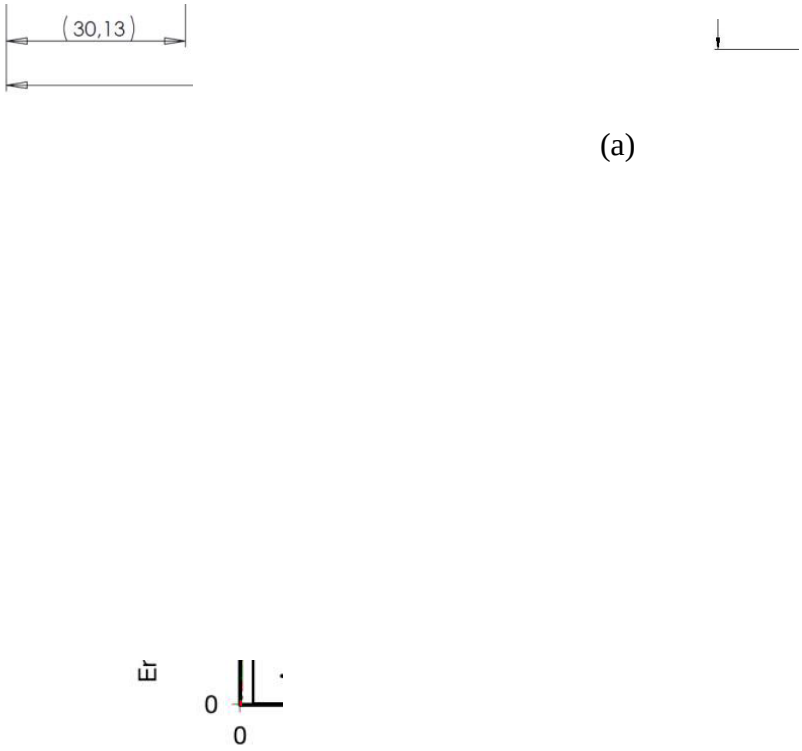

(a)

(b)

Fig 2.2.9. Micro specimens (a) and stress-strain diagrams for standard and micro tensile specimens (MTT) (Rund *et al.*, 2015).

A tensile test of samples cut from weld metal to investigate the local mechanical properties of the weld joint was studied by LaVan (1999), Kartal *et al.* (2007), Molak *et al.* (2009), and others. It was concluded that micro tensile testing had a good agreement with a standard tensile specimens when gauge contained all the regions of the weld.

Thus, using micro-specimens can be excellent method for express-analysis and evaluation of the DMLS process.

2.2.2. Peculiarities of mechanical tests of DMLS material

As it has been shown in sections 2.1.2 as-built DMLS samples can have anisotropy in mechanical properties since DMLS is layer-by-layer powder technology. Frey *et al.* (2009)

indicated that mechanical properties of DMLS samples depend on the specimen geometry, build orientation and surface finish (Fig. 2.2.10). Zwick/Roell Z050 machine with a maximum load of 50 kN was used for the testing. Loading rates was chosen in accordance with the standards and depending on the material being tested. Some typical values are 20 MPa s^{-1} in the elastic and 0.008 s^{-1} in the plastic region. The results confirm that more consistent and reliable results are to be expected when using machined cylindrical specimens. In all comparison the cylindrical results have high modulus of elasticity. It was found, that flat specimens (DIN 50125) have in every case both lower value and higher standard deviation than the corresponding cylindrical samples (DIN 50125); machined specimens have in every case both higher value and lower standard deviation than the corresponding un-machined (as built) samples. It was also shown, that the effect of orientation is material-dependent. For example, Maraging steel MS1 has slightly better properties in the horizontal direction, and Ti6Al4V alloy has significantly better yield strength and elongation at break in the vertical direction (Table 2.1.2).

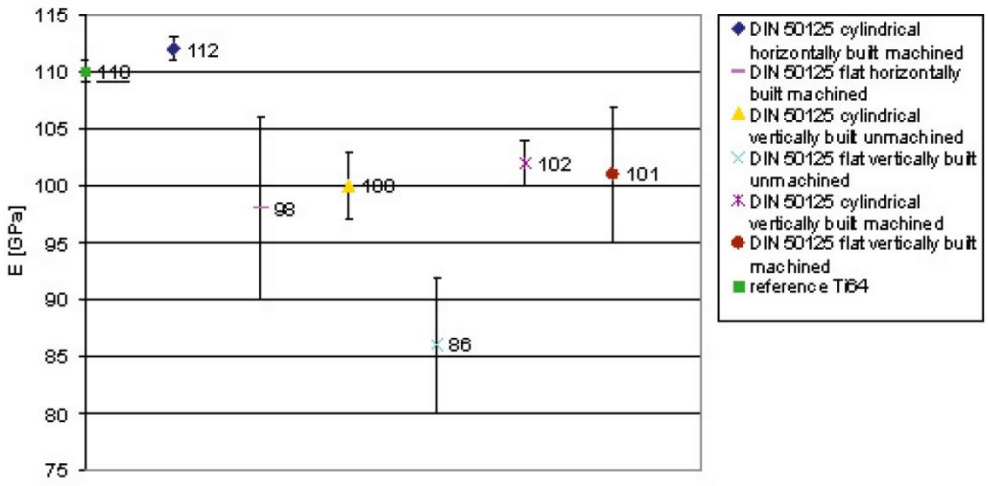

Fig. 2.2.10. Comparison of Young´s modulus (mean and standard deviation) for EOS Titanium Ti6Al4V depending on: (i) specimen geometry (cylindrical vs. flat); (ii) build orientation (vertical vs. horizontal); (iii) surface finish (as-built vs. machined) (Frey *et al.*, 2009).

Fig. 2.2.11 represents the surfaces of DMLS bar produced by EOSINT M280 machine at prescribed by EOS for Ti6Al4V alloy parameters and layer thickness of 30 μm. Surface roughness differs on the top, front and cut surfaces.

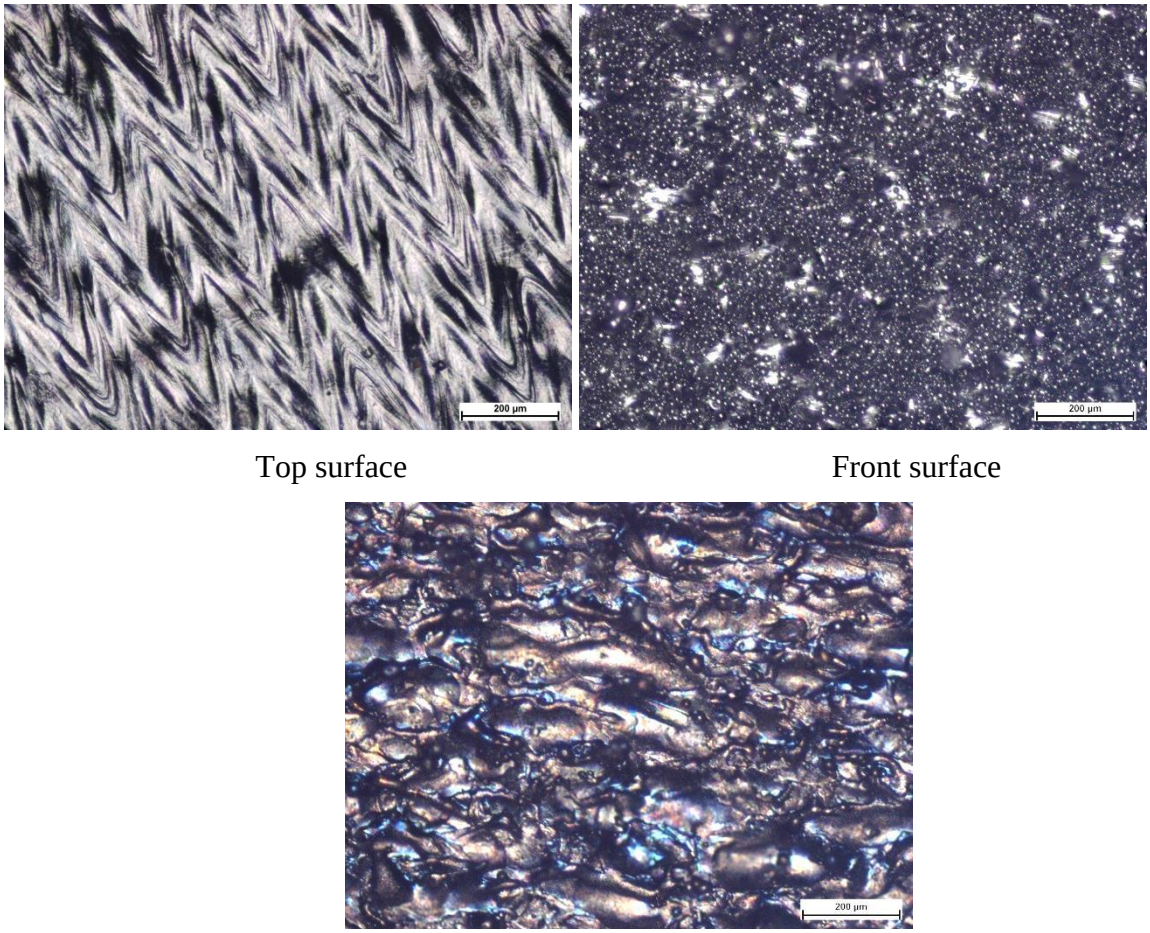

Top surface Front surface

Bottom surface (after cutting by EDM)

Fig. 2.2.11. Surfaces of as-built cut from the substrate DMLS sample.

Do & Li (2016) investigated the influence of laser energy input on the microstructure, physical and mechanical properties of titanium alloy. Ti6Al4V ELI was fused with different energy input 0.5E, E, 2E and different scanning speed the substrate was pre-heated and kept constantly at 200°C with constant process parameters of laser power (*P*), hatching spacing (*h*) and layer thickness (*t*). The main effect of porosity was caused by the process parameters of the SLM process as it was investigated in the study. The baseline value E_0 = 75 Jmm^{-3} was achieved with the laser power P_0 = 120 W, the scanning speed V_0 = 400 mm s^{-1}, the hatch spacing h_0 = 80 µm, and the layer thickness t_0 = 50 µm. Energy density E was defined as follows:

$$E = P/(V \times h \times t)$$

The table 2.2.2 shows the results of the measured microstructure, physical and mechanical properties as a function of laser energy input. At the low energy input $0.5E_0$ it was found that the porosity was maximum with 6.5% compared to the E_0 and $2E_0$ energy because the powder was not fully melted due to lower energy input. Studies done by Simchi (2006) explained that the higher energy causes higher temperature in the molten material, this enables liquid to flow and to fill out

the pores. The un-melted powder has an effect on the surface finish of the material. Increasing the laser energy from $0.5E_0$ to the baseline E generates the recoil pressure that facilitates to reduce the surface tension of the pool, increase the flattening effect, and hence improve the surface quality. The Table 2.2.2 shows that the increase of laser energy has an effect on the surface finish.

Table 2.2.2. Measured microstructure, physical and mechanical properties in the DMLS Ti6Al4V as a function of laser energy input (Do & Li, 2016)

Measured property	Laser energy input conditions		
	$0.5E_0$	E_0	$2E_0$
Relative density, %	93.5	99.0	99.2
Average roughness on top surface, *Ra* µm	94	8.9	24.7
Average roughness on side surface, *Ra* µm	19.5	7	13.2
Total roughness on top surface, *Rt* µm	286.3	27.3	74.2
Total roughness on the side surface, *Rt* µm	69.7	28.8	51
Martensitic lath length, µm	23.6±10.9	42.9±15.3	53.6±11
Vickers microhardness, HV	403±11	416±13	444±8

Frey *et al.* (2009) selected as standard for tensile testing proportional cylindrical tensile samples with 5 mm diameter and 25 mm length of the test section, and cylindrical (non-threaded) ends for clamping with the following reasons (Fig. 2.2.12). It was concluded that

- Cylindrical sample geometry ensures a homogenous distribution of stress.
- Cylindrical sample geometry is easy and efficient to produce, and also easier to post-machine with high tolerances (if desired) compared to e.g. flat specimens.

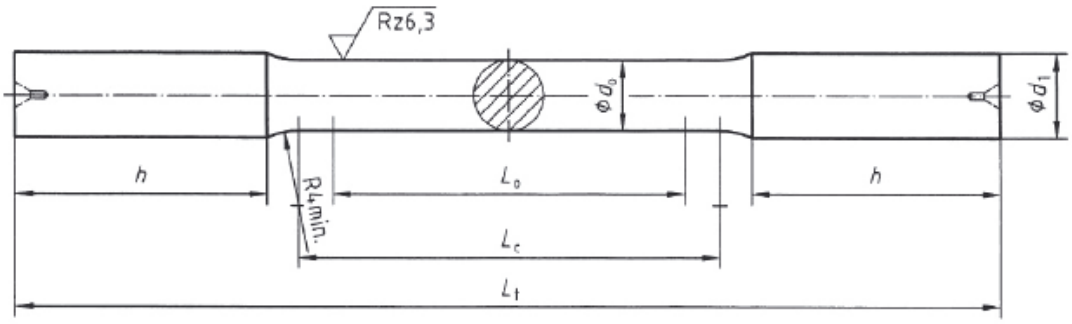

Fig. 2.2.12. The standard cylindrical sample geometry. Recommended tensile test sample for DMLS according to ISO 6892, DIN EN 10002-1 and DIN 50125, using L_t=80 mm, L_c=40 mm, L_0=25 mm, d_0=5 mm, d_1=6 mm, h=20 mm (Frey *et al.*, 2009).

- The results are also comparable to ASTM E 8M-04, because the dimensional guidelines correlate to ISO 6892, DIN EN 10002-1 and DIN 50125 by a factor of 0.8333.

- 5-mm diameter provides good reliability of results (smaller is less reliable, 4 mm is the smallest permitted by the ISO and DIN standards) combined with cost-effective production (larger sizes mean longer build times and higher costs).

Frey *et al.* (2009) also recommended for the tensile tests of DMLS samples:

1. To indicate whether the specimens were machined or not, building direction, post-stress relieving.
2. To test both horizontal and vertical samples.
3. As with all manufacturing methods, it should be remembered that the mechanical behaviour of real three-dimensional parts is not only determined by the bulk material properties, but also by surface roughness and other geometric effects, such as stress-concentrations at corners. This is especially relevant for fatigue behaviour.

Summary

Different mechanical testing of the material is essential to be analysed to be able to identify the quality of the material to prevent premature material failure. The geometry of the material specimen has standard to be followed during the mechanical testing. Mechanical properties of micro samples in mechanical testing is recommended to compare with the standard specimens.

As-built DMLS samples can have anisotropy in mechanical properties since DMLS is layer-by-layer powder technology. Building direction in DMLS samples can show different behaviour due to the tensile direction applied. The machined and un-machined samples mechanical properties of DMLS also can differ due to surface finish.

2.3. Titanium alloys

Titanium is an allotropic element; that exists in more than one crystallographic form. At room temperature, Ti has hexagonal close-packed (*hcp*) crystal structure, which is referred as "alpha" (α) phase (Fig. 2.3.1). When heating the α at a temperature of 888°C it changes to cubic crystal structure, which is referred as beta (β) phase (Donachie, 2000). The lowest temperature at which a 100% β-phase can exist is called the β-transus.

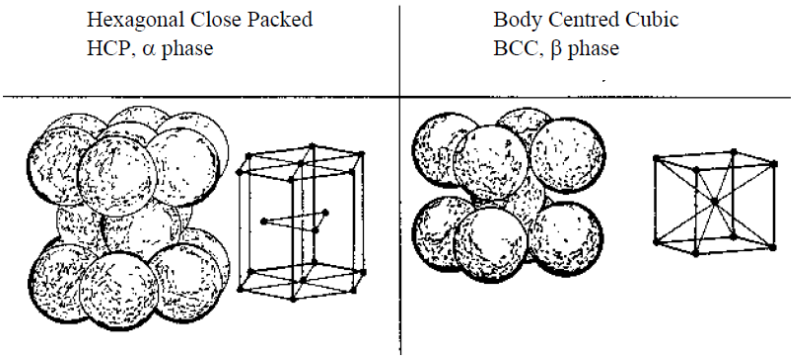

Fig. 2.3.1. Crystal structure of titanium (Pederson, 2002).

Titanium alloys have two main benefits: corrosion resistance and high strength-to-weight ratio. Titanium alloys are strong, non-toxic, biocompatible (non-toxic and not rejected by the body), long-lasting, non-ferromagnetic, osseointegrated (the joining of bone with artificial implant), long range availability, flexibility and elasticity rivals that of human bone (Hanawa, 2010; Clinning, 2012).

2.3.1. Classification of Titanium alloys

Elements to be alloyed with titanium can be categorised as either α-stabiliser, a β-stabiliser or as neutral. The distinction between α or β-stabiliser depends on which phase the element is most soluble in. Alloying elements affect the β-transus temperature. These influences are shown graphically in Fig. 2.3.2.

Important α-stabilising elements are Al (substitutional), O, N, and C (interstitial elements). Al is a widely used as α stabilising element, since it has a large solubility in α phase. Oxygen is a strong interstitial α-stabilising element, which must be accurately controlled in Ti alloys and is used in pure Ti to obtain the desired strength level.

Titanium at low temperature passivates and becomes completely inert to most mineral acids and chlorides. At high temperature titanium oxides quickly and its properties are greatly alert by the absorption of oxygen intestinal from the air. Heating titanium in air results not only in oxidation, but also in dissolution of oxygen and nitrogen in the surface layer of titanium causing

solid solution hardening of the surface. Titanium is chemically active at elevated temperatures and will oxidize in air; resulting in the formation of a scale the presence of the air contaminated layer reduces the fatigue strength and ductility. It is very important for the heat treatment to be done in a controlled atmosphere, using either a vacuum furnace or heat treatment in an inert atmosphere, such as argon for any heat treatment at temperatures above about 427°C (Donachie, 2000).

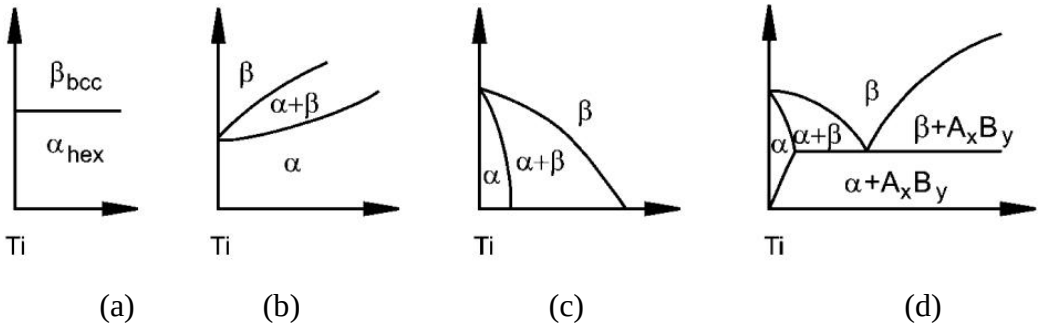

Fig. 2.3.2. The effect of alloying elements on phase composition: neutral elements Zr, Hf and Sn (a), α-stabilising elements Al, O, N, C (b), β-isomorphous elements V, Mo, Nb, Ta (c) and eutectoid elements Fe, Mn, Cr, Ni, Cu, Si, H (d) on titanium (Antonysamy, 2012).

The interstitial-enriched layer is commonly called “alpha case” (Fig. 2.3.3). Oxygen is absorbed at a much greater rate than nitrogen. Alpha case is detrimental because of the brittle nature of the oxygen-enriched alpha structure. The alpha case layer must be removed before the component is put into service; it can be removed by machining and also an antioxidant spray coating can be applied beforehand to clean sheet metal pans in order to minimize oxygen pickup during heat treatment (Donachie, 2000; Abbaschian *et al.*, 2010). It varies in thickness from 0.05 to 0.07 mm in the heat-treated condition to as much as 0.15 to 0.20 mm in the hot-rolled condition (Donachie, 2000).

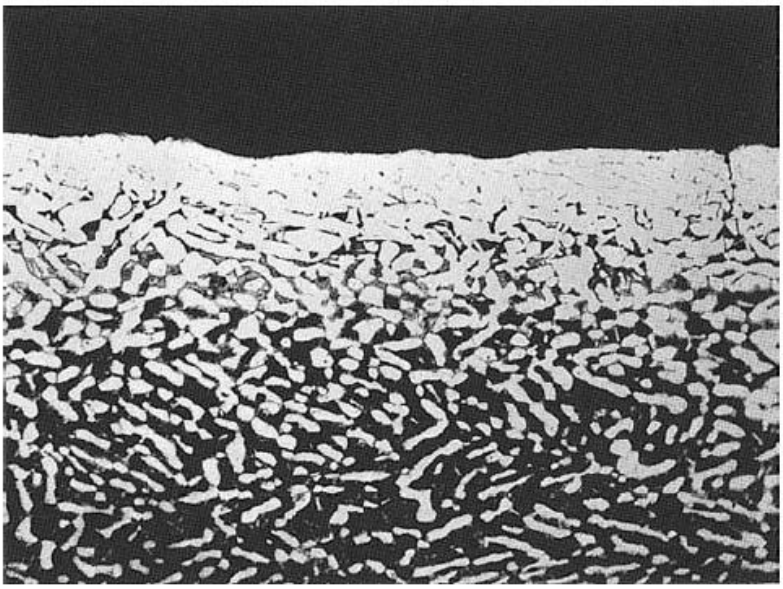

Fig. 2.3.3. Ti6Al4V alpha case. 250× (Donachie, 2000).

Elements that lower the transformation temperature, readily dissolve in and strengthen the β-phase and exhibit low α-phase solubility are known as β-stabilisers. The β-stabiliser can be divided into two categories according to their constitutional behaviour with titanium: 1) isomorphous – completely soluble in solid solution and 2) eutectoid – intermetallic particles are created. Molybdenum and vanadium are the most important beta isomorphous elements, while niobium and tantalum have also found application in some alloys β-eutectoid. Common β eutectoid forming elements are Cr, Fe, and Si, whereas Ni, Cu, Mn, and W, are not greatly used except in specialised alloys. Other β eutectoid forming elements, such as Co, Ag, Au, Pt, Be, Pb, and U, are not generally used. Hydrogen also belongs to these β eutectoid forming elements, but it leads to hydrogen embrittlement. A low eutectoid temperature of 300 °C, in combination with the high diffusivity of hydrogen, can however lead to a special process of microstructure refinement, by hydrogenation and dehydrogenation.

The other class of elements, like Zr, Hf and Sn, behave more-or-less neutrally, as shown in Fig. 2.3.2a. At lower concentrations they decrease the α/β transformation temperature slightly and then again increase the transformation temperature with higher concentrations (Clinning, 2012; Antonysamy, 2012; Donachie, 2000). The typical stabilisers for titanium alloys with the approximate range percentage are shown in Table 2.3.1.

Table 2.3.1. Ranges and effects of some alloying elements used in titanium (Donachie, 2000)

Alloying element	Approximate range, wt %	Effect on Structure
Aluminium	2-7	Alpha stabilizer
Tin	2-6	Alpha stabilizer
Vanadium	2-20	Beta stabilizer
Molybdenum	2-20	Beta stabilizer
Chromium	2-12	Beta stabilizer
Copper	2-6	Beta stabilizer
Zirconium	2-8	Alpha and Beta strengthener
Silicon	0.2-1	Improves creep resistance

Thus, in function of the dominant phase at room temperature, the different Ti alloys are classified in three categories α, α+β and β alloys. Pseudobinary titanium phase diagram (Fig. 2.3.4) shows effects of different alloy elements in Ti alloys. The martensitic start and finish (M_s/M_f) transformation behaviours are shown also in the Fig. 2.3.4.

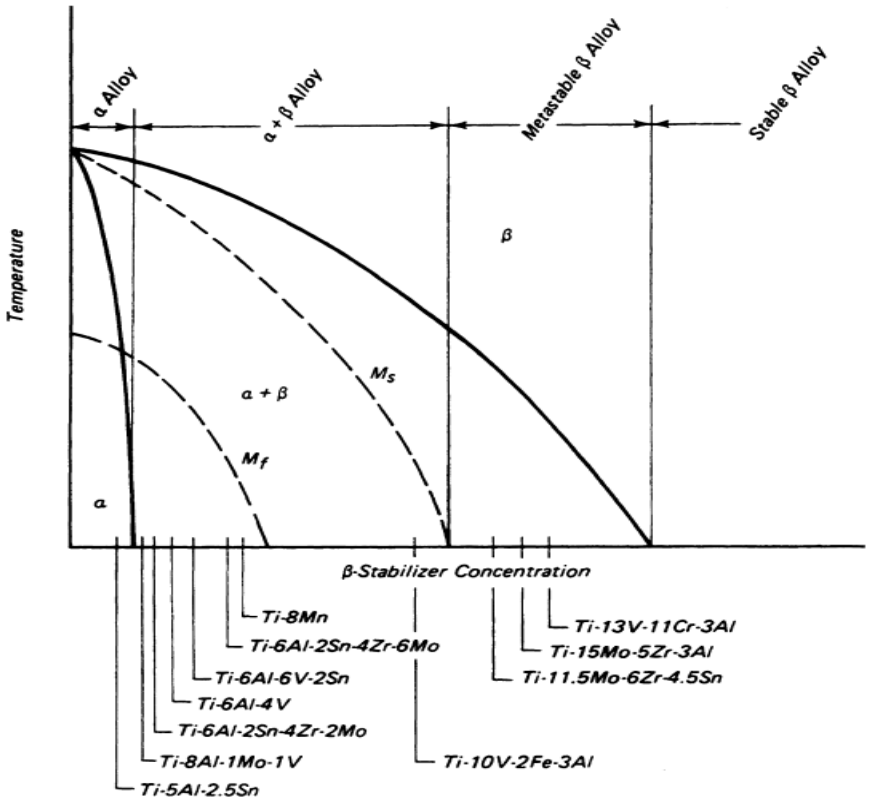

Fig. 2.3.4. A pseudo-binary titanium phase diagram (Donachie, 2000).

Al reduces density, stabilises and strengthens while V provides a greater amount of the more ductile phase for hot–working Ti alloys.

In α-alloys, Al is the main alloying element apart from Zr and Sn; the equivalence effect is expressed as

$$[Al]_{eq} = [Al] + 0{,}33\,[Sn] + 0{,}17\,[Zr] + 10\,[O + C + 2N]$$

If the Al equivalence exceeds 9 wt%, Ti_3X intermetalic particles may be formed which leads to embrittlement. 5-6% Al can lead to a finely dispersed, ordered phase (α_2), which is coherent to lattice deleterious ductility (Bhadeshia, 2005).

Molybdenum and vanadium have the largest influence on stability and are common β-alloying elements. In the beta stabilizer the Mo equivalence is important in terms of comparison of stabilizing effect of different element.

$$[Mo]_{eq} = [Mo] + 0{,}67\,[V] + 0{,}44\,[W] + 0{,}28\,[Nb] + 0{,}22\,[Ta] + 2{,}9\,[Fe] + 1{,}6\,[Cr] + 1{,}25\,[Ni] + 1{,}7\,[Mn] + 1{,}7\,[Co] - 1{,}0\,[Al]$$

From this equation, for example, it can be seen that β-stabilizer Fe is stronger than Mo in 3 times and in 4 times than V.

In function of the dominant phase at room temperature, the different Ti alloys are classified as follows:

- α-alloys (for example, Ti8Al1V1Mo) that cannot be heat treated to develop higher mechanical properties because they are single-phase alloys with almost mono-phase structure. They are quite stable until 650°C and resist against corrosion up to 1100°C.
- α-β-alloys (for example, Ti6Al4V, Ti6Al2Sn2Zr2Cr2Mo) are actually the most widely used titanium alloys. They are structurally quite stable up to 450°C and can be modified by thermal treatments. With appropriate heat treatment they have an excellent combination of strength and ductility; they also can be cold deformed.
- β-alloys (for example, Ti10V2Fe3Al, Ti15Mo) as their names indicate are in majority composed of β-phase. They are less stable than the two previous categories of alloys but they are industrially interesting because they are easier to form (Vanderhasten, 2007).

2.3.2. Heat treatment of α-β Ti alloys

Heat treatment is a controlled process that alters the microstructure of the material to enhance certain properties. Usually, heat treatment is performed to:

- Reduce residual stresses (*stress relieving*);
- Create the optimum combination of mechanical properties (*annealing*);
- Increase yield strength (*solution treating and aging*);
- Optimize properties such as fracture toughness, fatigue strength and high temperature creep strength.

Stress relieving is one of the most common heat treatments performed on titanium and its alloys. This treatment decreases undesirable residual stresses without adversely affecting the strength or ductility of the component. Removal of residual stress helps to maintain the shape stability. During stress relieve it is critical that the cooling rate is uniform, especially between 480 to 315°C. Quenching should not be used to accelerate the cooling process as it can induce residual stress. The recommended temperature and duration to stress relieve Ti6Al4V is 480 to 650 °C for 1 to 4 hours (Donachie, 2000).

The annealing process is performed to increase ductility, fracture toughness, creep resistance, thermal stability and dimensional stability. It is important to keep the intended use of the component in mind when annealing is done, as some properties are obtained at the expense of others. Some of the different annealing treatments include: mill annealing, duplex annealing, recrystallization annealing and beta annealing. Uniform cooling to 315°C is recommended to reduce the risk of distortion (Donachie, 2000).

Mill annealing is a general-purpose treatment given to all mill products. It may leave traces of cold or warm working in the microstructures of heavily worked products, particularly sheet.

Ti6Al4V is commonly used in the mill annealed condition. Annealing at temperature between 710 and 790°C during 1 to 4 hr followed by air cooling (Donachie, 2000; Vanderhasten, 2007).

Duplex annealing influences the microstructure and the distribution of phases to improve creep resistance or fracture toughness. Most of the time, this is realized by the introduction of acicular α. (First annealing at 900°C during 1 hr, air cooling and then annealing at 788°C during 0.25 hr and once again air cooling) (Vanderhasten, 2007).

Recrystallization annealing and β annealing are used to improve fracture toughness. In recrystallization annealing, the alloy is heated into the upper end of the α-β range, held for a time, and then cooled very slowly. In recent years, recrystallization annealing has replaced β annealing for fracture critical airframe components. To prevent excessive grain growth, the temperature for β annealing should be only slightly higher (30 – 50°C above) than the β transus. Annealing times are dependent on section thickness and should be sufficient for complete transformation. Time at temperature after transformation should be held to a minimum to control β grain growth. Larger sections should be fan cooled or water quenched to prevent the formation of α phase at the β grain boundaries (Donachie, 2000; Vanderhasten, 2007; Simonelli, 2014).

To achieve maximum strength levels, solution treating is done followed by aging. Solution treating is usually performed at a temperature slightly above or below the β transus temperature. The selection of an appropriate temperature for solution-treating depends on the type of alloy and desired properties to attain. For α/β alloys the selection of a solution treatment temperature is based on the combination of mechanical properties desired. The optimum combination of creep – and fatigue strength is at a solution temperature very close to the β transus but still just below. Only 10 to 15% untransformed α phase should remain (Donachie, 2000).

Summary of heat treatments for α-β titanium alloys is shown in Table 2.3.2.

Table 2.3.2. Summary of heat treatments for α-β titanium alloys (Donachie, 2000)

Heat treatment designation	Heat treatment cycle	Microstructure	Effect
Duplex anneal	Solution treat at 50–75°C below T_β, air cool and age for 2–8 h at 540–675°C	Primary α, plus Widmanstätten α – β regions	To improve creep resistance and fracture toughness
Solution treat and age	Solution treat at ~40°C below T_β, water quench and age for 2–8 h at 535–675°C	Primary α, plus tempered α′ or a β – α mixture	It's for strengthening
Beta anneal	Solution treat at ~15°C above T_β, air cool and stabilize at 650–760°C for 2 h	Widmanstätten α – β colony microstructure	To prevent excessive grain growth, the temperature for beta annealing should be only slightly higher than the beta transus.
Beta quench	Solution treat at ~15°C above T_β, water quench and temper at 650–760°C for 2 h	Tempered α′	
Recrystallization anneal	925°C for 4 h, cool at 50°C/h to 760°C, air cool	Equiaxed α with β at grain–boundary triple points	Recrystallization annealing to improve toughness.
Mill anneal	α – β hot work plus anneal at 705°C for 30 min to several hours and air cool	Incompletely recrystallized α with a small volume fraction of small β particles	Annealing is a general-purpose treatment given to all mill products.

Primary alpha is alpha phase that remains untransformed as opposed to alpha formed by transformation from the beta phase. The terms "acicular alpha" and "Widmanstatten" are generally interchangeable. Both are used to describe a transformation product brought about through nucleation and growth. However, acicular, by definition, refers primarily to grains with a fine, needle-like appearance, whereas the Widmanstatten basket weave pattern can exist as fine acicular or coarse plate-like grains (RMI Titanium Company, 2015). Plate-like alpha structures are characterized by relatively wide elongated grains. They are developed in the alpha and alpha-beta alloys as a result of slow cooling from the beta field, or from a temperature high in the alpha-beta field (RMI Titanium Company, 2015).

For very slow cooling rates high up in the region or above the β-transus temperature (995±20°C), the β phase mainly transforms into globular type of α. When increasing the cooling rate enhances α nucleation rate in the β grain boundaries thereby enhancing the formation and

growth of the plates into the prior β grains. The length and width of α platelets are determined by the cooling rate an increased cooling rate enhances the nucleation rate and slows the growth process. At a certain point the cooling rate is fast enough for nucleation of α to occur inside the prior β grains as well leading to the formation of basket-weave structure. If quenched, the β phase will fully or partly transform into a martensitic type α. This martensite exists in two different forms: α' and α'' structure. The type and amount of α' and α'' formed upon quenching depends on the chemical composition of the β phase existing at temperature prior to quenching.

The β phase experience large composition variation which is reflected in significant mechanical property changes. Vanadium enrichment of the β phase occurs in proportion to the reduction of the volume fraction of β phase. At vanadium contents ≥15wt%, the β phase is stabilised and retains its bcc crystal structure upon quenching. When β phase with 10 ± 2 wt% vanadium is quenched from 750°C to 900°C, it partly retains the bcc structure and partly transforms into soft orthorhombic α'' martensite. The higher the solution heat treatment the smaller is the vanadium enrichment in the β phase, leading to transformation into hexagonal α upon quenching from 900°C. Fig. 2.3.5 illustrates the principle transformations upon quenching.

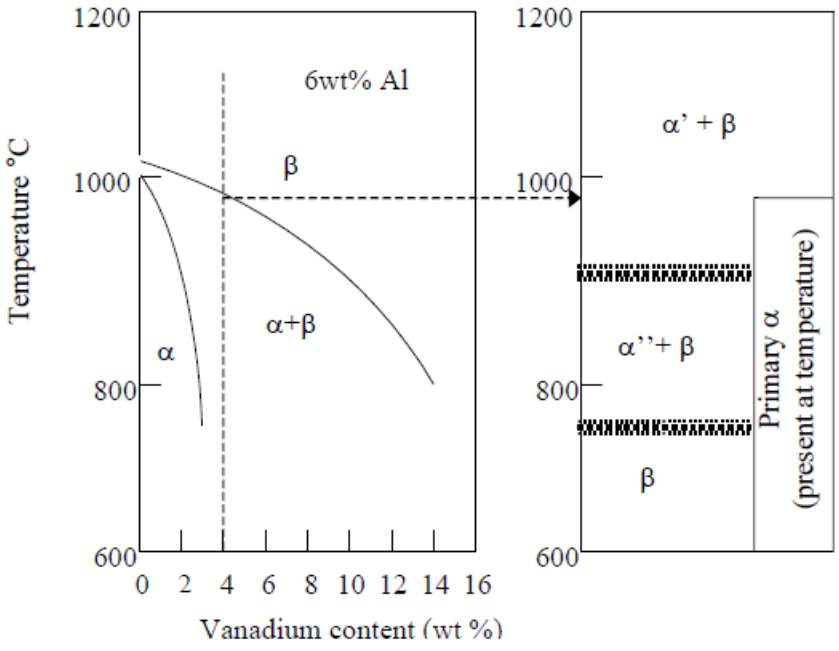

Fig. 2.3.5. A schematic illustration of microstructure occurring in Ti6Al4V after quenching from different temperatures (Pederson, 2002).

In titanium α-β alloys apart from alpha and beta phase there are other phase caused by the influence of thermo mechanical treatments:

- α’ (Hexagonal close packed martensite). When Ti6Al4V alloy is quenched from above 900°C, a part of the β-phase will transform in α’. Alpha prime has an acicular or fine lamellar microstructure. Alpha-prime α’, sometimes referred to as martensitic alpha, is a non-equilibrium supersaturated α structure formed by diffusionless transformation of the beta phase (RMI Titanium Company, 2015).
- α” (Orthorhombic martensite) α” is the result of a quenching of the β-phase from 750- 900°C. This martensite is softer than α’ (Vanderhasten, 2007).

Summary

Ti is allotropic element, other elements alloyed with titanium can create α, α+β and β alloys. There are different heat treatments that can be applied according to the desired mechanical properties and microstructure to be obtained for α-β titanium alloys: stress-relieving, quenching, annealing or their combination.

2.4. Ti6Al4V alloy

2.4.1. Microstructure and mechanical properties of wrought Ti6Al4V alloy

Ti6Al4V is one of the most widely used titanium alloys. Ti6Al4V is an α-β alloy with 6% aluminium stabilizing the alpha phase and 4wt% vanadium stabilizing the β phase. Ti6Al4V has an excellent combination of strength and toughness along with excellent corrosion resistance. Ti6Al4V as other titanium alloys has a high affinity for gases including oxygen, nitrogen, and hydrogen. When Ti6Al4V is heated in air, oxygen absorption results in the formation of an extremely hard, brittle oxygen-stabilized α-case layer (Donachie, 2000).

Depending on cooling rate and the prior heat treatment, the micro constituents and microstructure are divided into several types. There are different cooling methods that are used for Ti6Al4V alloys to obtain different microstructures: furnace cooling, air cooling, quenching from β and α+β phase fields, tempering of titanium martensite and decomposition of metastable phase.

As Smith (1981) indicated, furnace cooling from the β phase field (β annealed, 1066°C) causes transformation from β to α microstructure containing lamellar structure of similar crystal orientation. Furnace cooling from the α+β phase field (mill annealed, 954°C) produces microstructure approaching equilibrium equiaxed primary α phase surrounded with retained β phase. Microstructure is shown in Fig. 2.4.1. Air cooling from the β phase (1066°C) field produces fine acicular α, which is transformed from the β phase by nucleation and growth. Air cooling from the α+β phase (954°C) field provides equiaxed primary α phase in a matrix of transformed β phase (acicular) (Smith, 1981). The term "equiaxed" refers to a polygonal structure in which individual grains have approximately equal dimensions in all directions (RMI Titanium Company, 2015).

Quenching from β phase field the alloy experiences martensitic transformation passing through M_s point. Martensite α' consists of individual platelets which are heavily twinned and have *hcp* crystal structure.

When quenching is below β transus but above M_s temperature, microstructure consists of primary α phase embedded in transformed β phase (α' martensite).

There is also quenching below M_s temperature, microstructure consists of primary α phase and small amount of retained or untransformed β (Fig. 2.4.2).

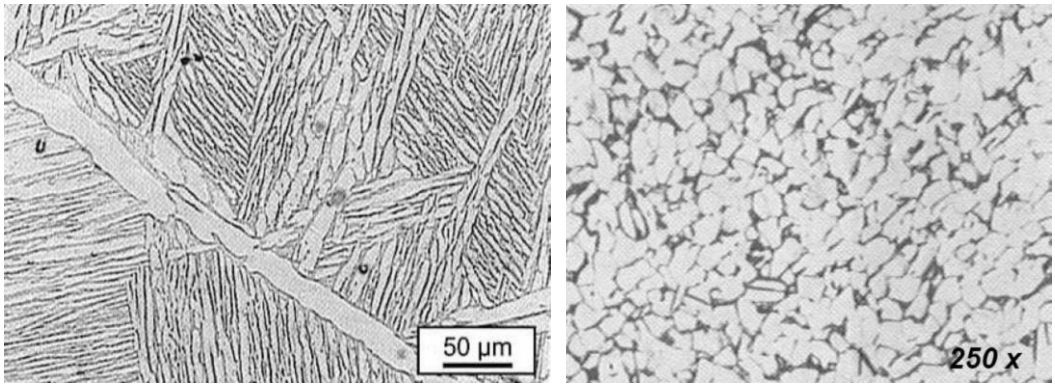

(a) (b)

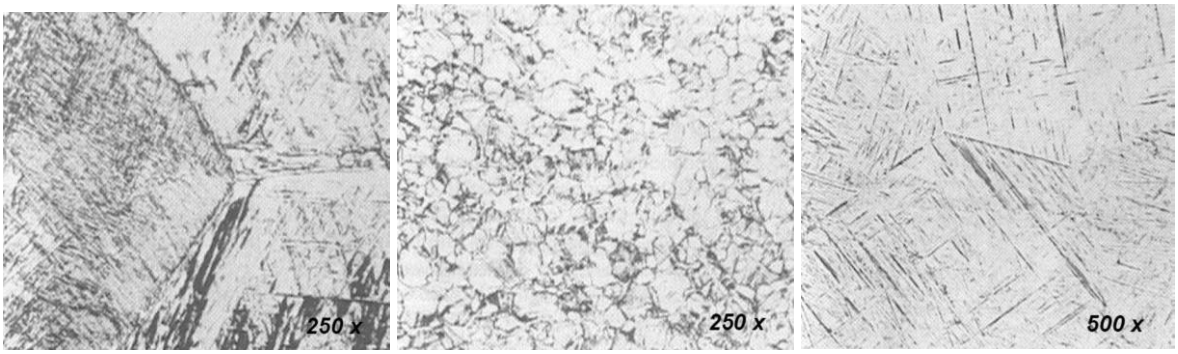

(c) (d) (e)

Fig. 2.4.1. Ti6Al4V alloy annealed from β phase field, showing transformed β phase or lamellar (basket weaves) microstructure (a) and annealed from α+β phase, showing equiaxed α grains (light) with inter-granular retained beta (dark) (b); air-cooled from β phase field giving transformed β phase (acicular) (c) and air-cooled from α+β phase field, showing primary α grains in a matrix of transformed β (acicular) (d); solution-heat-treated at 1066 °C /30 min and water quenched (e) (Smith, 1981).

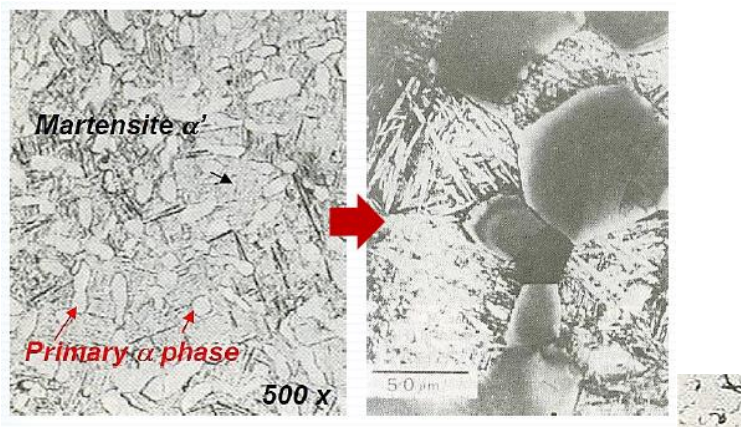

(a) (b)

Fig. 2.4.2. Ti6Al4V alloy solution treated at 954°C and then water quenched (a) and solution treated at 843°C and then water quenched (b) (Smith, 1981).

Fig. 2.4.3 shows some microstructures formed from Ti6Al4V alloy as a function of solution temperature and cooling rate. Different cooling methods are used after heat treatment of Ti6Al4V: water or air quenching, and furnace cooling. Water quenching cooling method is faster compared to air quenched and furnace cooling.

The cooling rates influence the microstructures in Ti6Al4V. Types of microstructure that can be found in Ti6Al4V alloy are:

1. Lamellar structures. Starting from above the β transus, the cooling rate will determine the size of the lamellae. Slow cooling (15 K/min) in the furnace will lead to the production of coarse plates of α-phase starting from the β-grain boundaries and quenching produces a needle like *hcp* martensite (α'). An aging treatment is used to strengthen the alloy (Fig. 2.4.4).
2. Equiaxed microstructures need extensive mechanical working (>75%) in the (α+β)-phases domain. During this process, α lamella are broken into equiaxed α grains. The process for creating an equiaxed structure is very similar to that shown in Fig. 2.4.5 for creating bi-modal structures, the only difference being the temperature of the recrystallisation step which, for an equiaxed microstructure, is lower to ensure that no β grains are formed. A subsequent annealing at about 700°C produces the so-called "mill-annealed" microstructure. In terms of mechanical properties, yield strength, ductility and high-cycle fatigue resistance depend on the slip length. The size of the equiaxed α grains determines the mechanical properties of Ti alloys. Another possibility to obtain equiaxed grains is a recrystallization of the deformed material in the α+β-phase field, at 925°C during 4 h, followed by slow cooling. In this second case, a more reproducible microstructure is obtained but, the resulting α grains are coarse (grain size about 15-20 μm instead of 8-10 μm). An equiaxed structure primarily consists of globular α grains, but does have some retained β phase (around 8%) present at either the grain boundaries or "triple points"

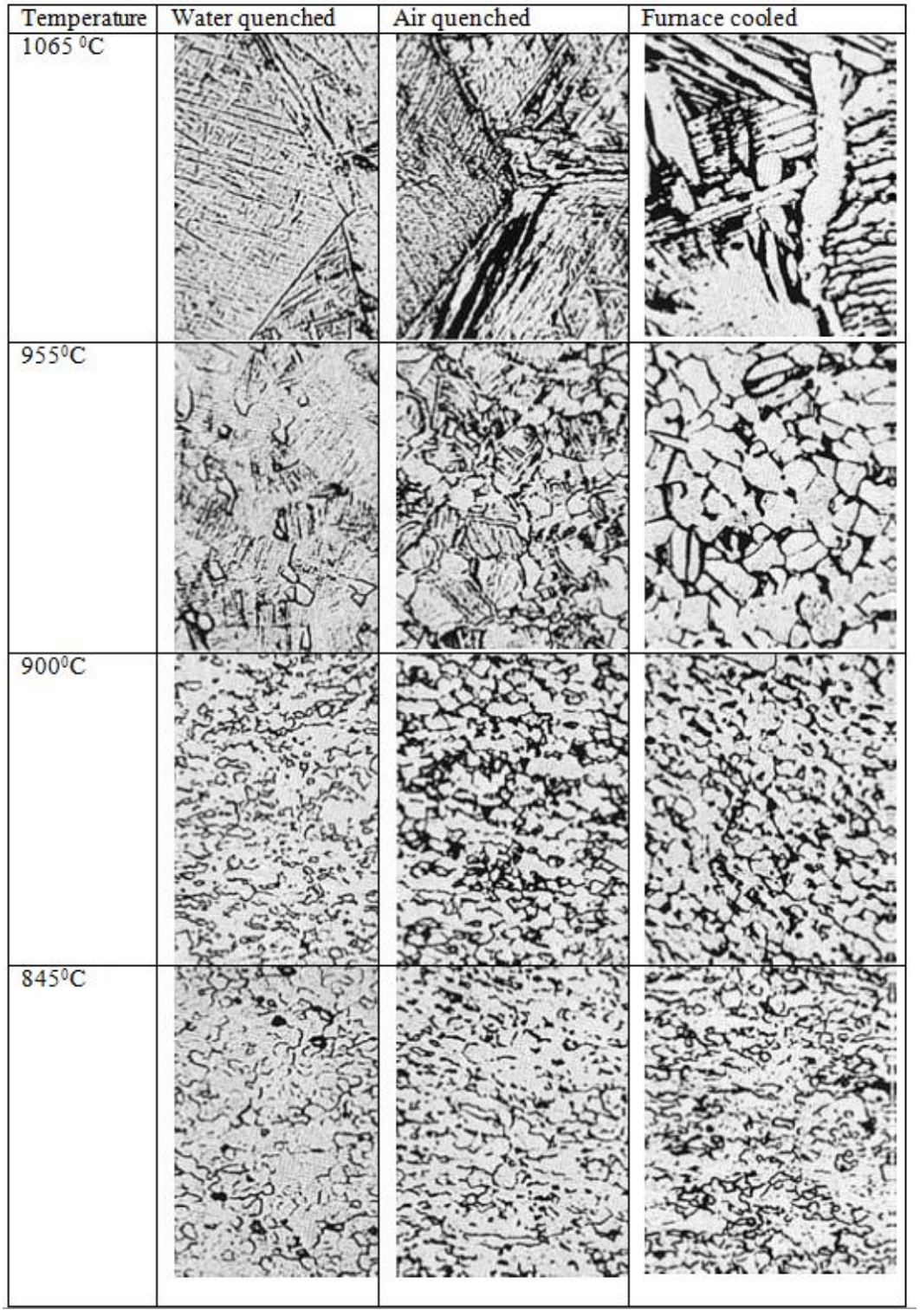

Fig. 2.4.3. Some microstructures formed from Ti6Al4V alloy as a function of solution temperature and cooling rate (Donachie, 2000).

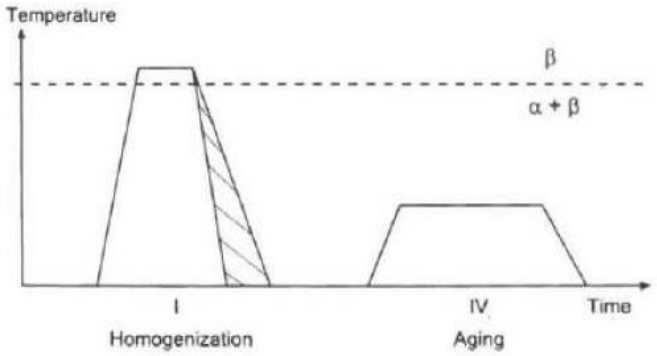

Fig. 2.4.4. Processing route for creating a fully lamellar microstructure (Clinning, 2012).

3. Bimodal microstructure consists of isolated primary α grains in a transformed β matrix. This type of microstructure is obtained by quenching from the α+β-phase field (approximately between 750 and 1000°C, Fig. 2.4.5). Bimodal process begins with a homogenisation step in the β phase, which upon cooling creates a lamellar structure. It is then deformed at an elevated temperature (but below that temperature creating new β phase) followed by a recrystallisation process at a temperature in the α+β region at which the structure comprises of equiaxed α grains as a result of the recrystallisation, and a portion of β grains in accordance with the temperature. Upon cooling, the equiaxed α is retained and the β decomposes into a lamellar structure.

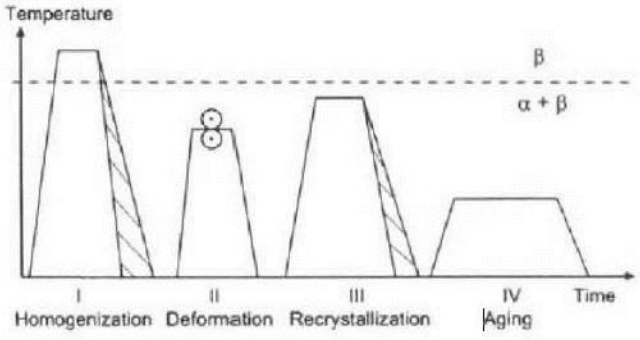

Fig. 2.4.5. Processing route for creating a bimodal microstructure of Ti6Al4V (Clinning, 2012).

As previously mentioned, the microstructure is influenced by heat treatment and the cooling rate fully lamellar microstructure can be obtained by the heating of the sample above β-transus followed by cooling.

When the alloys are cooled below the β transus, α phase first nucleates from the grain boundary and then intra granularly as plates/laths. Because of the close atomic matching along this common plane, the alpha phase thickens relatively slowly perpendicular to this plane but grows faster along the plane and plates are developed. It is observed that the darker regions are the β

phase left between the α plates that have formed (Fig. 2.4.6). It shows that the microstructure consists of parallel plates of α delineated by the β phase between them. Where α-plates formed parallel to one specific plane of β, meet α plates formed on another plane, a high-angle grain boundary exists between the α crystals and etches to reveal a line separating them (Kar, 2005; Donachie, 2000).

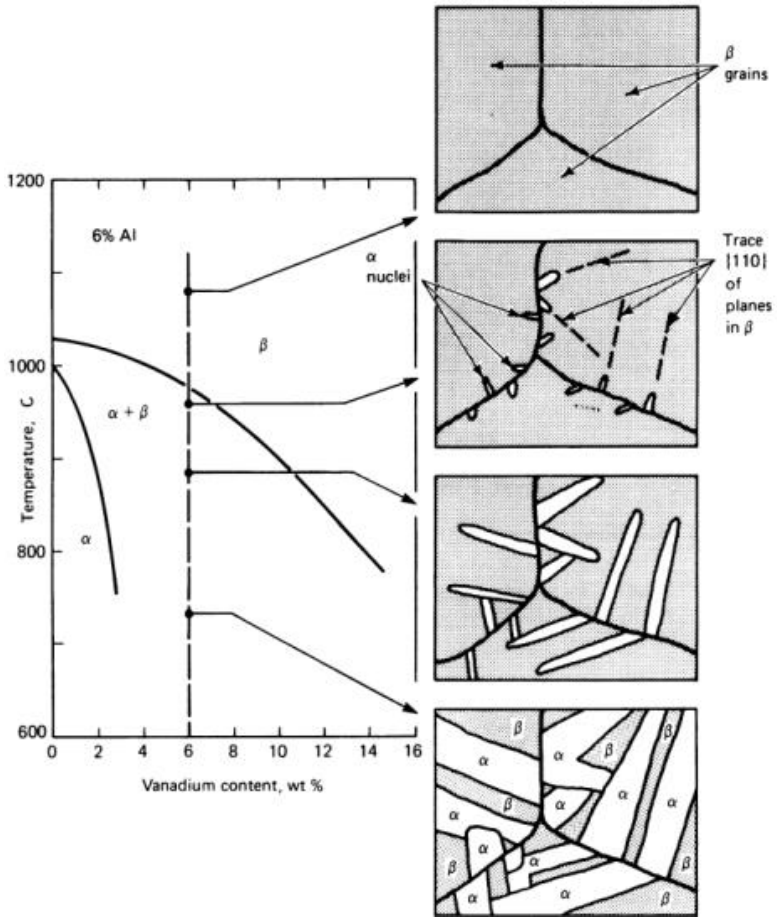

Fig. 2.4.6. The microstructure of an alpha-beta titanium alloys after slow cooling from above the beta transus is shown. The white plates are α, and the dark regions between them are β (Donachie, 2000).

The study according to the research done by Murr *et al.* (2009) illustrates two extremes for wrought Ti6Al4V. Sample A was a section from a billet forged at 1040°C (above the β-transus) to produce a coarse plate-like α with some intergranular β. Sample B was cut from a billet forged and solution treated 1 h at 950°C, air cooled and then annealed 2 h at 700°C. This produced an equiaxed, α/β microstructure very different from the large acicular α-plates for the sample A.

Mechanical properties of titanium samples are influenced by the microstructure. Fig. 2.4.8 shows the effect of heating Ti6Al4V bar to four different temperatures and cooling at three

different rates from each temperature. The tensile properties for each annealing treatment are listed in Table 2.4.1 (RMI Titanium Company, 2015).

Sample A Sample B

Fig. 2.4.7. Optical metallographic views of commercial wrought Ti6Al4V alloys: a primarily acicular α-plate microstructure (a) and equiaxed α/β mixture and coarse, acicular alpha (b) (Murr *et al.*, 2009).

Data from Table 2.4.1 shows that (1) tensile properties didn't change after aging for the samples with furnace cooling; (2) only a slight response occurs on air cooling; and (3) the greatest response is experienced with a water quench from the solution temperature. Good response to aging occurs on water quenching from the beta field; however, ductility values are quite low. The best combination of tensile properties can be achieved by solution treating at temperatures in the α-β field (RMI Titanium Company, 2015).

Kar (2005) indicated the following microstructural parameters which affect the mechanical properties of the Ti6Al4V alloy: β-grain size, α-colony size, thickness of grain boundary α and lamellar α. Results showed that while prior beta grain size has little or no influence on the yield strength, it has a strong influence on ductility. Ductility depends on β grains, the length of β grain boundary limits the maximum slip in the boundary layer.

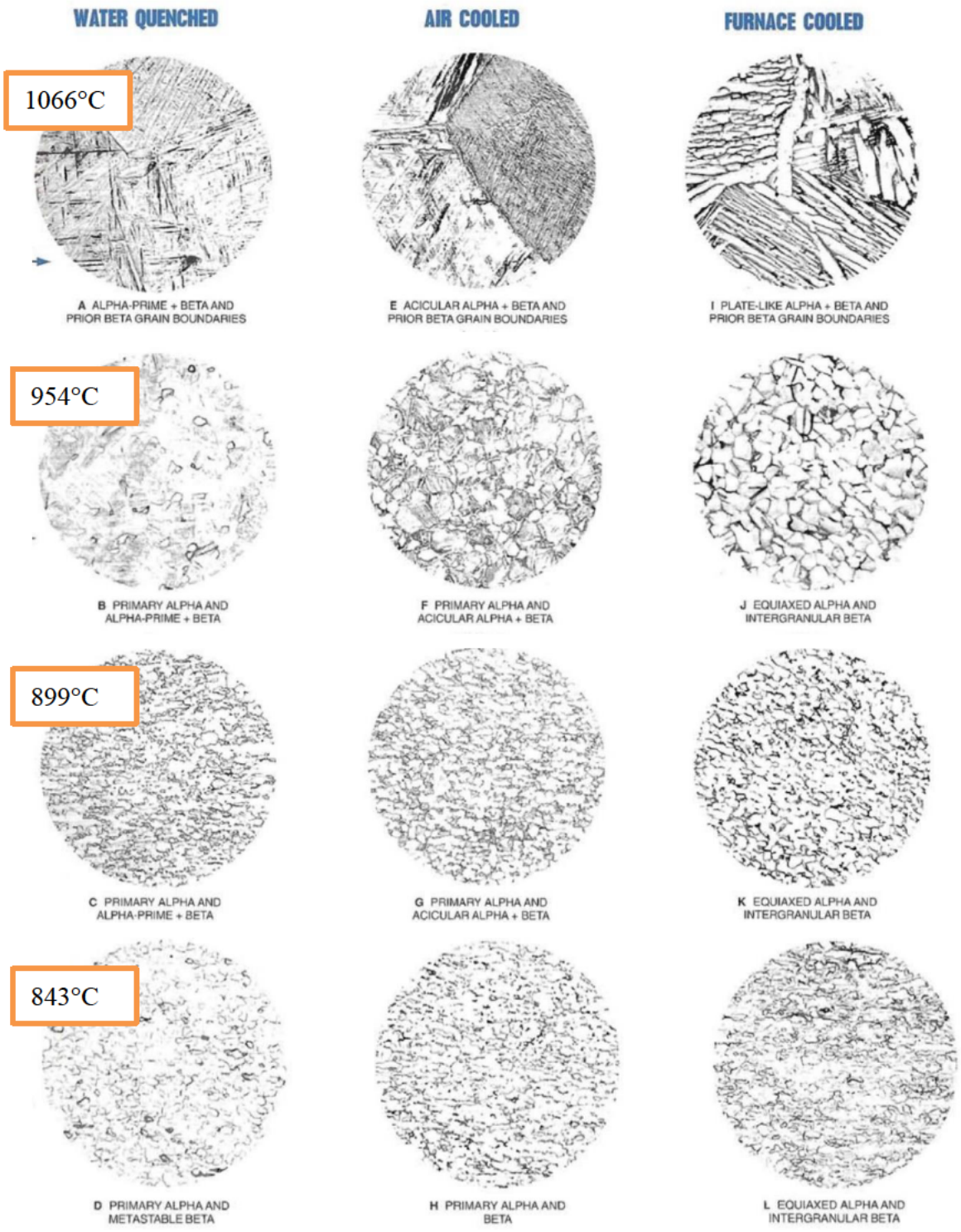

Fig. 2.4.8. RMI Ti6Al4V 5/8" dia. bar microstructures resulting from various cooling rates from several temperatures (RMI Titanium Company, 2015).

Table 2.4.1. Mechanical properties of Ti6Al4V 5/8"·dia. bar following various heat treatments (RMI Titanium Company, 2015)

Type	Treatment, °C	UTS, MPa	0.2% YS, MPa	Elongation, %	RA, %
A	1066°C /WQ	1108	953	7.7	19:2
	After aging	1170	1057	8.5	19.2
B	954°C /WQ	1119	953	17.0	60:2
	After aging	1183	1069	16.5	56.4
C	899°C /WQ	1117	924	15.2	53.9
	After aging	1117	1013	15.3	47.5
D	843°C /WQ	1009	772	20.0	54.7
	After aging	1077	977	16.5	48.8
E	1066°C /AC	1060	945	7.0	10.3
	After aging	1060	940	9.8	16.0
F	954°C /AC	995	846	17.8	54.1
	After aging	1020	896	16.1	45.7
G	899°C /AC	1002	869	17.5	54.7
	After aging	1029	938	17.3	50.2
H	843°C /AC	1020	878	17.8	477
	After aging	1034	931	16.8	46.9
I	1066°C /FC	1041	938	10.5	15.6
	After aging	1011	938	9.5	15.4
J	954°C /FC	940	836	18.8	46.0
	After aging	967	883	18.2	49.1
K	899°C /FC	963	855	16.5'	43.3
	After aging	963	876	16.8	48.3
L	843°C /FC	997	924	17.3	48.9
	After aging	1062	954	17.0	49.6

Aging in all cases: 538°C/4 hours, air cool

Dabrowski (2011) obtained, that martensitic transformation occurred in the Ti6Al4V alloy cooled from the β phase range (1020°C) at 23.1°C/s. After cooling at 7.3°C/s both dispersed α and α' martensite were present in the alloy, whereas during cooling at 2.5°C/s or slower only diffusional transformation took place resulting in entirely α structure. The α phase morphology was strongly affected by the cooling rate and appeared as Widmannstatten lamellas (7.3-0.065°C/s) or equiaxed grains (0.015-0.012°C/s); decreased cooling rate increased the lamella/grain size (Fig. 2.4.9).

Simonelli (2014) indicated that the length of the prior β grain has influence on mechanical properties since the β grain is known as the weakest point in the microstructure, where crack can be easily initiated. Fully lamellar microstructures with long prior β grain boundaries exhibit, in

general, poor ductility and resistance to short crack propagation. Long prior β grain boundaries can retard the spread of large cracks as they induce crack deflection similarly to the crack propagation behaviour for large α colonies. It has been shown that large cracks are deflected along the grain boundaries and thus crack path of microstructure with long grain boundary are generally tortuous and thus crack propagation in these microstructures is associated with more energy expense (Simonelli, 2014).

The colony size determines the effective slip length, and thus an increase in cooling rate will effectively reduce the slip length. This will in turn cause the yield stress to increase (Kar, 2005; Antonysamy, 2012).

The α colony size also influences the mechanical properties of Ti6Al4V because this size is limited by the size of the prior β grain. It was demonstrated by Sieniawski *et al.* (2013) when the correlation of higher strengths with faster cooling rates was found; the faster cooling rates result in a finer transformed structure leading to higher strength. Fig. 2.4.10 shows that as the cooling rate increases, the ductility increases too, but when it reaches maximum, the ductility decreases. The influence is believed to be from the reduction of the slip length by increasing the cooling rate. As the cooling rate increases beyond this reduces the pile-up length and decreases the stress concentrations, thereby delaying crack nucleation which results in higher ductility. After reaching maximum the ductility curve declines. Such behaviour was reported and recognised to the change of fracture mode from ductile trans-crystalline for low cooling rates to ductile inter-crystalline fracture along continuous α phase layers at primary β grain boundaries (Sieniawski *et al.*, 2013).

The size of the colonies of α lamellae having the same crystallographic orientation have significant influence on the mechanical properties of the alloy as it is a measure of effective slip length. However transition to the ‘basket weave’ type of microstructure makes the determination of colonies size even more difficult. Because of that the thickness of α-lamellae was also taken into account as the quantitative parameter illustrating the effect of microstructure refinement on mechanical properties (Sieniawski *et al.*, 2013).

Thus, different microstructures have different mechanical properties. Temperature gradients during processing influences microstructure and properties of Ti6Al4V alloy.

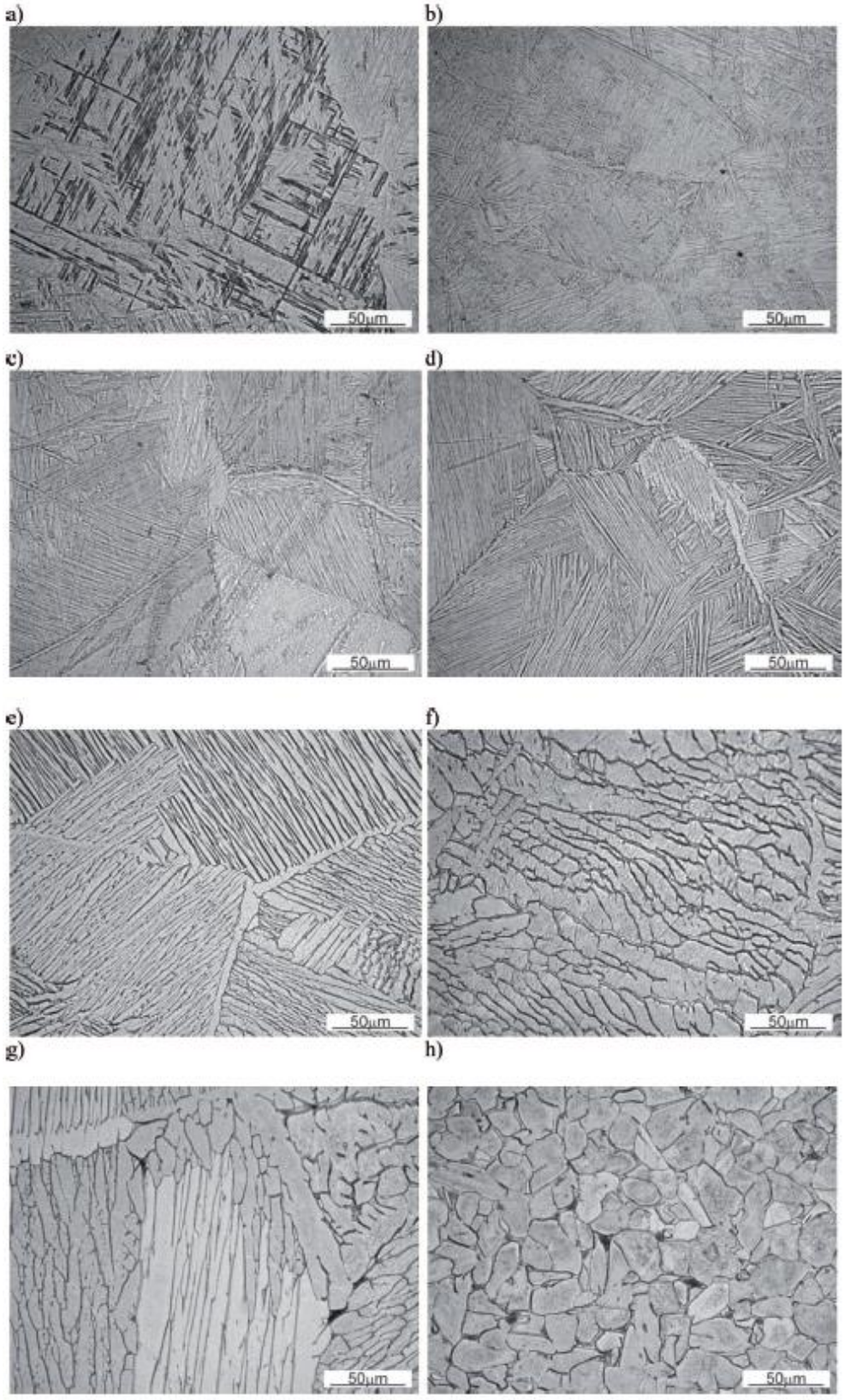

Fig. 2.4.9. Ti6Al4V alloy cooled from 1020°C at: 23.1°C/s (a), 7.3°C/s (b), 2.5°C/s (c), 0.94°C/s (d), 0.065°C/s (e), 0.030°C/s (f), 0.015°C/s (g) and 0.012°C/s (h) (Dabrowsky, 2011).

Fig. 2.4.10. The effect of cooling rate from β-phase range on elongation and yield stress (Sieniawski *et al.*, 2013).

2.4.2. Microstructure and mechanical properties of DMLS Ti6Al4V alloy

Microstructure

Shunmugavel *et al.* (2015) compared to DMLS and wrought Ti6Al4V Ti6Al4V cylindrical bars. The wrought Ti6Al4V consisted of a fully equiaxed microstructure (Fig. 4.2.11a). DMLS material showed a martensite microstructure due to rapid heating and rapid cooling (Fig. 2.4.11b). The difference in microstructure caused the yield strength and ultimate strength to be higher in DMLS material compared to the wrought. There was higher ductility in wrought Ti6Al4V compared to the DMLS material. It was found that DMLS Ti6Al4V have higher yield strength and ultimate tensile strength compared to its wrought counterparts. This difference in their material behaviour can be explained in terms of the difference in microstructure as titanium alloy's mechanical properties are strongly influenced by its microstructure (Shunmugavel *et al.*, 2015).

The as-built microstructure of the material produced by DMLS has a very fine, acicular morphology. DMLS Ti6Al4V microstructure is interpreted as martensitic with the typical needles visible on the etched metallographic section (Fig. 2.4.12). DMLS microstructure is a result of rapid solidification and its features correlate with heat conducting direction (Facchini *et al.*, 2010; Yadroitsev *et al*, 2014).

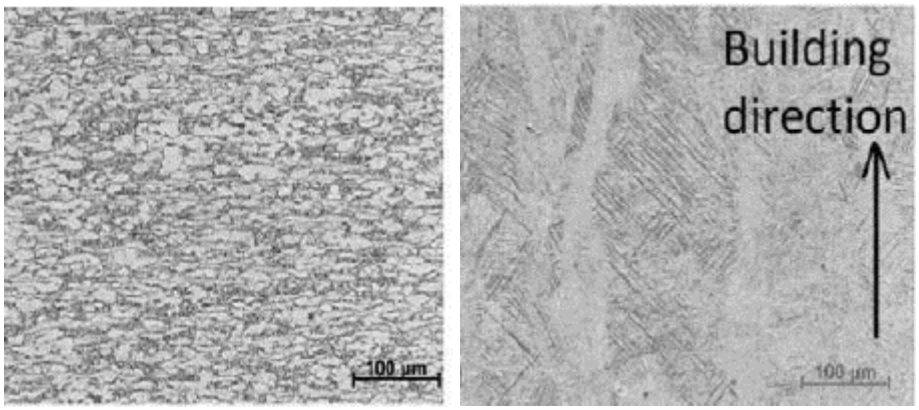

(a) (b)

Fig. 2.4.11. Microstructure of wrought and as-built DMLS (Shunmugavel *et al.*, 2015).

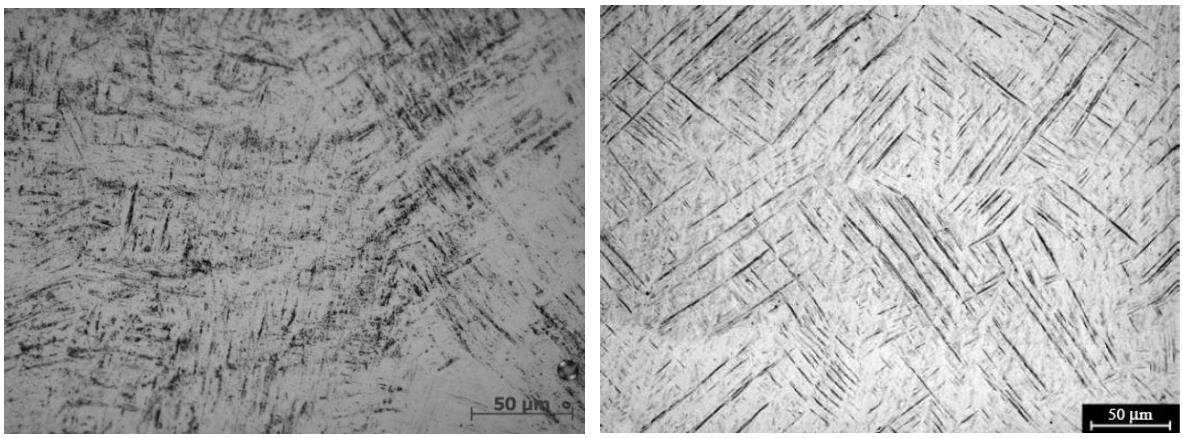

(a) (b)

Fig. 2.4.12. The microstructure of Ti6Al4V as-built DMLS parts (a) (Yadroitsev *et al.*, 2014) and (b) (Facchini *et al.*, 2010).

Vrancken *et al.* (2012) studied DMLS Ti6Al4V ELI (Grade 23 Ti alloy). A laser with continuous laser mode and a spot size of 52 µm was used. Samples were produced with a scanning speed V=1.6 m/s, a laser power P of 250 W, h=60 µm hatch spacing and a 30 µm layer thickness Layers were scanned by a zigzag pattern, which was rotated 90° between each layer. Fig. 2.4.13 indicates that a fully acicular α' martensitic microstructure was developed during the DMLS process. At a smaller magnification, the side view reveals long, columnar grains which are oriented more or less in the building direction. These are identified as prior β grains which grow epitaxial during the process, up to several millimetres in length.

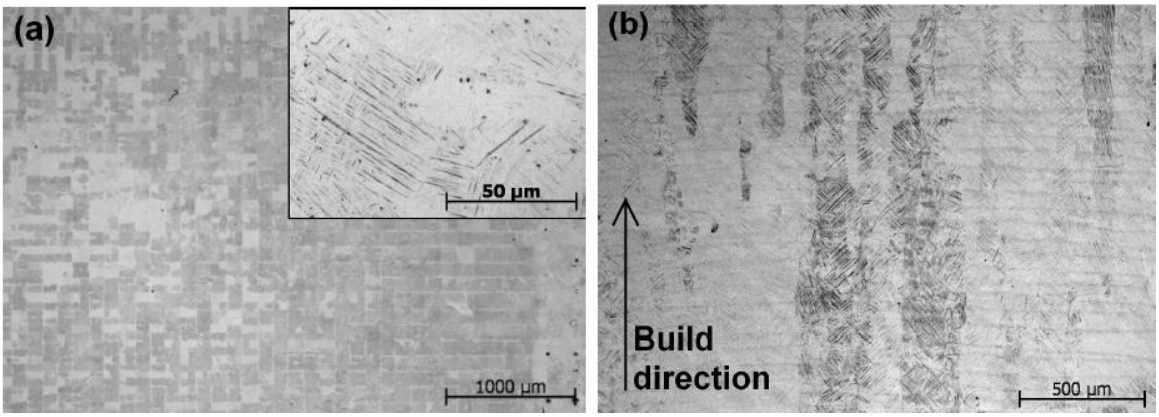

Fig. 2.4. 13. The microstructure untreated Ti6Al4V produced by DMLS in (a) and (b) is fully martensitic. (Vrancken *et al.*, 2012).

Facchini *et al.* (2010) showed by the XRD analysis the presence of *hcp* phase only in as-built Ti6Al4V (Fig. 2.4.14). The *hcp* pattern can be attributed to both the α-phase and the α' martensite, as they have the same crystalline structure and very similar lattice parameters.

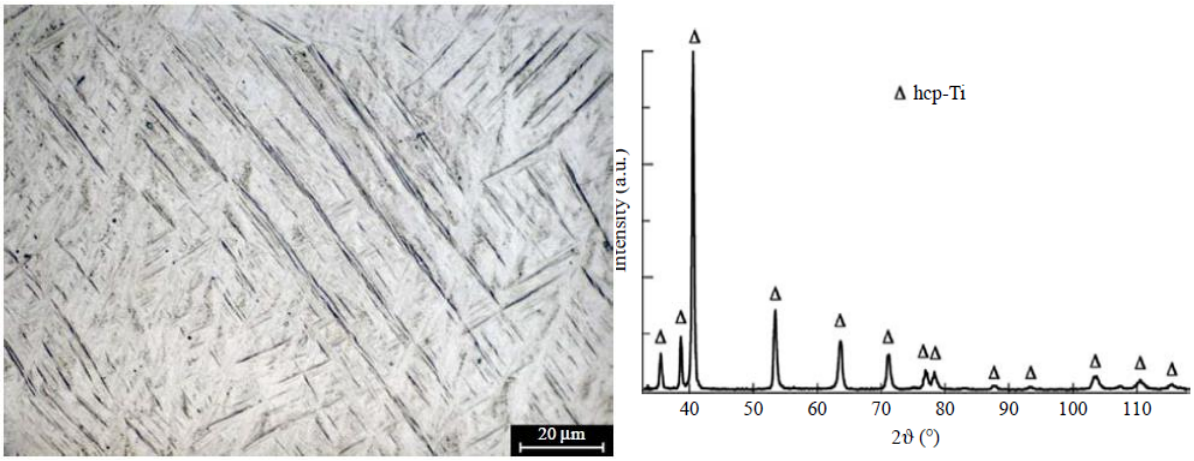

Fig. 2.4. 14. Oriented martensitic plates containing acicular hcp phase and XRD pattern of the as-built DMLS Ti6Al4V (Facchini *et al.*, 2010).

In as built of Ti6Al4V DMLS parts the martensitic microstructure has an influence on the mechanical properties. The yield strength are high, the ductility is very low. Vrancken *et al.* (2012) showed the combination effect of martensite, microcracks and residual stress are responsible for low ductility.

Post-processing heat treatment has influence on the microstructure of DMLS Ti6Al4V (Fig. 2.4.15, Tab. 2.4.2) since cooling rate and temperature and holding time influence the morphology of microstructure. When treated above the β-transus, the cooling rate is the most important parameter that determines the final dimensions of the α phase and even the morphology. At high cooling rates, the large undercooling leads to the formation of many a nuclei resulting in

smaller α colony size and a finer spacing between individual α plates. Furnace cooling results in lamellar α + β and air cooling results in Widmanstätten microstructure or basket weave structure. The cooling rate during water quenching is higher than 410°C/s leads to α' martensite (Becker *et al.*, 2015).

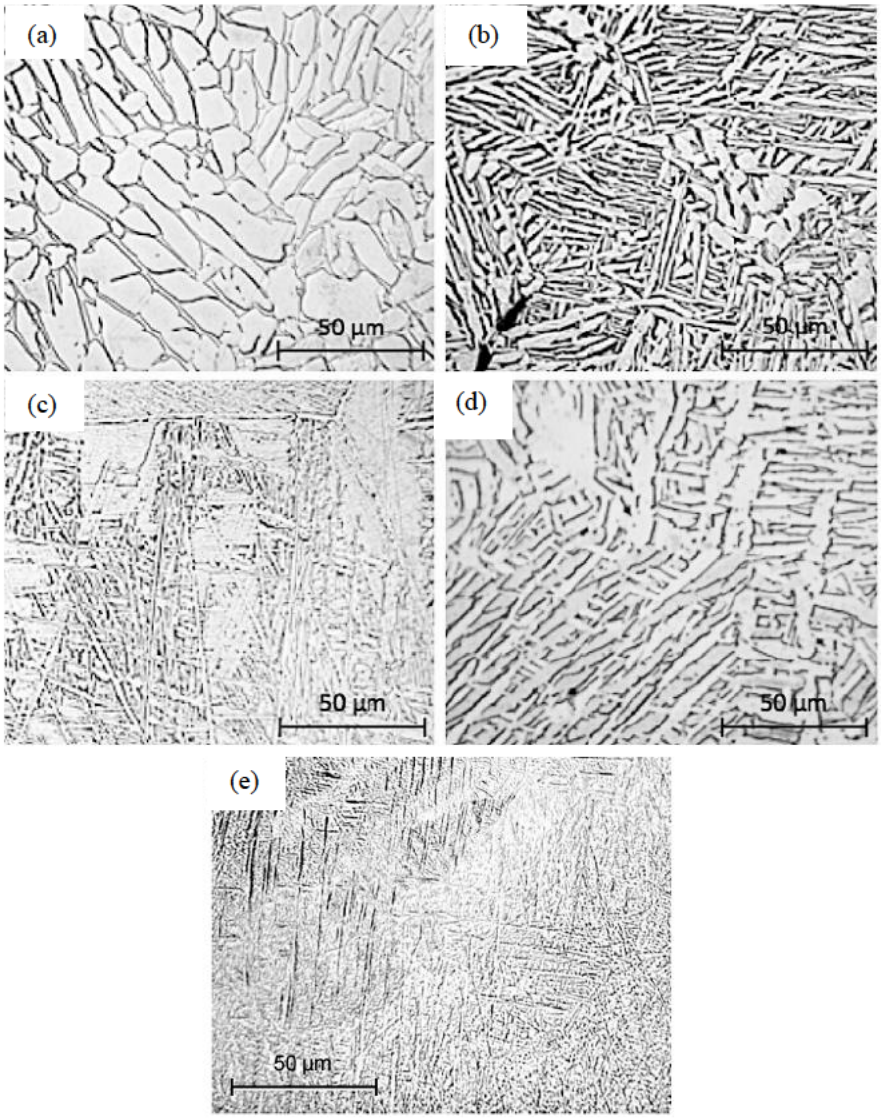

Fig. 2.4.15. Microstructures obtained through various heat-treatments of DMLS Ti6Al4V: (a) duplex anneal, (b) recrystallisation anneal, (c) beta anneal, (d) hot isostatic pressing (HIP), and (e) as-built condition (Becker *et al.*, 2015).

Table 2.4.2. Heat-treatments and resultant microstructure in DMLS Ti6Al4V (Becker *et al.*, 2015)

Heat treatment	Holding temperature	Microstructure
As built	-	Fine acicular α' martensite
Recrystallization anneal	950°C, 1-hour holding period, FC	Plate-like α - β, small amount of equiaxed α
HIP	915°C at 1000 bar isostatic pressure, 2-hour holding period, FC at 11°C/min	Plate-like α – β, small amount of equiaxed α
Duplex anneal	1-hour holding period followed by AC; 700°C, 2-hour holding period, AC	Equiaxed and acicular α with intergranular β
Beta anneal	1030°C, 1-hour holding period AC; 630°C, AC	Widmanstätten α + β colony

Study done by Ramosoeu (2015) showed that 700ºC heat treatment temperature did not show much difference on the microstructure of the DMLS samples. During both air cooling and water quenching the cooling rate is too high for significant grain growth to occur. Low cooling rates, such as during furnace cooling, allow the grains to grow. The very fine martensitic as-built microstructure changed to a coarser alpha colony with a beta phase on the grain boundaries (Fig. 2.4.16). The slowest cooling rate (furnace cool) resulted in a fully lamellar microstructure comprising colonies of parallel alpha laths separated by beta laths which are in different lath orientation. The grain sizes are larger and the grain boundaries consisted of a globular alpha phase after heat treatment at 1000ºC for 1 hour and furnace cooling.

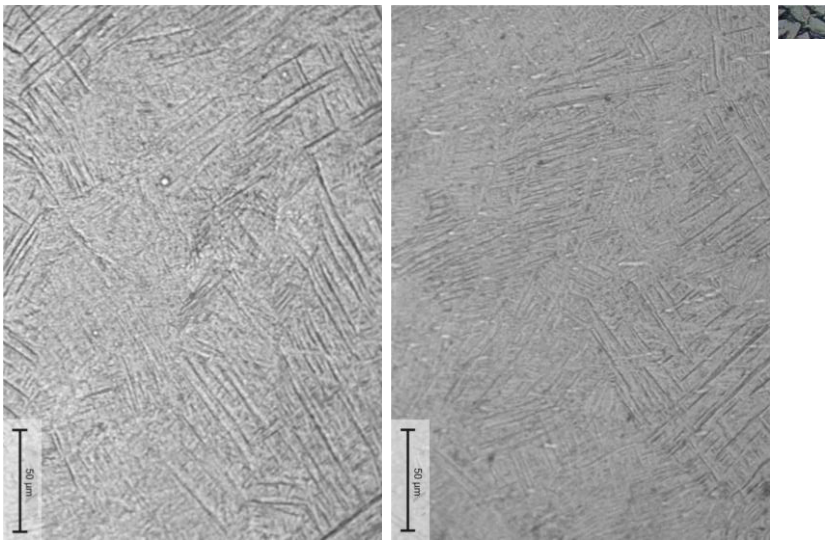

(a) (b) (c)

Fig. 2.4.16. Microstructures of DMLS Ti6Al4V samples heat treated (a) at 700ºC, soaked for 1 hour then furnace cooled; (b) air cooled; (c) samples heat treated at 1000ºC, soaked for 1 hour then furnace cooled (Ramosoeu, 2015).

Mechanical properties

For Ti6Al4V heat treated at intermediate temperatures below the β-transus (so-called "the low-temperature heat treatment"), the initial fine martensitic structure can be transformed to a mixture of α and β, in which the α phase is also present as fine needles as stated by Vrancken *et al.* (2012). When annealing above the β-transus (so-called "high-temperature heat treatment"), the martensitic material can restore into a structure similar to the conventional Ti6Al4V, which observation is supported by the comparative study of Vilaro *et al.* (2011) and Facchini *et al.* (2010). The transformed structures are essential for the preferred mechanical properties of the materials. The high-temperature heat treatment leads to slightly lower yield strength and ultimate tensile strength than the conventional microstructure. The low- temperature heat treatment, in contrast, increases the yield strength and ultimate tensile strength in comparison to 'as-cast' and wrought materials. However, the tensile strength of as built DMLS Ti6Al4V alloy is higher compared to the wrought TiAl6V4 therefore ductility and fatigue strengths are inferior. This is caused by a combination of martensitic α' microstructure and un-molten particles, pores, or micro cracks when DMLS process-parameters were non-optimal (Facchini *et al.*, 2010).

According to the ASTM F1472 standard of recommended the yield strengths must be minimum of 825-860 MPa and elongation more than 8% (Tables 2.4.3 and 2.4.4). These tables show properties of the samples that were built in and at different process-parameters.

The difference in powder can also effect on the mechanical properties. Ti6Al4V4ELI (Extra Low Interstitials) contains oxygen less than 0.13%. This confers improved ductility and fracture toughness with reduction in strength.

Rafi *et al.* (2013) found that recycled titanium has an effect on tensile results due to the fact that over time titanium picks up oxygen due to the high affinity of titanium for oxygen which can lead to embrittlement. It was shown for wrought alloys, that the corrosion resistance the strength and ductility are similar for Ti6Al-4V(ELI) and Ti6Al4V but the fracture toughness of the ELI grade is about 25% higher than the standard grade (United titanium, 2016).

The surface finish of the DMLS sample can effect on the mechanical properties of the samples (Rafi *et al.*, 2013). The surface roughness and micro-pores at or near surface the sample have stress concentration gives opportunity for crack initiation on a component (Leicht & Wennberg, 2015; Kasperovich & Hausmann, 2015). Elongated pores might evolve due to incorrect melting of the built layers and the spherical due to gaseous protective gas in the raw powder. The tensile tests concluded that effect of pores could be more limited in samples with layer orientation parallel to the tensile direction, since those samples will not include as many layers and thus

possibly decrease the risk of pores being present. Fig. 2.4.17 shows the build orientation sample of the SLM to be focused on this study vertical built and horizontal built (Leicht & Wennberg, 2015).

But in terms of pore's risk, mechanical tests done by Leicht & Wennberg (2015) with Ti6Al4V powder with constant process parameters but different built orientation (vertical and horizontal) showed that vertical samples had higher yield strength and tensile strength compared to the horizontal samples. The effect of this difference was concluded might be connected to the microstructure and especially the growing direction of the prior β-grains. The dog-bone specimens of Ti6Al4V (ELI) were build using EOS M280 the sample were stresse relived before they were removed from the substrate for 2 hours at 300°C temperature. The as build sample surface horizontally and vertically grown showed few pores with surface roughness and solidified beads of melted powder. During tensile testing the vertical samples had high modulus of elasticity and it was stiffer compared to the horizontal build and HIP samples.

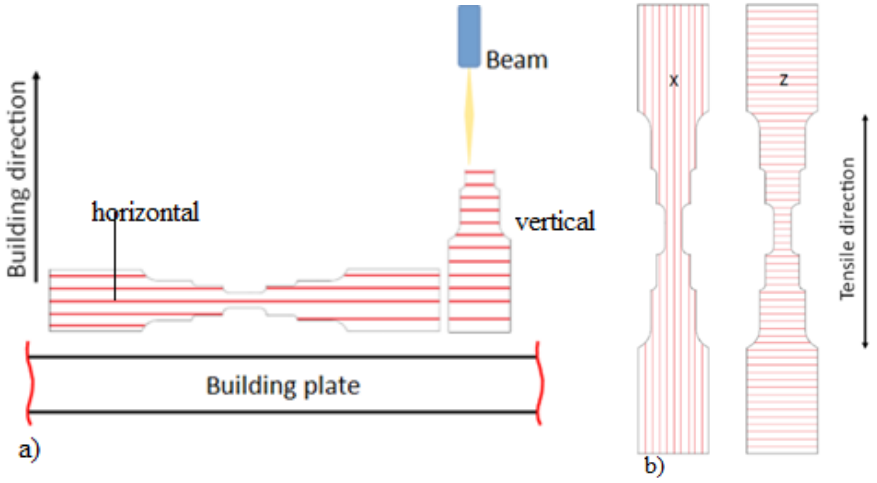

Fig. 2.4.17. Demonstration of horizontal and vertical built on the building plate during DMLS process (a) and demonstration of horizontal and vertical built during tensile testing (b) (Leicht &Wennberg, 2015).

The study done by Vracken *et al.* (2012) (Table 2.4.5) shows the effect of different heat treatment of the same build sample of Ti6Al4V ELI vertical samples produced under the same process parameter. The change of microstructure was found by high temperature level or a longer annealing time for heat treatment. The fine martensite gives higher strength but less elongation this is an influence of rapid cooling rate for water quenching. The slow air cooling and furnace cooling showed the improvement in ductility this is due to the coarse microstructure developed.

Table 2.4.3. Tensile properties of as-built and heat-treated DMLS vertical build Ti6Al4V samples

Reference	Type of powder	Process parameters	Machined or not machined	Heat treatment	UTS (MPa)	YTS (MPa)	Elongation (%)	Young Modulus, GPa
Frey *et al.* (2009)	Ti6Al4V	EOS M270			1201	1088	10.6	111
Mower and Long (2016)	Ti6Al4V ELI	EOS M280 Laser spot 100 µm Layer thickness 30 µm	As built	Thermal stress relieve at 300°C for 2 hours	1130	1096	0.012 (failure strain)	114
Xu *et al.* (2015)	Ti6Al4V ELI		machined (martensite)	None	1197	1029	8	
			machined (lamellar)	None	Not specified	1106±6	11.4	
Kasperovich & Hausmann (2015)	Ti6Al4V ELI	LaserCusing	Not machined	None	1051	736	11.9	110
			Machined	None Heat treated 700°C	1155 1115	986 1051	10.9 11.3	112.4 117.4
			Machined	Heat treated 900°C	988	908	9.5	118.8
Vrancken *et al. (*2012)	Ti6Al4V ELI	LM-Q SLM Laser power 250W Layer thickness 30 µm Hatch spacing 60 µm	As built	None	1267	1110	7.28	109.2
Ti6Al4V								
Thone *et al.* (2012)	Ti6Al4V	SLM250HL Laser power 175 Layer thickness 30µm	Not specified	Vacuum with 20°C	Not specified	1080	1.6	
	750			1062			3.7	
	800			1040			5.1	
	850			1009			5.2	
	950			972			10.1	
	1050			945			11.6	
EOS (2013)	Ti6Al4V	EOSINT M 280 400W.		None	1250±50	1130±75	9±3%	112±13
				800 °C 2hours in argon.	1080±30	1005±40	15±4	115±20
Facchini *et al.* (2010)	Ti6Al4V		Machined	None	1095±10	990±5	8.1±0.3	110±5
			Machined		990	870	11	117
Rafi *et al.* (2013)	Ti6Al4V	EOS M270	Machined	None	1219±19	1143±38	4.89±0.6	
Rekedal *et al.* (2015)	Ti6Al4V	EOS M280	Not machined	None	1140	938	6.7	91.8±0.5
	Ti6Al4V	EOS M280	Not machined	Heat treated 4h at 800°C	937	862	11.4	98.0±1.2
Edwards & Ramulu (2014)	Ti6Al4V	MTT 250	Not machined	None	1035±29	910±10	3±0.8	
Leuders *et al.* (2013)	Ti6Al4V	SLM 250 Laser power 400 W	Machined	None	1080	1008	1.6	

Reference	Type of powder	Process parameters	Machined or not machined	Heat treatment	UTS (MPa)	YTS (MPa)	Elongation (%)	Young Modulus, GPa
		Layer thickness 30 µm Particle size 40 µm						
		800 for 2 hours vacuum or argon	Machined		1040	962	5	
		1050 for 2 hour vacuum or argon	Machined		945	798	11.6	

Table 2.4.4. Tensile properties of as-built and heat-treated DMLS horizontal build Ti6Al4V samples

Reference	Process parameters	Machined / not machined	Heat treatment	UTS (MPa)	Yield (MPa)	Elongation (%)	Young's Modulus (GPa)
	Ti6Al4V ELI						
Mower and Long (2016)	EOS M280 Laser spot 100 µm Layer thickness 30 µm	Not machined	Thermal stress relieve at 300°C for 2 hours	1034	972	0.055 (failure strain)	108.8
Facchini *et al.* (2010)				1095±10	990±5	8.1±0.3	110±5
	Ti6Al4V						
Rafi et al (2013)	M 270	Machined	None	1269±9	1195±19	5.5	
Vilaro *et al.* (2011)	Trumpf LF250			1206±8	1137±20	7.6±2	105±5
Becker *et al.* (2015)	EOSINT M280, layer thickness of 30 µm 200 W	Not machined	None	1155±20		4.1±2	
			Stress relived	1230±20		7±2	
EOS (2013)	M280	As built	None	1260± 40	1125±65	7±3	108±20
		Not machined	800°C 2 hours in argon.	1075±30	1000±40	13±3	111±20
Frey *et al.* (2009)	EOS M270		None	1248	1043	8.5	112
Murr *et al.* (2009)	EOS M270	Not machined	None	1407	1333	4.54	
Facchini *et al.* (2010)	EOSINT M270 195 W, 225 mm/s	Machined		1095±10	990±5	8.1±0.3	110±5
		Machined		1140±10	1040±10	8.2±0.3	
Edwards & Ramulu (2014)	MTT 250	Not machined	None	1035±29	910±10	3±0.8	

Table 2.4.5. Mechanical properties of SLM material after different heat treatment (Vrancken *et al.*, 2012)*

Temperature (°C)	Time (hours)	Cooling rate	UTS(MPa)	Yield (MPa)	Elongation (%)	Young Modulus
540	5	WQ	1223±52	1118±39	5.36±2.02	112.6±30.2
850	2	FC	1004±6	955±6	12.84	114.7
850	5	FC	965±20	909±24	premature failure	112±3.4
1015	0.5	AC				
Followed by			874±23	801±20		114.9±1.5
843	2	FC				
1020	2	FC	840±27	760±19	13.45±1.18	114.7±0.9
705	3	FC	1082±34	1026±35	14.06±2.53	114.6±2.2
940	1	AC				
Followed by			948±27	899±27	13.59±0.32	115.5±2.4
650	2	AC				
1015	0.5	AC				
Followed by 730	2	AC	902±19	822±25	12.74±0.56	112.8±2.9

* WQ= Water quenching, AC = air cooling, FC= furnace cooling

The study DMLS Ti6Al4V (ELI) was done by Kasperovich & Hausmann (2015) for the sample build vertically. The samples were tensile tested as built, machined and heat treated in different temperatures as shown in Fig. 2.4.18. As built results shows higher strength compared to heat treated. After different heat treatment the elongation didn't show improvement according to the expected results of improving the mechanical properties this is shown through the tensile fracture analysis ,the heat treated fracture at 700ºC resembled the non-heat treated which has effect on less elongation after heat treating. The reference material shows the superior elongation results compared to as built this is due to microcracks, unmolten particles and pores.

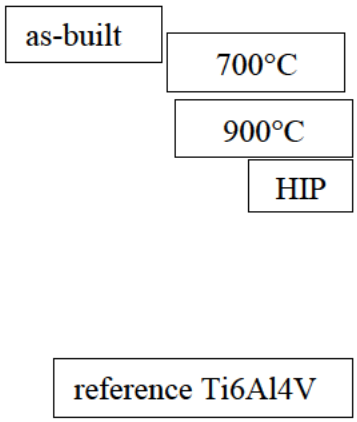

Fig. 2.4.18. Comparison of Ti6Al4V DMLS parts on stress-strain graph (Kasperovich & Hausmann, 2015).

Applying the heat treatment can improve the common properties including tensile strength, creep strength and fracture toughness. Heat treatment shows the improvement in the ductility but decrease in the yield strength from investigation done by Thöne *et al.* (2012) (Fig. 2.4.19). Yadroitsev *et al.* (2014) also suggested that the mechanical strength after heat treatment of DMLS Ti6Al4V alloy is usually lower compared to the as-made state and the coarsening of lamellar microstructure at high treatment temperatures is the factor causing the strength decrease.

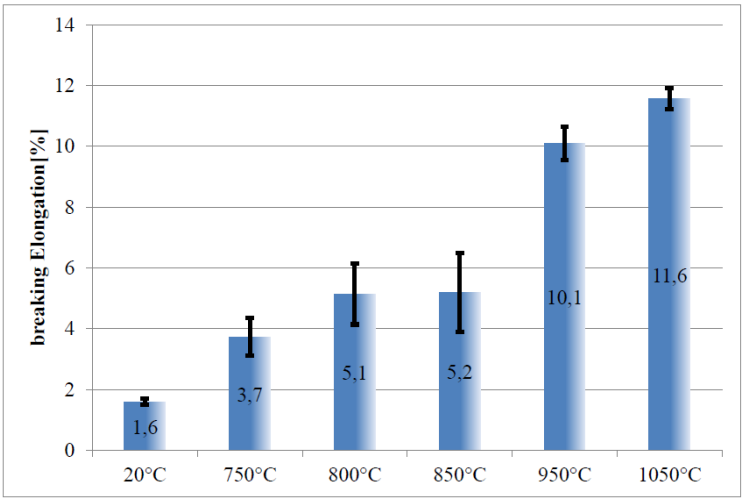

(a)

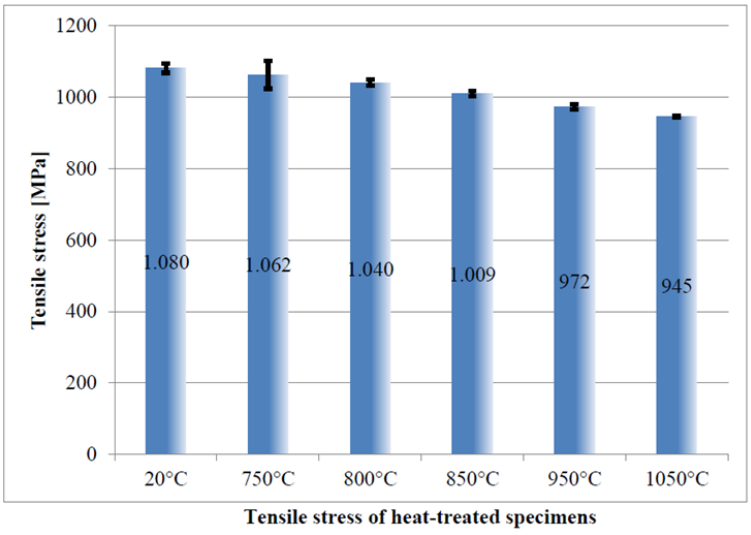

(b)

Fig. 2.4.19. Elongation (a) and tensile strength (b) of DMLS Ti6Al4V samples at different heat treatment (Thone *et al.*, 2012).

Thöne *et al.* (2012) showed the three cases of heat treatment DMLS Ti6Al4V microstructures. As said above, DMLS as-built parts have residual stress and very fine microstructure (Fig. 2.4.20). In case 1 heat-treatment at low temperature caused the reduction of residual stress without any changing of microstructure. The reduction of stress leads to higher

elongation at break. Case 2 shows the changing of microstructure of DMLS parts by using a higher temperature level or a longer annealing time for heat treatment to enlarge the grain size or the laminar structure (to α'-constellation transform a α/β-constellation). HIP can be applied to change microstructure combining with reduction of pores (case 3).

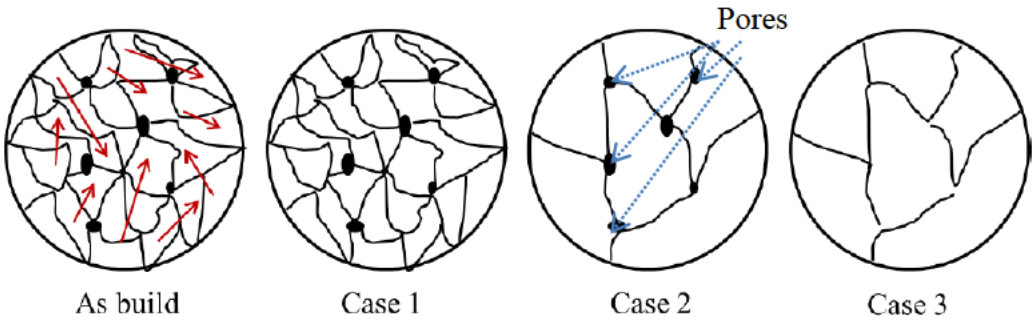

Fig. 2.4.20. Three cases of heat treatment DMLS microstructures (Thöne *et al.*, 2012).

The study by Yadroitsev *et al.* (2014) showed that the hardness of as-made Ti6Al4V alloy depends on the process parameters. The Fig. 2.4.21 showed higher micro-hardness of as-made Ti6Al4V alloy as compared to the heat treated. Under different heat treatment the micro-hardness is decreased.

In the study by Kasperovich & Hausmann (2015), Vickers micro-hardness tests showed higher hardness values for the samples with the martensitic structure in comparison to the 'Reference' and HIPed materials (Fig. 2.4.22). After HIP, the micro-hardness values are almost restored to the values of the reference material or slightly higher due to the elongated structure.

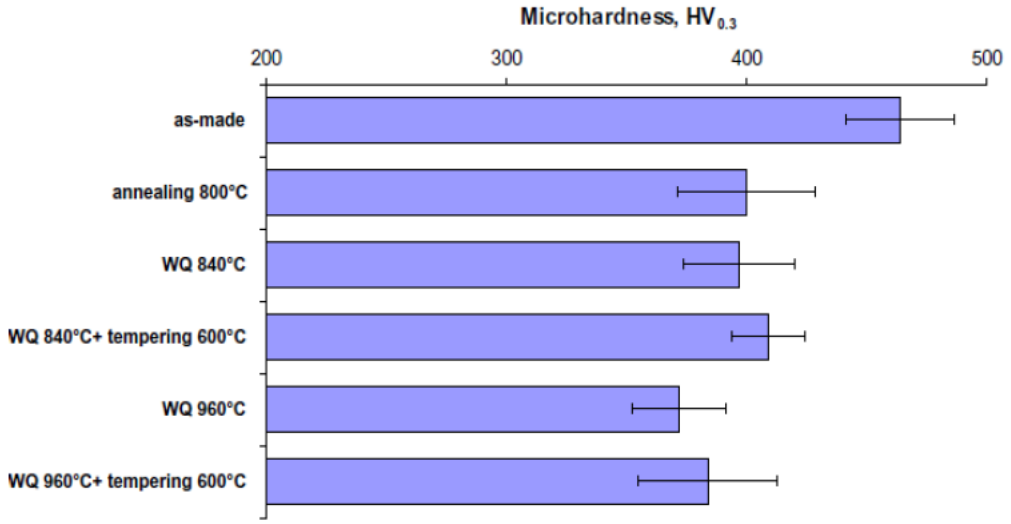

Fig. 2.4.21. Vickers micro-hardness of Ti6Al4V alloy (Yadroitsev *et al.*, 2014).

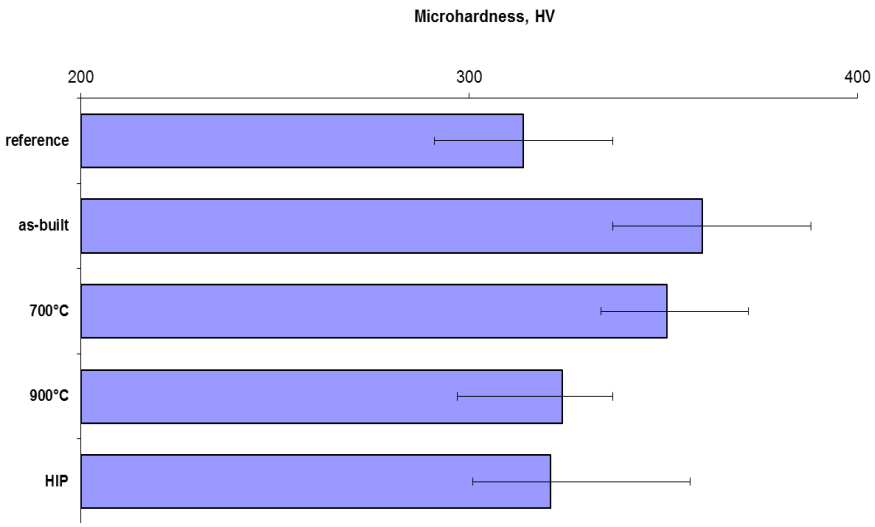

Fig. 2.4.22. Vickers micro-hardness tests of TiAl6V4 Average (min -max) reference and DMLS samples without and with thermo-mechanical treatment (Kasperovich & Hausmann, 2015).

Kasperovich & Hausmann (2015) indicated that TiAl6V4 samples produced by DMLS had a brittle fracture in the middle region (Fig. 2.4.23). The inner region was asymmetrical and has an irregular structure. It is observed that fracture in DMLS as built sample starts from outside to the middle of the sample. Heat treated samples show lower ultimate tensile strength compared to the as-built DMLS specimens (Tab.2.4.3).

bril
failu

Fig. 2.4.23. Fractures of DMLS Ti6Al4V samples (Kasperovich & Hausmann, 2015).

Summary

Titanium and titanium alloys are used in biomedical applications because of their excellent specific strength, corrosion resistance, non–allergic properties and biocompability. Allotropic properties of titanium allow to use alloying and heat treatment for the enhancement of certain mechanical properties.

Fine martensitic microstructure of DMLS Ti6Al4V is confirmed in all studies. But different studies showed different results of mechanical properties as-built DMLS samples. Under vertical and horizontal building direction the mechanical tests showed different results. The machined and unmachined tensile specimen showed different mechanical results due to the surface roughness. Ductility of DMLS as-built and heat treated Ti6Al4V varied significantly.

Powder properties, process parameter, building strategy and machine parameters have influence on the final properties of the DMLS component. It was found out that the as built of the DMLS mechanical properties cannot meet medical standards because of the fine martensite microstructure and poor ductility.

References

3DSystems, 2013. 3DSystems. [Online]
Available at: http://www.thesolidexperts.com/application/files/4514/3819/2068/direct-metal-brochure-1013-usen-web_0.pdf[Accessed 20 December 2015].

ASTM Standard F2792-12a, 2013. Standard terminology for additive manufacturing Technologies, West Conshohocken: *ASTM International*, pp 10–12.

ASTM E8 / E8M-13, *Standard test methods for tension testing of metallic materials*, ASTM International, West Conshohocken, PA, 2013.

Abbaschian, R., Abbaschian, L. & Reed-Hill, R. E., 2010. *Physical metallurgy principles*. 4th ed. PWS-KENT publishing company, Boston.

Alkahari, M. R., Furumoto, T., Ueda, T., Hosokawa, A., Tanaka, R. & Abdul Aziz, M. S., 2012. Thermal conductivity of metal powder and consolidated material fabricated via selective laser melting. *Key Engineering Materials*, 523, pp. 244-249.

Antonysamy, A., 2012. *Microstructure, texture and mechanical property evolution during additive manufacturing of Ti6Al4V alloy for aerospace applications.* Doctoral thesis. University of Manchester.

Bhadeshia, H.K.D.H., 2005. Titanium & its Alloys. *Materials Science & Metallurgy*, Cambridge University, pp.1-12.

Becker, T. H., Beck, M. & Scheffer, C., 2015. Microstructure and mechanical properties of direct metal laser sintered Ti-6AL-4V. *The South African Journal of Industrial Engineering*, 26(1), pp. 1-10.

Becker, T., van Rooyen, M. & Dimitrov, D., 2015. Heat treatment of Ti-6Al-4V produced by lasercusing. *The South African Journal of Industrial Engineering*, 26(2), pp.93-103.

Becker, W.T. & Lampman, S., 2002. Fracture appearance and mechanisms of deformation and fracture. *Materials Park, OH: ASM International, 2002*.

Clinning, N., 2012. *Thermomechanical processing of blended elemental powder Ti-6Al-4V alloy*. Masters Dissertation, University of Cape Town, 146 p.

Conceptlaser, 2012. Conceptlaser. [Online] Available at: http://www.concept-laser.de/[Accessed 20 December 2015].

Dąbrowski, R., 2011. The kinetics of phase transformations during continuous cooling of the Ti6Al4V alloy from the single-phase β range. *Archives of Metallurgy and Materials*, *56*(3), pp.703-707.

Donachie, M., 2000. Titanium: A Technical Guide. Materials Park, Ohio 44073-0002: ASM International , Technology & Engineering .

Do, D.K. & Li, P., 2016. The effect of laser energy input on the microstructure, physical and mechanical properties of Ti-6Al-4V alloys by selective laser melting. *Virtual and Physical Prototyping*, *11*(1), pp.41-47.

Edwards, P. and Ramulu, M., 2014. Fatigue performance evaluation of selective laser melted Ti–6Al–4V. *Materials Science and Engineering: A*, *598*, pp.327-337.

EOS, 2015. EOS. [Online] Available at: www.eos.info [Accessed 20 December 2015].

Facchini, L., 2010. Ductility of a Ti6Al4V alloy produced by selective laser melting of pre-alloyed powders. *Rapid Prototyoing Journal*, 16(6), pp. 450-459.

Frey, M., Shellabear, M. & Thorsson, L., 2009. Mechanical testing of DMLS parts. *EOS whitepaper*.

Gu, D., 2014. New metallic materials development by laser additive manufacturing. *Laser Surface Engineering*, pp. 163-180.

Hanawa, T., 2010. Overview of metals and applications. In: Metals for Biomedical Devices. pp. 3-24.

Kandil, F. A., Lord, J. D., Fry, A. T. & Grant, P. V., 2001. A review of residual stress measurement methods. *A Guide to Technique Selection*, Volume 4.

Kar, S., 2005. Modelling of mechanical properties in alpha/beta-titanium alloys. Doctoral dissertation. Ohio State University.

Kartal, M., Molak, R., Turski, M., Gungor, S., Fitzpatrick, M. E. & Edwards., L., 2007. Determination of weld metal mechanical properties utilising novel tensile testing methods. *Applied Mechanics and Materials*, 7-8, pp. 127-132.

Kashaev, N., Horstmann, M., Ventzke, V. & Riekehr, S., 2013. Comparative study of mechanical properties using standard and micro-specimens of base materials Inconel 625, Inconel 718 and Ti-6Al-4V. *Journal of Materials Research and Technology*, 2(1), pp. 43-47.

Kasperovich, G. & Hausmann, J., 2015. Improvement of fatigue resistance and ductility of TiAl6V4. *Journal of Materials Processing Technology*, Volume 220, pp. 202-214.

Klocke F., Wagner C. & Ader C., 2003. Development of an integrated model for selective laser sintering. *36th CIRP International Seminar on Manufacturing Systems*, 03-05 June, pp. 387-392.

Knowles, C. R., Becker, T. H. & Tait, R., 2012. Residual stress measurements and structural integrity implications for selective laser melted Ti6Al4V. *The South African Journal of Industrial Engineering*, 23(3), pp. 119-129.

Krakhmalev, P., Yadroitsava, I., Fredriksson, G. & Yadroitsev, I., 2015. In situ heat treatment in selective laser melted martensitic AISI420 stainless steels. *Materials & Design*, 87, pp. 380-385.

Kruth, J.P., Badrossamay, M., Yasa, E., Deckers, J., Thijs, L. & Van Humbeeck, J., 2010, April. Part and material properties in selective laser melting of metals. In *Proceedings of the 16th international symposium on electromachining*.

LaVan, D.A., 1999. Microtensile properties of weld metal. *Experimental Mechanics*, 23 (3), pp. 31-34.

Leicht, A. and Wennberg, E.O., 2015. *Analyzing the mechanical behavior of additive manufactured Ti-6Al-4V using digital image correlation*. MS thesis, Chalmers University of technology Gothenburg, Sweden.

Leuders, S., Thöne, M., Riemer, A., Niendorf, T., Tröster, T., Richard, H.A. and Maier, H.J., 2013. On the mechanical behaviour of titanium alloy TiAl6V4 manufactured by selective laser melting: Fatigue resistance and crack growth performance. *International Journal of Fatigue*, 48, pp.300-30

Löhe, D., Lang, K.H., Vöhringer, O., Totten, G., Howes, M. & Inoue, T., 2003. *Handbook of residual stress and deformation of steel*. Materials Park, OH: ASM International.

Manfredi, D. *et al.*, 2014. Additive manufacturing of Al alloy and Aluminium matrix composites. *Light metal alloys applications*, InTech: Rijeka, pp. 1-32.

Mercelis, P. and Kruth, J.P., 2006. Residual stresses in selective laser sintering and selective laser melting. *Rapid Prototyping Journal*, *12*(5), pp.254-265

Micro-manufacturing, 2014. Sintering 3D parts from powdered metal is on the rise. [Online] Available at: http://www.micromanufacturing.com/content/sintering-3d-parts-powdered-metal-rise [Accessed 9th March 2015].

Mier, H. & Harbeland, C., 2008. Experimental studies on selective laser melting of metallic parts. *Materialwissenschaft und Werkstofftechnik*, 39(8), pp. 665-670.

Molak, R., M., Paradowski, K., Brynk, T., Ciupinski, L., Pakiela, Z., Kurzydlowski, K.J., 2009. Measurement of mechanical properties in a 316L stainless steel welded joint. *International Journal of Pressure Vessels and Piping*, 86 (1), pp. 43-47.

Mower, T.M. and Long, M.J., 2016. Mechanical behavior of additive manufactured, powder-bed laser-fused materials. Materials Science and Engineering: A, 651, pp.198-213.

Murr, L. E; Quinones, S. A; Gaytan, S. M; Lopez, M. I., Rodela, A., Martinez, E. Y.& Wicker, R. B, 2009.Microstructure and mechanical behaviour of Ti6Al4V produced by rapid-layer manufacturing, for biomedical application. *Journal of the mechanical behaviour of biomedical materials*, pp. 20-32.

Paranjpe, A., 2014. *Residual stresses in machined titanium (Ti-6Al-4V)*. Doctoral dissertation. The University of Utah.

Pederson, R., 2002. *Microstructure and phase transformation of Ti-6Al-4V*. Licentiate thesis. Lulea University of technology

Qiu, C., Adkins, N. & Attallah, M., 2013. Microstructure and tensile properties of selectively laser-melted and of HIPed laser-melted Ti–6Al–4V. *Materials Science and Engineering*, 578, pp. 230-239.

Rafi, H.K., Karthik, N.V., Gong, H., Starr, T.L. and Stucker, B.E., 2013. Microstructures and mechanical properties of Ti6Al4V parts fabricated by selective laser melting and electron beam melting. *Journal of materials engineering and performance*, 22(12), pp.3872-3883.

Ramosoeu, M. K. E., 2015. Characterisation and static behaviour of the DMLS TI-6AL-4V for biomedical applications. Masters dissertation. Central University of technology, Bloemfontein.

Rekedal KD, Liu D. Fatigue life of selective laser melted and hot isostatically pressed Ti–6Al–4V absent of surface machining. *Proceedings of the 56th AIAA/ASCE/AHS/ASC structures, structural dynamics, and materials conference*, Kissimmee, FL; 2015.

RMI Titanium Company [online], 2015. Titanium Armor. Available at www.titanium.org/resource/resmgr/Technical_Library/RMI_Metallography_brochure.pdf [Accessed 28 January 2016].

Rund, M., Procházka, R., Konopík, P., Džugan, J. and Folgar, H., 2015. Investigation of Sample-size Influence on Tensile Test Results at Different Strain Rates. *Procedia Engineering*, *114*, pp. 410-415.

Seguineau, C., Ignat, M., Malhaire, C., Brida, S., Lafontan, X., Desmarres, J.M., Josserond, C. and Debove, L., 2008, April. Micro-tensile tests on micromachined metal on polymer specimens: Elasticity, plasticity and rupture. *Design, Test, Integration and Packaging of MEMS/MOEMS, 2008. MEMS/MOEMS 2008. Symposium on* (pp. 8-10). IEEE.

Shifeng, W. *et al.*, 2014. Effect of molten pool boundaries on the mechanical properties of selective laser melting parts. *Journal of Materials Processing Technology*, 214(11), pp., 214(11), pp. 2660-2667.

Shunmugavel, M., Polishetty, A. & Littlefair, G., 2015. Microstructure and Mechanical Properties of Wrought and Additive Manufactured Ti-6Al-4V Cylindrical Bars. *Procedia Technology*, 20, pp. 231-236.

Sieniawski, J., Ziaja, W., Kubiak, K. & Motyka, M., 2013. Microstructure and mechanical properties of high strength two-phase titanium alloys. *Titanium Alloys-Advances in Properties Control*, pp. 69-80.

Simchi, A., 2006. Direct laser sintering of metal powders: Mechanism, kinetics and microstructural features. *Materials Science and Engineering*, 428(1), pp. 148-158.

Simonelli, M., 2014. *Microstructure evolution and mechanical properties of selective laser melted Ti-6Al-4V.* Doctoral thesis. Loughborough University.

SLM, 2014. SLM solution. [Online] Available at: http://www.stage.slm-solutions.com/ [Accessed 20 December 2015].

Slotwinski, J. A., Garboczi, E. & Hebenstreit, K. M., 2014. Porosity Measurements and Analysis for Metal Additive Manufacturing Process Control. *Journal of research of the national institute of standards and technology*, 119, pp. 494-528.

Smith, W.F., 1981. *Structure and properties of engineering alloys*. New York: McGraw-Hill Book Co.

Tensile testing, 2004. Ed. by J.R. Davis. 2nd ed. ASTM International, Materials Park, Ohio.

Thijs, L., Verhaeghe, F., Craeghs, T., Humbeeck, J.V. and Kruth, J.P. A study of the microstructural evolution during Selective Laser Melting of Ti6Al4V, 2010. *Acta Materialia*, 58(9): 3303-3312.

Thöne, M., Leuders, S., Riemer, A., Tröster, T. and Richard, H.A., 2012. Influence of heat-treatment on selective laser melting products–eg Ti6Al4V. *Solid freeform fabrication symposium SFF, Austin Texas*.

Vanderhasten, M., 2007. Ti-6Al-4V: *Deformation map and modelisation of tensile behaviour*. PhD thesis. Katholieke Universiteit Leuven.

Vilaro, T., Colin, C. and Bartout, J.D., 2011. As-fabricated and heat-treated microstructures of the Ti-6Al-4V alloy processed by selective laser melting. *Metallurgical and Materials Transactions A*, *42*(10), pp.3190-3199.

Vrancken, B., Thijs, L., Kruth, J. & Van Humbeeck, J., 2012. Heat treatment of Ti6Al4V produced by Selective Laser Melting: Microstructure and mechanical properties. *Journal of Alloys and Compounds*, Volume 541, pp. 177-185.

United Titanium, 2016. Titanium and Titanium alloys [Online] Available at http://www.unitedtitanium.com/ [Accessed 10th March 2016]

Yadroitsava I., Els J., Booysen G., Yadroitsev I., 2015. Peculiarities of single track formation from TI6AL4V alloy at different laser power densities by SLM. *SAJIE*, 26 (3): 86-95.

Yadroitsev, I., 2009. Direct manufacturing of 3D objects by selective laser melting of metal powders. LAP Lambert Academic Publishing, ISBN: 3838317947, 309 p.

Yadroitsev, I., Krakhmalev, P. & Yadroitsava, I., 2015. Hierarchical design principles of selective laser melting for high quality metallic objects. *Additive Manufacturing*, 7, pp.44-56.

Yadroitsev, I; Yadroitsava, I, 2015. Evaluation of residual stress in stainless steel 316L and Ti6Al4V samples produced by selective laser melting. *Virtual and Physical Prototyping*, (ahead-of-print), pp. 1-10.

Yadroitsev, I., Gusarov, A., Yadroitsava, I. & Smurov, I., 2010. Single track formation in selective laser melting of metal powders. J*ournal of Materials Processing Technology*, 210(12), pp. 1624-1631.

Yadroitsev, I., Krakhmalev, P. & Yadroitsava, I., 2014. Selective laser melting of Ti6Al4V alloy for biomedical applications: Temperature monitoring and microstructural evolution. *Journal of Alloys and Compounds*, 583, pp. 404-409.

Yadroitsev, I., Pavlov, M., Bertrand, P. & Smurov, I., 2009. Mechanical properties of samples fabricated by selective laser melting. 14èmes Assises Européennes du Prototypages & Fabrication Rapide.

Yadroitsev, I. & Smurov, I., 2010. Selective laser melting technology: from the single laser melted track stability to 3D parts of complex shape. *Physics Procedia*, 5, pp. 551-560.

Yadroitsev, I. & Smurov, I., 2011. Surface morphology in selective laser melting of metal powders. *Physics Procedia*, 12, pp. 264-270.

Yasa, E., Kempen, K., Kruth, J.P., Thijs, L. and Van Humbeeck, J., 2010.Microstructure and mechanical properties of maraging steel 300 after selective laser melting. *Solid Freeform Fabrication Symposium Proceedings* (pp. 383-396).

Xu, W., Brandt, M., Sun, S., Elambasseril, J., Liu, Q., Latham, K., Xia, K. and Qian, M., 2015. Additive manufacturing of strong and ductile Ti–6Al–4V by selective laser melting via in situ martensite decomposition. *Acta Materialia*, *85*, pp.74-84.

Chapter 3. MATERIALS AND METHODS

This chapter describes the experimental procedures used to produce the DMLS sample of Ti6Al4V including the parameters used. The Ti6Al4V alloy used for the entire study is characterised. The chapter then describes the samples types evaluated and the methods used to analyse them. It covers also the mechanical testing carried out and microstructure analysis machines used.

3.1. Manufacturing of DMLS Ti6Al4V (ELI) samples

EOSIONT M280 machine was used to produce Ti6Al4V (ELI) samples in Argon atmosphere (Fig. 3.1.1). The samples were built on the Ti6Al4V substrate following the recommended by EOS process-parameters and strategy (laser spot size of 80 μm, laser power of 170 W, scanning speed of 1.25 m/s, zigzag scanning by stripes with changing scanning direction with 67° from layer to layer, layer thickness of 30 μm).

Fig. 3.1.1. EOSINT M 280 machine.

3.2. Powder characterisation

TiAl6V4 ELI powders from TLS Technik were used for the study. Chemical composition of employed powders is shown in Table 3.2.1.

Table 3.2.1. Chemical composition of employed powders (wt. %)

Samples	Ti	Al	V	O	N	H	Fe	C	Y
Horizontal	Bal.	6.44	3.99	0.12	<0.002	0.001	0.19	0.007	<0.001
Vertical		6.34	3.94	0.058	0.006	0.001	0.25	0.006	<0.001
ASTM - 1472	Bal.	5.5-6.75	3.5-4.5	0.20 max	0.05 max	0.015 max	0.30 max	0.08 max	
ASTM F3001 − 14		5.5-6.5	3.5-4.5	0.13 max	0.05 max	0.012 max	0.25 max	0.08 max	0.005 max

The 10th, 50th and 90th percentiles of equivalent diameter (weighted by volume) of the powder particles were d_{10}=11.2 µm, d_{50}=20.6 µm and d_{90}=31.8 µm for horizontal samples and d_{10} = 13 µm, d_{50}= 23 µm and d_{90}= 37 µm for vertical ones.

3.3. Heat treatment of DMLS samples

Stress relieving heat treatment of the specimens with the substrate was done in Ar atmosphere at 650°C for 3 hours in the over oven (Fig. 3.3.1).

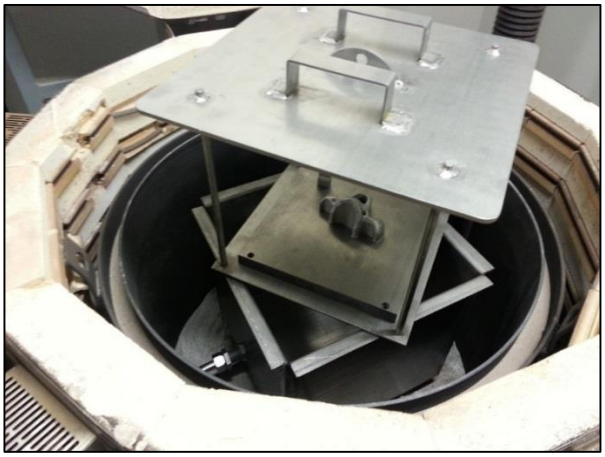

Fig. 3.2.1 Oven for heat treatment of the samples.

3.4. Samples for mechanical testing

3.4.1. Standard test specimens (type I)

The Ti6Al4V rectangular blocks 10 mm ×10 mm ×60 mm were built in the vertical and horizontal directions. Fig. 3.4.1 shows the as build samples on a substrate firstly for horizontal blocks and vertical blocks. The as built Ti6Al4V ELI blocks were removed from the substrate with wire cutter. Other blocks were heat treated with the substrate

Fig. 3.4.1. As-built vertical/ horizontal samples on the substrate.

The samples for tensile tests were made according to dimensions recommended by ASTM E8 standard (2016) (Fig. 3.4.2a). The machining process was completed on the lathe at the speed of 650 rev/min using coolant in a mixture of dinate water, stabilio cut 003, scrub lubricant. The CAD model with the dimensional values of the machined specimen is shown in Fig 3.4.2(a). The machined specimen shows the shiny surface with absence of surface finish, notches, chatter marks, grooves and gouges (Fig 3.4.2b).

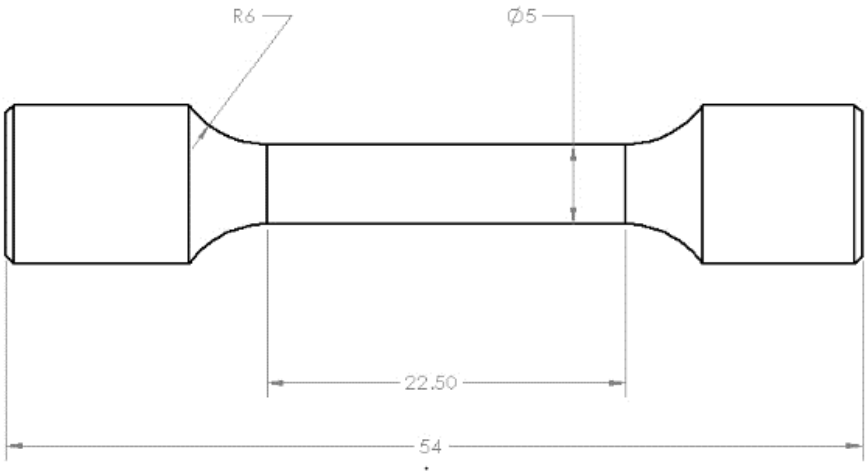

(a)

(b)

Fig. 3.4.2. Geometry of machined tensile samples (a) machined Ti6Al4V ELI specimen (b).

3.4.2. Mini-specimens (type II)

16 rectangular pin-loaded mini samples with 10 mm gauge length, 2 mm width and 1 mm thickness were directly built at the same process-parameters by the EOSINT M280 system. Dimensions of the tensile mini samples are shown in Fig. 3.4.3(a).

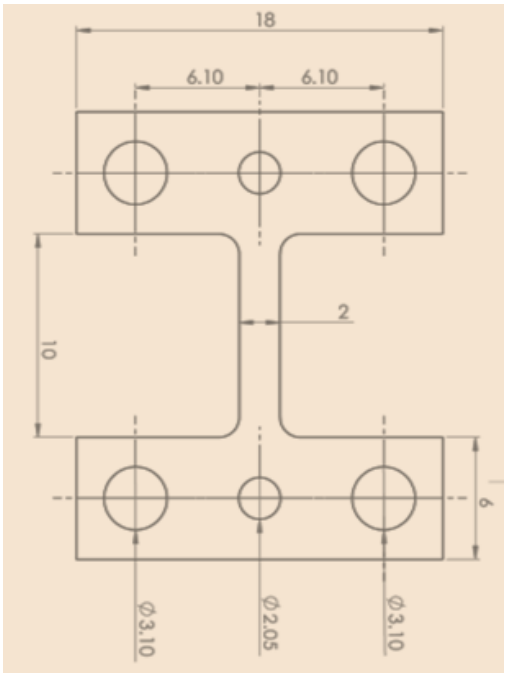

(a)

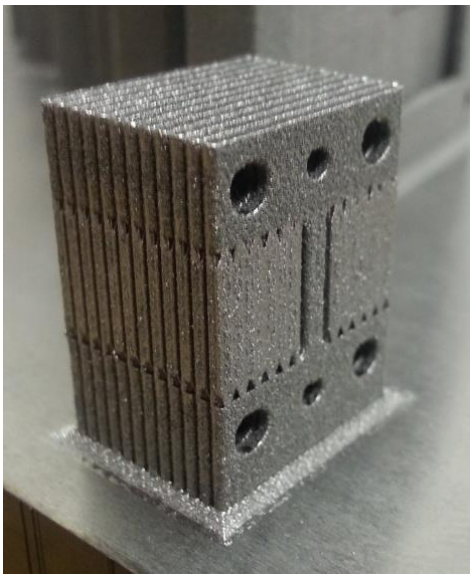

(b)

Fig. 3.4.3. Dimensions sketch of mini specimens b) as-built mini specimens

3.5. Mechanical testing

Tensile tests of the samples (Type I) were done at CSIR using INSTRON tensile machine (Fig. 3.5.1). The pre-load was 0.5kN and load was increasing linearly. Initially the extensometer was placed on the middle of the gauge length of the specimen until it reaches the 2% of the proof strength depending on the results wished to be accomplished. The extensometer is removed to prevent it from damage when the sample are allowed to break. The speed of the applied strain was

1.5 mm/min. The stress relieved and as-built samples were pulled until fracture. The other samples were pulled until a certain elongation is reached to investigate by CT scans.

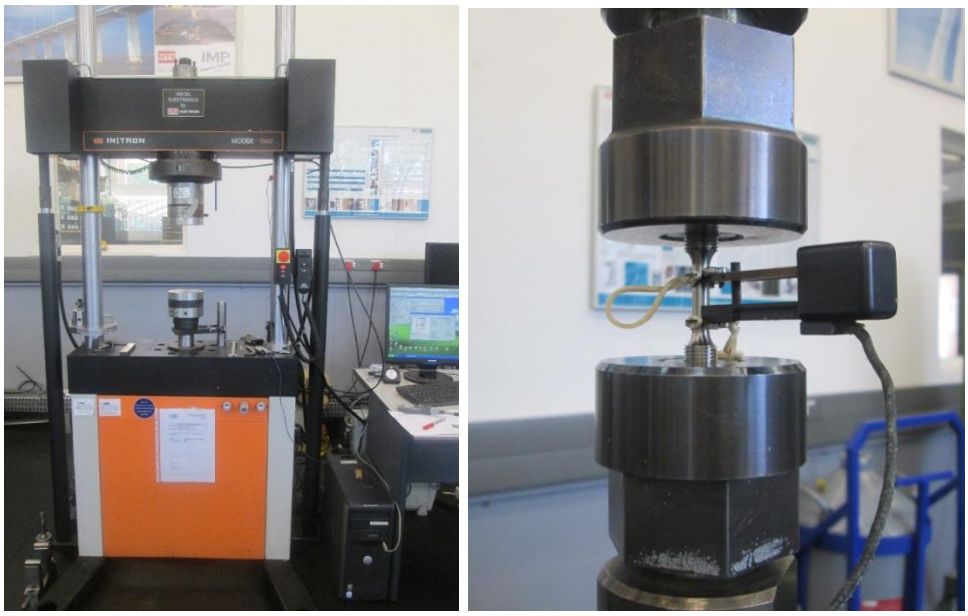

(a) (b)

Fig. 3.5.1. INSTRON tensile machine (a) specimen clamped for tensile tests (b).

Tensile tests for mini-samples were performed with an MTS Criterion Model 43 electric testing machine with wedge grips and without extensometer under constant strain rate of 0.25 mm/min.

Fig 3.5.2. MTS Criterion model 43 Electromechanical Universal Test Systems machine.

3.6. Microhardness testing

The micro-hardness as a part of the metallographic analysis was done using FM-700 Digital micro-hardness Tester from Future-Tech Corporation (Fig. 3.6.1).

Fig. 3.6.1. FM-700 microhardness tester.

3.7. Surface roughness testing

The surface roughness of the specimens were measured with Surftest SJ-210 portable surface roughness tester from Mitutoyo Corp. (Fig 3.7.1) in different directions for as-built and stress-relieved samples.

Fig. 3.7.1. Surface roughness measuring tester SJ-210 measuring the flat specimen.

3.8. Residual stress

The residual stress measurements were done with an X-ray diffractometer from ProtoXRD (Fig. 3.8.1). The residual stresses were determined using the $\sin^2 \psi$ method. The lattice deformations of the Ti-α were determined using a CuKα radiation source. Scans were performed around a {213} Bragg diffraction peak (2θ~139.69°) at 9 tilting angles ψ between –44.16° + 44.16°.

Fig. 3.8.1. ProtoXRD employed by NMMU.

The residual stresses were calculated considering plane stress conditions using X-ray elastic constants shown in Table 3.5.1. Principal stresses and their directions were analysed. XRD measurements were done at the Department of Mechanical Engineering in NMMU.

Table 3.5.1. Parameters used for the X-ray analysis

Test material	Collimator, mm	Wavelength, Å	Radiation	Bragg angle 2θ, °	*hkl*	1/2 S_2, MPa^{-1}	$-S_1$, MPa^{-1}
Ti α	3	1.5418	Cu Kα	139.69	{213}	11.89×10^{-6}	2.83×10^{-6}

3.9. Metallographic analysis

Samples were cut to be a square by the wire cutter for microstructure analysis. The small templates from Ti6Al4V were incorporated into MultiFast resin by CitoPress (Fig. 3.9.1a). Samples were polished with Tegramine-25 system (Fig. 3.9.1b) as recommended by Taylor & Weidmann (2016) and etched by Kroll's reagent. Optical microscope was used for metallographic analysis.

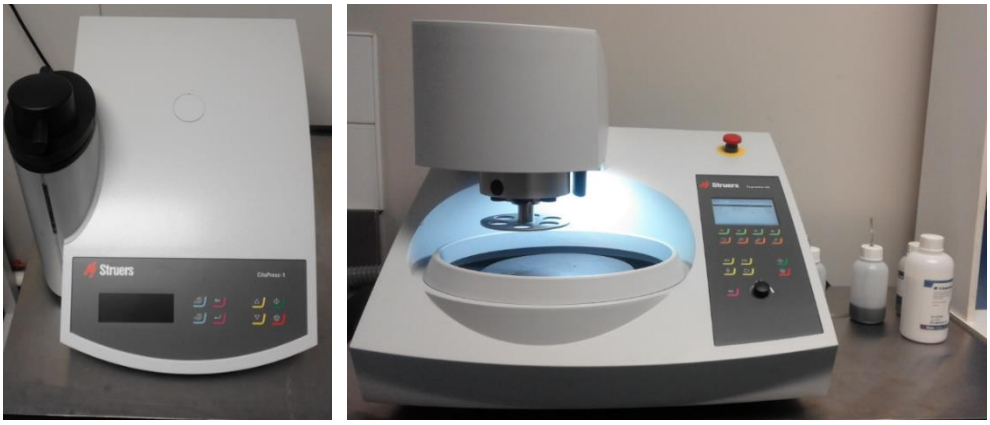

(a) (b)

Fig. 3.9.1. CitoPress-1 (a) and polishing machine Tegramin-25 (b).

3.10. Fracture surface analysis

Scanning electron microscope NeoScope JCM 500 was used for fracture analysis (Fig. 3.10.1).

Fig. 3.10.1. NeoScope JCM 5000 scanning electron microscope.

3.11. X-ray micro computed tomography

Tensile samples were subjected to X-ray micro computed tomography (MicroCT), before and after stress relieving and tensile tests. MicroCT scans were done with a General Electric Phoenix V|Tome|X L240 system at 160 kV and 200 μA, including beam filtering of 0.5 mm copper; the resolution was 10 μm. Detailed procedure is described in Chapter 4.2.

References

ASTM E8 / E8M-16a, 2016, *Standard Test Methods for Tension Testing of Metallic Materials*, ASTM International, West Conshohocken, PA, www.astm.org

Taylor, B., Weidmann, E., 2016. Metallographic preparation of titanium. *Application notes*. http://www.struers.com/-/media/Struers-media-library/Materials/Application-reports/Application_Note_Titanium_2015_ENG.pdf

Chapter 4. RESULTS AND DISCUSSION

4.1. Direct Metal Laser Sintering of Ti6Al4V (ELI) Powder for Rapid Prototyping

4.1.1 Abstract

Direct metal laser sintering (DMLS) is an innovative technology which allows the production of fully dense objects or fine-structured parts with complex shapes. Ti6Al4V (ELI) alloy is typically used for biomedical implants, aerospace components and cryogenic applications. Stability and certification of the properties of DMLS objects is an important task for all producers and end-users. Drawbacks of this technology are high residual stress in as-made DMLS objects and anisotropy of mechanical properties. Final mechanical properties of the SLM object depend on the thermal history of the bulk material that was subjected to previous heating and cooling cycles many times during the multipass laser treatment. Numerical simulation allows estimation of temperature distribution and stresses during DMLS of Ti6Al4V (ELI).

4.1.2 Introduction

Direct Metal Laser Sintering (DMLS) is an additive manufacturing technology which produces parts from metal powder deposited in a thin layer utilizing laser beam scanning. The powder material absorbs energy from the laser and melts. The laser beam scans over the powder thus melting the powder particles and also heating the previous layer. Sequentially, track by track, layer by layer, a 3D DMLS object is created. Parts with complex inner structures are in demand for automotive, aerospace and medical industries. Temperature gradients play a key role in the genesis of the residual stresses in DMLS objects. Residual stresses in as-built DMLS parts are tensile and high (Shiomi *et al.*, 2004; Merselis and Kruth, 2006; Furumoto *et al.*, 2010; Yadroitsava *et al.*, 2014; Yadroitsev *et al.*, 2015). Ti6Al4V (ELI) is a key material especially for bio-medical and aerospace application due to its bio-compatibility, high strength to weight ratio and also corrosion resistance. With regard to the nature of application in the various industries mentioned, it is of utmost importance to have sound knowledge of material and mechanical properties of DMLS produced samples, for safe implementation. The Centre for Rapid Prototyping and Manufacturing at the Central University of Technology, Free State specializes in producing medical implants from Ti6Al4V (ELI) and is where the following experiments and analyses were conducted.

4.1.3. Materials and methods

Manufacturing of Ti6Al4V (ELI) samples

Ti6Al4V alloy is a low density, high strength-to-weight ratio, extraordinary corrosion resistant material and it is biocompatible. Ti6Al4V alloy is α/β titanium being a heat treatable alloy which makes it more attractive due to the versatility it offers (Donachie, 2000). The Ti6Al4V (ELI) powder used was pre-alloyed gas atomized powder. The chemical composition was as follows: Ti – balance, Al – 6.31%, V –4.09%, O – 0.12%, N – 0.009%, H – 0.003%, Fe – 0.20%, C – 0.005% (weight %). The equivalent diameters (weighted by volume) of the powder particles were d_{10} = 13 µm, d_{50} = 23 µm and d_{90} = 37 µm. Ti6Al4V samples were produced by the EOSINT M280 system. A back-and-forth scanning by strips with the hatch distance of 100 µm was applied for manufacturing specimens. The substrate and powder materials were similar in chemical composition. Argon was used as the protective atmosphere.

Numerical simulation of laser melting of Ti6Al4V alloy

When the laser beam scans the surface of the solid sample, the evolution of the temperature due to heat conduction can be estimated from (1):

$$\rho c_p \frac{\partial T}{\partial t} - \nabla(k\nabla T) = Q \qquad (1)$$

T is the temperature, t is the time, ρ is the density of material, (c_p) is the specific heat capacity, k is the thermal conductivity, Q is the source term, i.e. power absorbed from the laser beam. The laser beam intensity had a Gaussian profile. Equation (1) takes into consideration only the effect of conduction into a solid (Sanders, 1984). For numerical simulations, properties of Ti6Al4V are temperature-dependent (Mills, 2002; Boivineau *et al.*, 2006; Hodge *et al.*, 2014). Temperature-dependent specific heat capacity (c_p) was selected with respect to latent heat of fusion.

Marangoni flow which occurs due to a local difference in the surface tension of the liquid, can contribute significantly to temperature distribution and the shape of molten pool (Davis, 1987; Edwards *et al.*, 1991; Sternling *et al.*, 1959; Limmaneevichitr and Kou, 2000). Effective thermal conductivity of the liquid metal has been introduced by Kim *et al.* 2003, Zhang *et al.* 2004, He *et al.*, 2003 for taking into account changing in heat balance due to flows. For Ti6Al4V alloy the effective thermal conductivity of the liquid metal was introduced as a value multiplied by a factor of 1.5-3. Except for the top surface, all other boundaries are assumed to be thermally insulated. The heat flux on the top surface simulates convective cooling (Eq. 2). Heat losses due to convection is expressed by

$Q_c=h_c(T-T_o)$ (2)

where T_0=293 K is initial temperature, h_c = 10 W/(m^2×K) is convection coefficient.

To validate the model, the actual experimental true temperatures from Yadroitsev *et al.* (2014) were used as input for the simulation. 4 scan lines were simulated. 3D numerical simulation of the laser processing was carried out using the COMSOL 5.1 (COMSOL, Inc.) a heat transfer module. In order to obtain accurate results, the density of the mesh in the region around the irradiation, and on the top region of the sample (100 μm), was higher than in the sample as a whole, the minimal mesh size was 0.1 μm.

Residual stress measurements

The residual stress measurements were done with an X-ray diffractometer from ProtoXRD. The residual stresses were determined using the sin2 ψ method. The lattice deformations of the Ti-α were determined using a CuKα radiation source. Scans were performed around a {213} Bragg diffraction peak (2θ~139.69°) at 9 tilting angles ψ between –44.16+44.16°. The residual stresses were calculated considering plane stress conditions using X-ray elastic constants: -S_1= 2.83×10^{-6} MPa^{-1}; ½ S_2=11.89×10^{-6} MPa^{-1}.The electrolytic removal technique was used to determine in-depth residual stress distribution. Since the rotation of the scanning direction is the standard strategy incorporated by the EOS machine, principal stresses and their directions were analysed.

Roughness measurements

At prescribed Ti6Al4V process-parameters, the last layers of the parts are rescanned twice, without stripes, at 90° for each layer ("upskin" regime). Fig. 4.1.1 presents typical view of the top surface of the DMLS specimens.

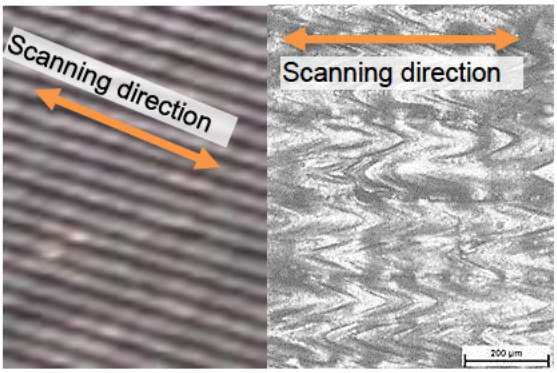

Fig. 4.1.1. Top surface of the samples.

Roughness was measured in perpendicular directions by a surface roughness tester Mitutoyo SJ-210 (ISO 1997).

4.1.4. Results and discussion

DMLS samples were produced at process-parameters and the strategy recommended by EOS for the M280 machine for Ti6Al4V powder. Layer thickness was 30 μm. Ten samples 10×10mm with prescribed thickness 0 (without powder), 1, 5, 10, 15 up to 40 layers and cubes 10×10×10mm with/without support structures were manufactured and analysed.

Fig. 4.1.2 shows the variation in average surface roughness with powder layer. After laser scanning of the smooth substrate, which has *Ra*=0.7±0.32 μm and *Rz*=4.0±1.83 μm, the roughness slightly increased. Delivering and laser scanning of the first layer significantly increases the surface roughness of the synthesized layer. Delivering of the first powder layer has some peculiarities: plate curvature (if existed), bias in mounting base plate (substrate) parallel to the horizontal level influence on the amount of the powder involved in synthesizing tracks of the first layer. With the delivering of subsequent layers the situation improves and from the 10th layer upwards the roughness is practically constant and its average was *Ra*=4.3±0.77 μm and *Rz*=22.1±3.79 μm.

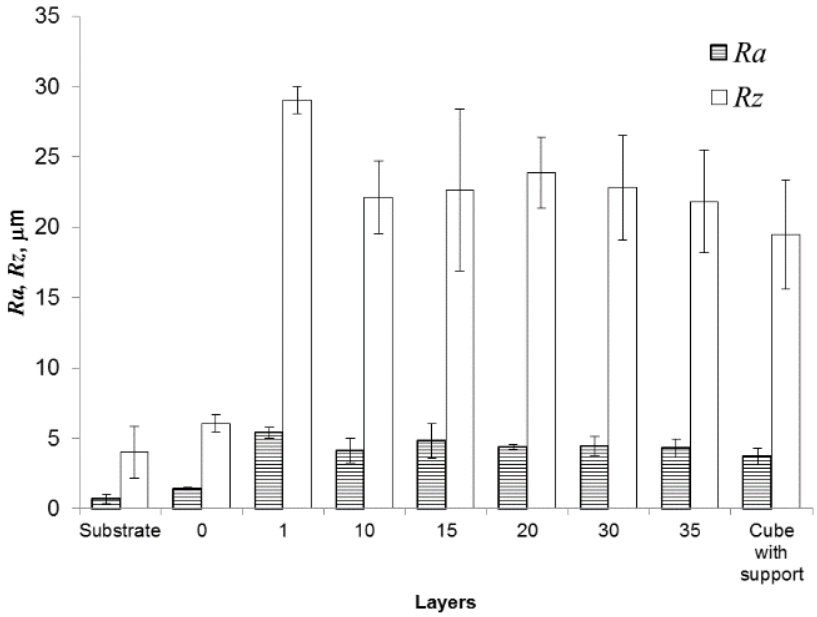

Fig. 4.1.2. Roughness of the DMLS samples.

Fig. 4.1.3 shows optical microscope photo of etched as-built Ti6Al4V specimen. As received martensitic α' microstructure is typical for Ti6Al4V samples manufactured by DMLS. In the built direction columnar growth is observed. The microstructure of the DMLS samples differs from the microstructure of wrought Ti6Al4V alloy since the cooling rates during DMLS reach 10^5–10^6 K/s (Rafi *et al.*, 2013).

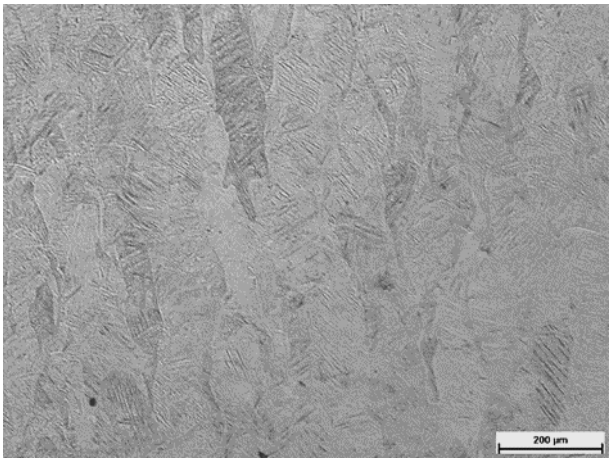

Fig. 4.1.3. Microstructure of as-built DMLS sample.

Temperatures during back-and-forth laser scanning of the Ti6Al4V sample with length of 1 cm, laser power density of 19.1 kW/mm^2 and scanning speed of 1.2 m/s at the top surface reaches about 3000 K, rapidly decreases to 400 K, then increases up to 1450 K during second scan (Fig. 4.1.4).

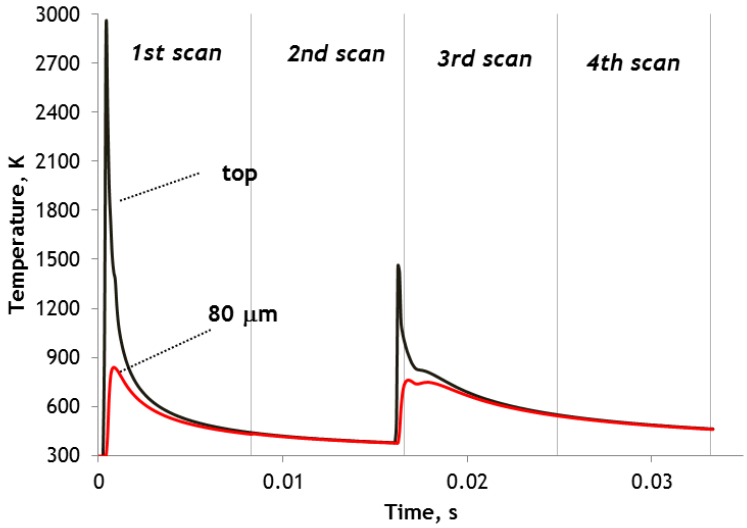

Fig. 4.1.4. Temperatures during back-and-forth laser scanning of the Ti6Al4V sample with length of 1 cm, the laser power density of 19.1 kW/mm2 and the scanning speed of 1.2 m/s; the hatch distance is of 100 µm.

Various layers of material cool down at different rates, therefore contraction also occurs at different speeds. During laser melting, high compressive and tensile stresses are present under the front of the molten pool (Yadroitsava *et al.*, 2015; Yadroitsev *et al.*, 2015). As a result, deformations in the surrounding material and the solidifying track occur.

Residual stresses measured by XRD method in the middle point near the surface of as-built DMLS samples, are shown in Fig. 4.1.5. Residual stresses were tensile and their values are significantly varied: from 800 MPa for major stress to 220 MPa for minor residual stress. No

significant correlation was found between the number of powder layers, the surface roughness and value of the maximum principal residual stresses.

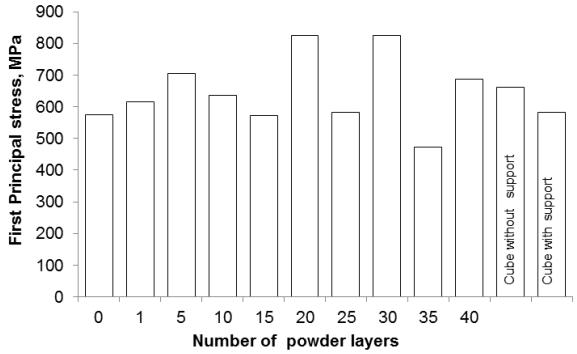

(a)

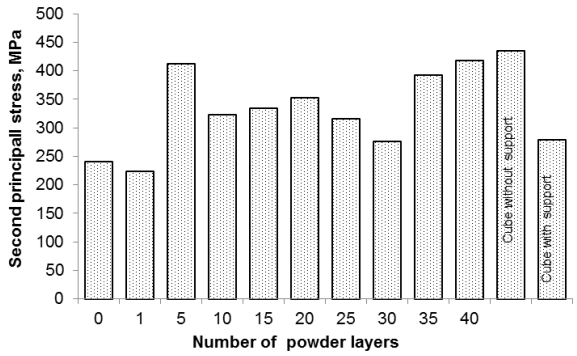

(b)

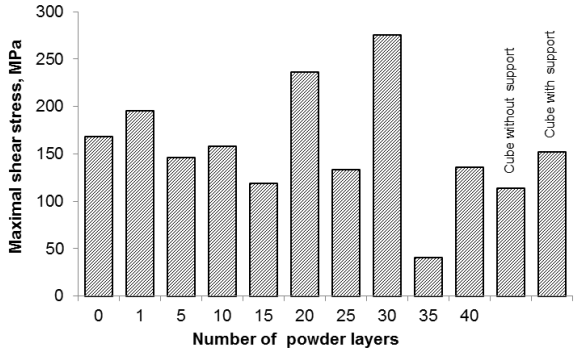

(c)

Fig. 4.1.5. Residual stresses on the top surface of the samples: maximal (a), minimal (b) and maximal shear stresses (c).

The direction of the maximal principal stress coincided with the direction of the laser scanning of each of the top layers. It was found, that the average maximum height of profile Rz correlated with second principal stress, which is perpendicular to the scanning direction. Coefficient of correlation was of – 0.8479 (Fig. 4.1.6).

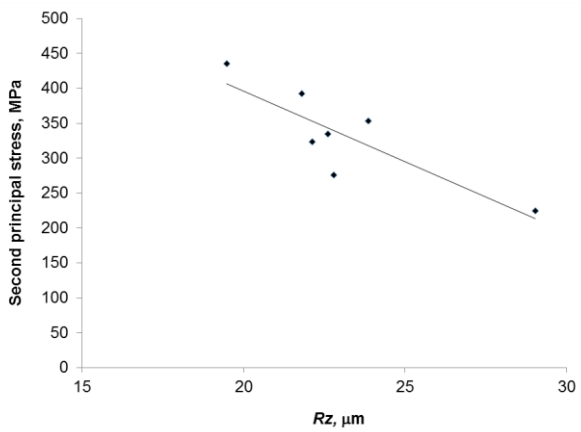

Fig. 4.1.6. Second principal stress versus *Rz* for powder layers.

Electrolytic removing of 15–80 µm was used to determine residual stresses of the samples consists of 1, 5, 25 and 40 layers. Results are shown in Fig. 4.1.7. After electrolytic removal of top layers, measured principal residual stresses were 630–150 MPa, which is lower than those measured near the surface.

The reason can be in-situ heat treatment happened during scanning of upper layers. As was calculated, due to thermal diffusivity at depth of 80 µm the temperature reaches about 840 K which is close to stress-relieving temperature 750-920 K (Fig. 4.1.4). Also, M280 machine applied different process-parameters and scanning strategy for top and inner layers. Different energy input can lead to different residual stresses. As indicated by Fitzpatrick *et al.* (2005), sources of uncertainty in residual stress measurements and the accuracy of calculations depends on elastic constants, non-linearity due to texture, stress gradients with depth and micro-stresses due to plastic deformation or grain interactions, etc. A surface roughness or interference of the sample geometry with the diffracted X-ray beam can result in systematic error in residual stress measurements (Prevéy, 1986).

Residual stresses near the surface of the cube produced without support (Fig. 4.1.8) were close to the values of 40-layers sample. Separation from the support structures during manufacturing of the cube (Fig. 4.1.8) indicates that during the process, at some point, the limit value of ultimate tensile strength for Ti6Al4V alloy (1.17 GPa), was exceeded. This, in turn, indirectly indicates that measurements were correct.

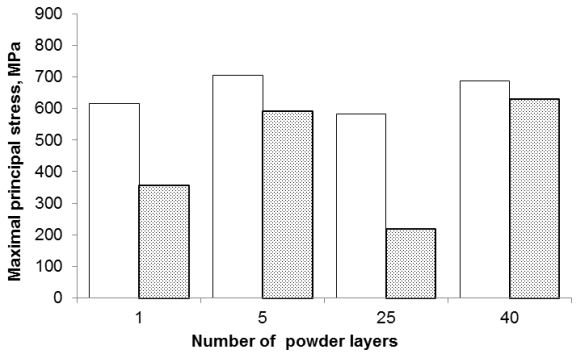

(a)

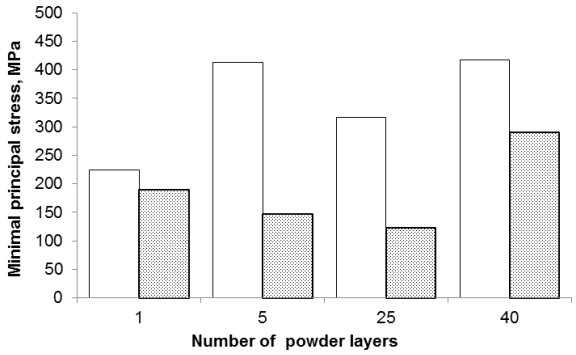

(b)

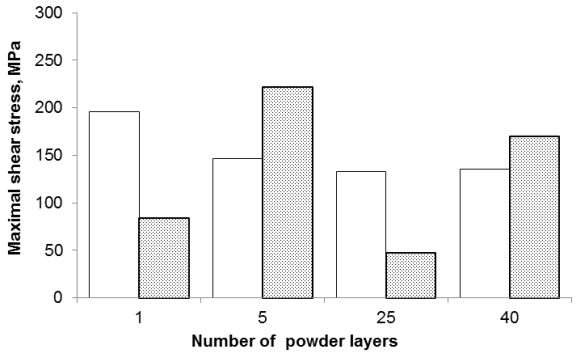

(c)

Fig. 4.1.7. Residual stresses on the top surface (white) and in depth of 15-80 μm (grey colour).

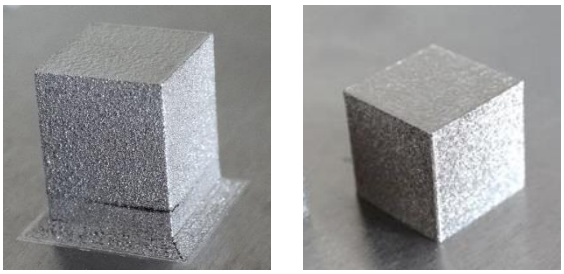

Fig. 4.1.8. Ti6Al4V cubes with/without support.

Conclusions

In the present work, experimentally measured residual stresses in DMLS specimens attached to the substrate were tensile and very high. XRD measured residual stresses had high variability, especially maximal shear stress. The direction of the maximal principal stress coincided with the direction of the laser scanning. The average maximum height of the surface profile correlated with the second principal stress, which is perpendicular to the scanning direction.

Acknowledgements

This work is based on the research supported by the South African Research Chairs Initiative of the Department of Science and Technology and National Research Foundation of South Africa (Grant №97994) and the Collaborative Program in Additive Manufacturing. This work benefited from the cooperation between the Central University of Technology, Free State and Nelson Mandela Metropolitan University (NMMU). Authors would like to acknowledge Director of eNtsa NMMU Prof. D.Hattingh for his help and wish to express their thanks to S. Grewar and R. Brown from NMMU for performing the XRD measurements.

References

Boivineau, M. Cagran, C. Doytier, D., Eyraud, V., Nadal, M.-H., Wilthan, B. and Pottlacher, G., 2006. Thermophysical properties of solid and liquid Ti-6Al-4V alloy, *International Journal of Thermophysics*, 27 (2), pp 507-529.

Davis S. H. 1987. Thermocapillary instabilities. *Ann. Rev. Fluid Mech.* 19, pp. 403–435.

Donachie, M.J. 2000. *Titanium: A Technical Guide*, 2nd Ed, Materials Park, Ohio: ASM International, Technology & Engineering.

Edwards D. A., Brenner H., Wassan D.T. *Interfacial transport processes and rheology*. Butterworth Heinemann, 1991.

Fitzpatrick M. E., Fry, A. T., Holdway, P., Kandil, F. A., Shackleton, J., Suominen, L. (2005). Determination of residual stresses by X-ray diffraction. *A National Measurement Good Practice Guide*, 52(2), 68 p.

Furumoto, T., Ueda, T., Abdul Aziz M.S., Hosokawa, A., Tanaka, R., 2010. Study on reduction of residual stress induced during rapid tooling process: influence of heating conditions on residual stress. *Key Engineering Materials*, 447-448, pp. 785-789.

He, X., Fuerschbach, P.W., DebRoy, T., 2003. Heat transfer and fluid flow during laser spot welding of 304 stainless steel, *J. Phys. D: Appl. Phys.* 36 , pp. 1388–98.

Hodge, N.E., Ferencz, R. M. and Solberg J. M., 2014. Implementation of a thermo-mechanical model for the simulation of selective laser melting, *Computational Mechanics*.

Kim, C.H., Zhang W., DebRoy, T., 2003. Modeling of temperature field and solidified surface profile during gas-metal arc fillet welding, *J. Appl. Phys.* 94, pp. 2667-79.

Limmaneevichitr C., Kou S. 2000. Visualization of Marangoni convection in simulated weld pools. *Welding Journal*. 79, pp. 126–135.

Limmaneevichitr C., Kou, S., 2000. Experiments to simulate effects of Marangoni convection on weld pool shape. *Welding Journal*. 79, pp. 231-237.

Mercelis, P. and Kruth, J.-P., 2006. Residual stresses in selective laser sintering and selective laser melting. *Rapid Prototyping Journal*, 12 (5), pp. 254 – 265.

Mills, K.C. 2002. Recommended values of thermophysical properties for selected commercial alloys. ASM International, Cambridge, England.

Prevey, P.S., 1986. X-ray diffraction residual stress techniques. *ASM International, ASM Handbook., 10*, pp.380-392.

Rafi, H.K., Karthik, N.V., Gong, H., Starr, T.L. and Stucker, B.E., 2013. Microstructures and mechanical properties of Ti6Al4V parts fabricated by selective laser melting and electron beam melting. *Journal of materials engineering and performance*, *22*(12), pp.3872-3883.

Sanders, D.J., 1984. Temperature distributions produced by scanning Gaussian laser beams. *Applied optics*, *23*(1), pp.30-35.

Shiomi, M., Osakada, K., Nakamura, K., Yamashita, T. and Abe, F., 2004. Residual stress within metallic model made by selective laser melting process. *CIRP Annals-Manufacturing Technology*, *53*(1), pp.195-198.

Sternling, C.A. and Scriven, L.E., 1959. Interfacial turbulence: hydrodynamic instability and the Marangoni effect. *AIChE Journal*, *5*(4), pp.514-523.

Yadroitsava, I., Grewar, S., Hattingh, D. and Yadroitsev, I., 2015. Residual Stress in SLM Ti6Al4V Alloy Specimens. In *Materials Science Forum*, 828, pp. 305-310. Trans Tech Publications.

Yadroitsev, I., Krakhmalev, P. and Yadroitsava, I. 2014. Selective laser melting of Ti6Al4V alloy for biomedical applications: temperature monitoring and microstructural evolution, *Journal of Alloys and Compounds*, 583, pp 404-409.

Yadroitsev, I., Yadroitsava, I. (2015). Evaluation of residual stress in stainless steel 316L and Ti6Al4V samples produced by selective laser melting, *Virtual and Physical Prototyping*.

Zhang, W., Kim, C.H. and DebRoy, T., 2004. Heat and fluid flow in complex joints during gas metal arc welding—Part II: Application to fillet welding of mild steel. *Journal of Applied Physics*, *95*(9), pp.5220-5229.

4.2. Tensile properties and microstructure of standard vertical and horizontal DMLS Ti6Al4V (ELI) samples

4.2.1 Abstract:

Direct metal laser sintering is an additive manufacturing technology where powder is melted/solidified by laser beam layer-by layer to produce complex components. Due to the fast heating/cooling during the process, the DMLS microstructure differs from cast/wrought Ti6Al4V alloy. Track-by-track, layer-by layer DMLS method also has an effect on mechanical properties of the samples. The aim of this work is to study the influence of DMLS process build strategy on mechanical properties of Ti6Al4V samples. The vertical and horizontal DMLS blocks were machined for tensile testing. Microstructure and tensile mechanical properties were analysed.

4.2.2 Introduction

Titanium alloys are strong, lightweight, corrosion resistant, cost-efficient, non-toxic, biocompatible, long-lasting, non-ferromagnetic, they have osseointegration capabilities, flexibility and elasticity (Hanawa, 2010; Clinning, 2012). Ti6Al4V is α/β alloy that is heat treatable to achieve the desired mechanical properties (Donachie, 2000).

As built Ti6Al4V DMLS objects have fine martensitic microstructure which has an influence on the following mechanical properties: the yield strength is high and the ductility is quite low. It was shown that a combination of martensite microstructure and residual stress is responsible for low ductility at DMLS as built samples (Vrancken *et al.*, 2012; Becker *et al.*, 2015; Facchini *et al.*, 2010). Shunmugavel *et al.* (2015) found that DMLS Ti6Al4V has higher yield strength and ultimate tensile strength compared to its wrought counter parts but inferior in ductility. Post-processing heat treatment from different research showed the improvement of mechanical properties due to stress-relieving or transformation of microstructure under different temperatures (Thone *et al.*, 2012; Becker *et al.*, 2015). Table 4.2.1 below shows the mechanical properties of Ti6Al4V (ELI) samples with different building directions.

Table 4.2.1. Properties of as-built and annealed DMLS vertical and horizontal Ti6Al4V (ELI) samples at different process-parameters

Process	UTS, MPa	YTS, MPa	E, GPa	Elongation at break, %	Microstructure	Source
vertical						
As-built	1051	736	110	11.9	martensitic α', column width < 0.5 µm	Kasperovich & Hausmann (2015)
Heat treated at 700°C	1115	1051	117.4	11.3	martensitic α', column width <1 µm	
Heat treated at 900°C	988	908	118.8	9.5		
As-built	-	1106±6		11±0.4	lamellar	Xu et al (2015)
horizontal						
As-built	1267±5	1110±9	109.2±3.1	7.28±1.12	martensitic, acicular α'	Vrancken *et al.*, (2012)
Heat treatment 3 h at 705°C, air cooling	1082±34	1026±35	114.6±2.2	9.04± 2.03		
As-built, preheating 500°C	1206±8	1137±20	105±5	7.6±2	martensitic, acicular α'	Vilaro *et al.*, (2011)
Annealing at 730°C 2 hours, air cooling	1046±6	965±16	101±4	9.5±1	martensitic, needle α' phase embedded in α+β phases	
ASTM F136-14	Min 825	Min 760		Min 8		

4.2.3 Materials and methods

Powder and manufacturing of the DMLS samples

A chemical composition of the employed spherical argon-atomized Ti6Al4V (ELI) powders from TLS Technik is indicated in Table 2. The 10th, 50th and 90th percentiles of equivalent diameter (weighted by volume) of the powder particles were d_{10}=11.2 µm, d_{50}=20.6 µm and d_{90}=31.8 µm for horizontal samples and d_{10} = 13 µm, d_{50}= 23 µm and d_{90} = 37 µm for vertical ones.

Table 4.2.2. Chemical composition of employed powders (wt. %)

	Ti	Al	V	O	N	H	Fe	C	Y
Horizontal	Bal.	6.44	3.99	0.12	<0.002	0.001	0.19	0.007	<0.001
Vertical		6.34	3.94	0.058	0.006	0.001	0.25	0.006	<0.001

20 vertical and horizontal rectangular blocks Ti6Al4V (ELI) were produced by the EOSINT M280 system. A back-and-forth (zig-zag) scanning by strips with the hatch distance of 100 µm was applied. The substrate and powder materials were similar in chemical composition. All blocks were built without supports, directly on the substrates. Argon was used as the protective atmosphere; the oxygen level in the chamber was 0.07–0.12%. A first set of as-built bars were cut off from the substrates; a second sets of specimens remained on substrates were heat treated in Ar atmosphere at 650°C (3 hours).

Tensile tests

Round metal specimens with threaded ends were machined from DMLS rectangular bars 10 mm×10 mm×60 mm in size according to geometry recommended by ASTM E8M standard (gauge length four times the diameter). Tensile tests were performed with an Instron 1342 servo-hydraulic testing machine with clip-on extensometer of 12.5 mm and under constant strain rate of 1.5 mm/min.

4.2.4 Results

Mechanical properties results

Figure 4.2.1 shows the mechanical properties of 5 as-built samples compared to the 5 stress relieved specimens. The yield strength for both cases increase approximately the same and the difference it's the ultimate strength. It is observed that the as built samples had high maximum strength compared to the stress relived specimens. Repeatability of the mechanical properties in each series of the experiments was very high, coefficient of variations were less than 0.1% for all measured values.

From the stress-strain graphs (Fig. 4.2.2), it is clear that the as built horizontal samples have slightly higher values if compared with the vertical samples. After stress relieving heat treatment both values for the horizontal and vertical were reduced, but it was higher than minimum requirements of ASTM standard for cast Ti6Al4V (ELI) material for biomedical applications.

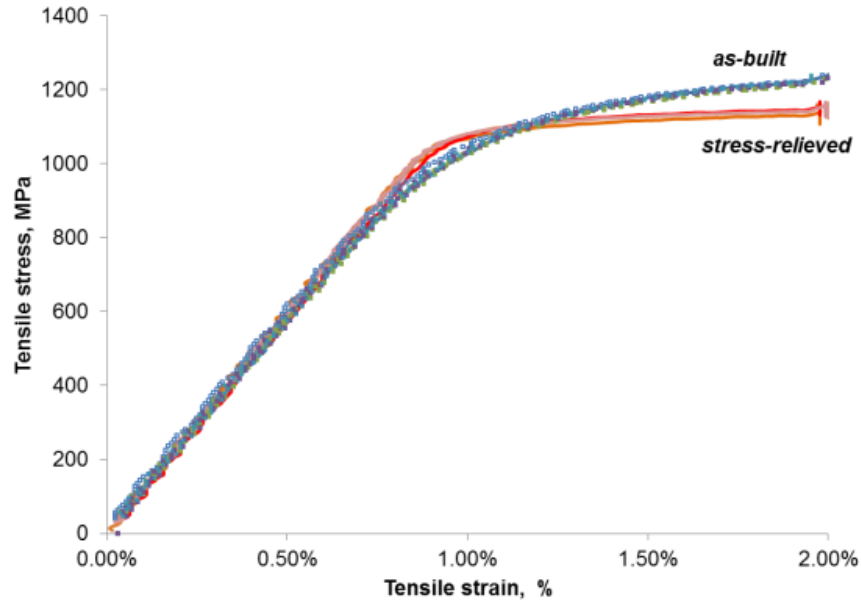

(a)

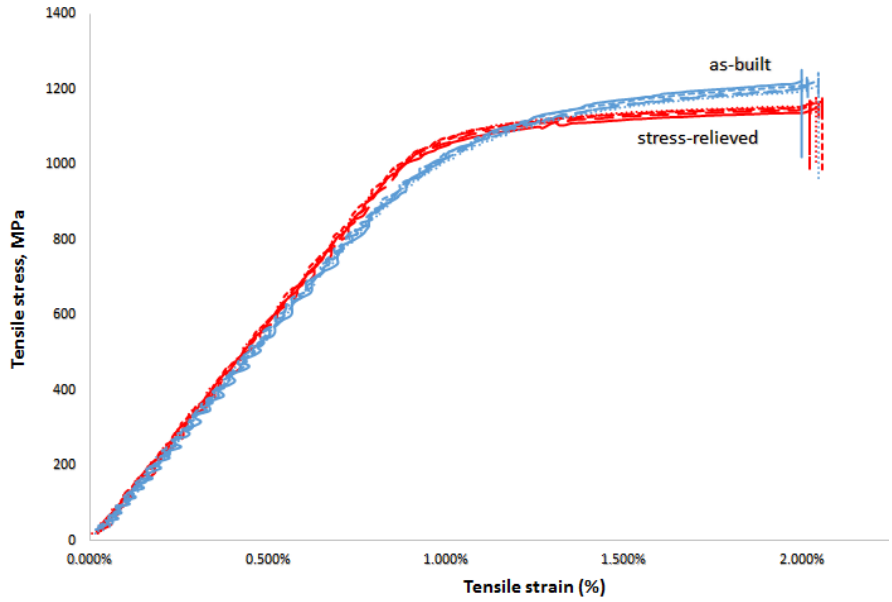

(b)

Fig. 4.2.1. The stress strain diagrams for horizontal (a) and vertical (b) as built and stress relieved samples.

A lack of fusion between tracks and/or stripes and/or islands can be critical in terms of ductility. For vertically fabricated samples, interlayer pores play a role of stress concentrators also deteriorating properties (Beese *et al.*, 2016). When DMLS process is stable, increasing the number of layers has no effect on ductility of the vertical and horizontal samples. In the present case, as built vertical samples were even more ductile in comparison with horizontal ones (Fig.4.2. 3). It can be the result of lower level of oxygen in initial powder material for vertical samples,

peculiarities of the geometry of the primary beta grains or martensitic colonies for different building directions. These hypothesis should be subject to further studies.

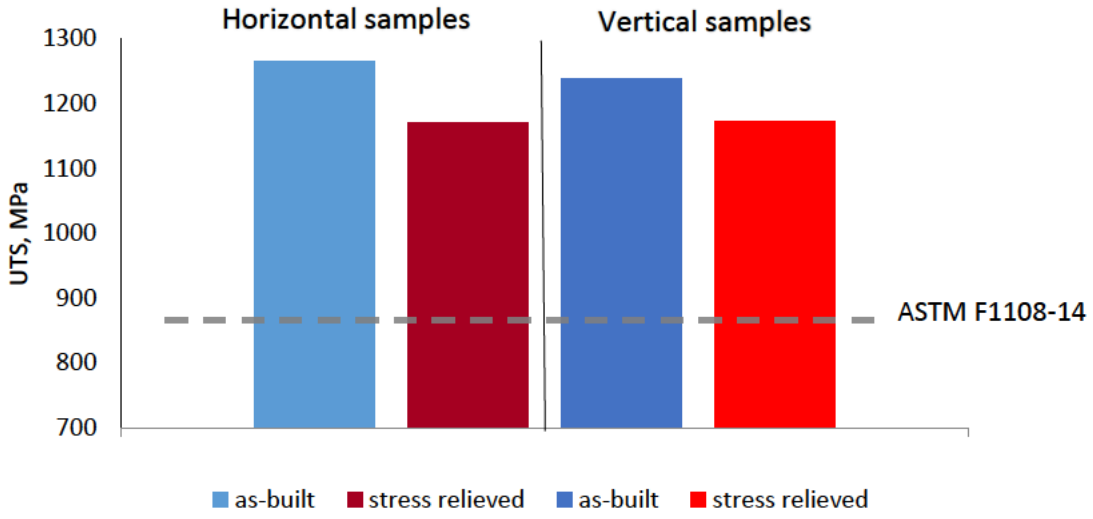

Fig. 4.2.2. Ultimate tensile stresses for horizontal and vertical samples.

Due to the rapid heating/cooling during DMLS, as-built Ti6Al4V samples had martensitic microstructure which increased tensile strength. Any visible difference in the microstructure of as-built and stress-relived samples have not been found by analysis of cross-sections by optical microscope. The elongation found for both built direction exceed 8% biomedical standards minimum requirements (Fig.4.2. 3, Table 4.2.1).

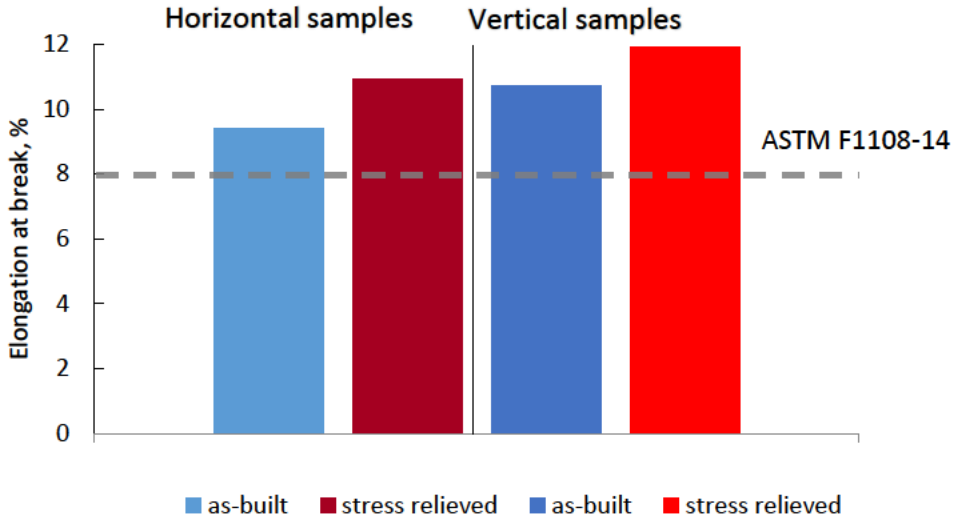

Fig. 4.2.3. Elongation at break for horizontal and vertical samples.

Analysis of fracture surfaces

The surface fracture were analysed for as built both horizontal and vertical and middle part of the fracture showed the irregularities. Surface analysis showed typical cup and cone fracture for as built horizontal and vertical specimens (Fig. 4.2.4). This type of fracture is commonly classified as ductile, which is confirmed by observation of micro-dimples at the fracture. Nevertheless, quasi-cleavage facets features of brittle fracture were observed also (Fig. 4.2.5).

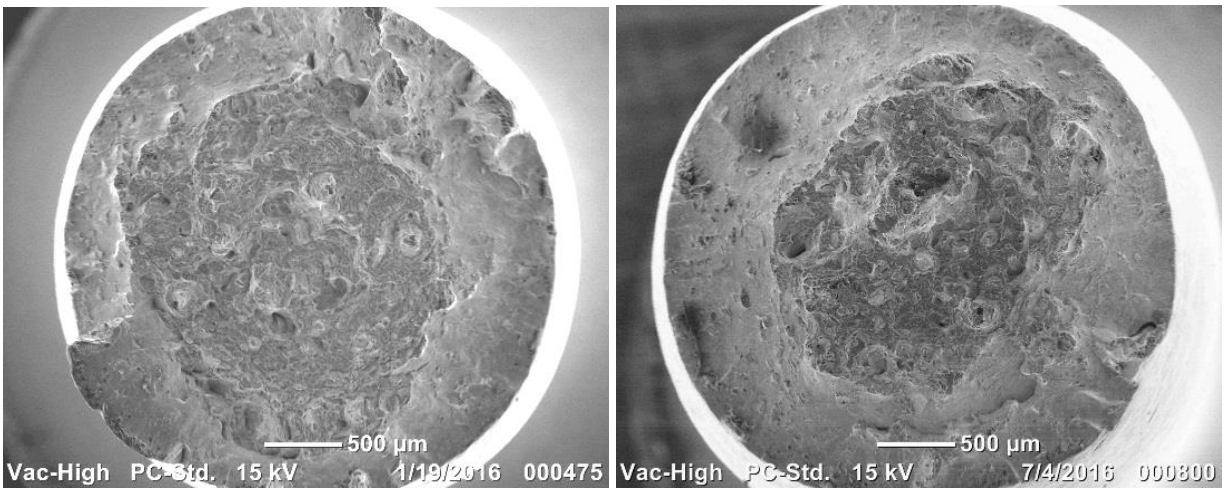

(a) (b)

Fig. 4.2.4. Fractured surfaces of horizontal (a) and vertical (b) samples.

Comparison of the microstructure and fracture surfaces in corresponding directions showed that when the crack reaches a pore, primary beta grain boundary or fusion boundary, the direction of crack grow was changed (Fig. 4.2.5). Higher magnification analysis showed that quasi-cleavage surfaces were formed when the crack propagates along martensitic colonies (Fig. 4.2.5, 4.2.6). Thus the interface acts as a crack deflector preventing quick failure of DMLS Ti6Al4V ELI samples.

Conclusion

The fracture analysis showed that DMLS material has complex tensile behaviour: neck creation and cup and cone fracture is typical for ductile material and quasi-cleavage facets featured for brittle material. The vertical samples were slightly more ductile as compared with horizontal samples. The process parameters used for vertical and horizontal build samples were the same, according to the results it shows the build direction does not affect significantly mechanical properties of the DMLS samples. The stress-relieved DMLS samples have good tensile properties that correspond to ASTM standard for biomedical applications.

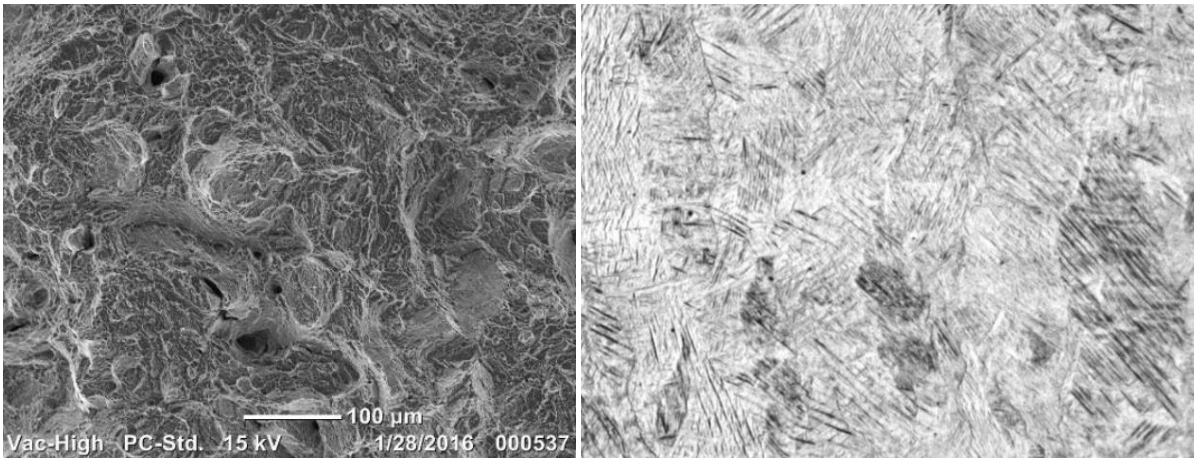

(a) (b)

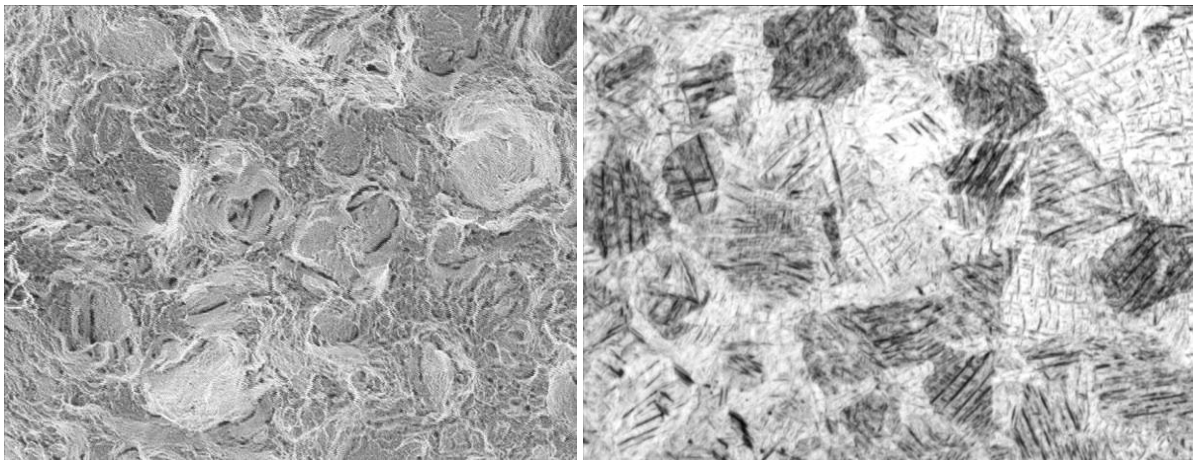

(c) (d)

Fig. 4.2.5. Fractured surface of horizontal and vertical samples (a, c) and microstructure of the samples at *zy* (b) and *zy* (d) cross-sections.

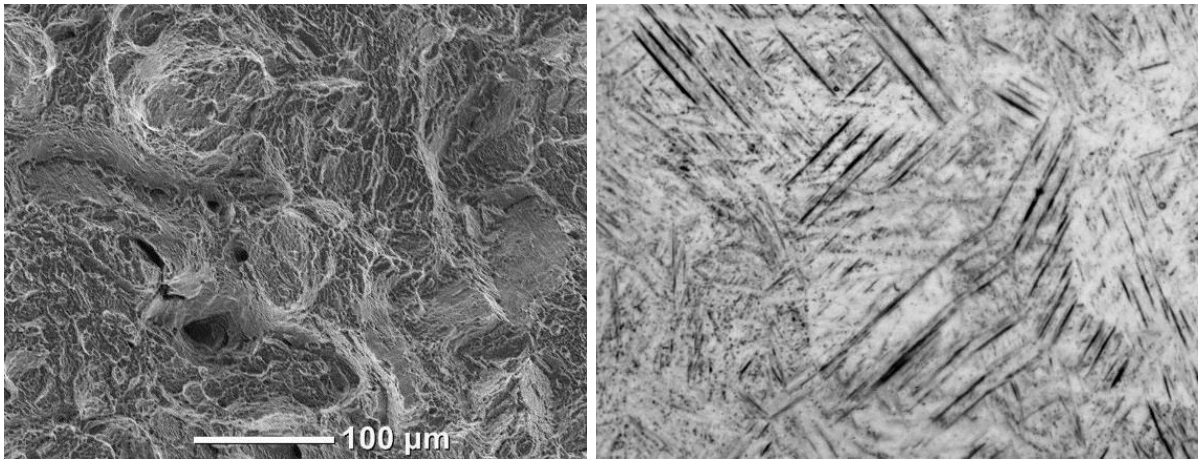

(a) (b)

Fig. 4.2.6. Fractured surface of horizontal sample (a) and microstructure of the sample of *zy* cross-section (b) at high magnification.

Acknowledgements

This work is based on the research supported by the South African Research Chairs Initiative of the Department of Science and Technology and National Research Foundation of South Africa (Grant №97994) and the Collaborative Program in Additive Manufacturing (Contract №CSIR-NLC-CPAM-15-MOA-CUT-01). Mechanical testing has been performed in mechanical testing laboratory in CSIR and authors are grateful to Chris McDuling. The authors also wish thanks to CRPM for manufacturing DMLS samples.

References

Becker, T., van Rooyen, M. & Dimitrov, D., 2015. Heat treatment of Ti-6Al-4V produced by lasercusing. *South African Journal of Industrial Engineering*, 26(2), pp. 93-103.

Beese, A.M., Carroll, B.E. 2016. Review of mechanical properties of Ti-6Al-4V made by laser-based additive manufacturing using powder feedstock. *JOM*, 68, 724-734.

Clinning, N., 2012. Thermomechanical processing of blended elemental powder Ti-6Al-4V alloy. *Masters Dissertation*, University of Cape Town, 146 p.

Donachie, M., 2000. *Titanium: A technical guide*. Materials Park, Ohio, ASM International, Technology & Engineering.

Edwards, P. & Ramulu, M., 2014. Fatigue performance evaluation of selective laser melted Ti–6Al–4V. Materials Science and Engineering: A, 598, pp.327-337.

Hanawa, T., 2010. Overview of metals and applications. In: *Metals for Biomedical Devices*. Woodhead, Cambridge, pp. 3-24.

Facchini, L., 2010. Ductility of a Ti6Al4V alloy produced by selective laser melting of pre-alloyed powders. *Rapid Prototyping Journal*, 16(6), pp. 450-459.

Shunmugavel, M., Polishetty, A. & Littlefair, G., 2015. Microstructure and mechanical properties of wrought and additive manufactured Ti-6Al-4V cylindrical bars. *Procedia Technology*, 20, pp. 231-236.

Thöne, M., Leuders, S., Riemer, A., Tröster, T. & Richard, H.A., 2012. Influence of heat-treatment on selective laser melting products–e.g. Ti6Al4V. *In: Solid freeform fabrication symposium*, Austin Texas.

Kasperovich, G. & Hausmann, J., 2015. Improvement of fatigue resistance and ductility of TiAl6V4. *Journal of Materials Processing Technology*, 220, pp. 202-214.

Rafi, H.K., Karthik, N.V., Gong, H., Starr, T.L. & Stucker, B.E., 2013. Microstructures and mechanical properties of Ti6Al4V parts fabricated by selective laser melting and electron beam melting. *Journal of Materials Engineering and Performance*, 22(12), pp.3872-3883.

Leuders, S., Thöne, M., Riemer, A., Niendorf, T., Tröster, T., Richard, H.A. & Maier, H.J., 2013. On the mechanical behaviour of titanium alloy TiAl6V4 manufactured by selective laser melting: Fatigue resistance and crack growth performance. *International Journal of Fatigue*, 48, pp.300-307.

Vandenbroucke, B. & Kruth, J.P., 2007. Selective laser melting of biocompatible metals for rapid manufacturing of medical parts. *Rapid Prototyping Journal*, 13(4), pp.196-203.

Vrancken, B., Thijs, L., Kruth, J. & Van Humbeeck, J., 2012. Heat treatment of Ti6Al4V produced by Selective Laser Melting: Microstructure and mechanical properties. *Journal of Alloys and Compounds*, 541, pp. 177-185.

Vilaro, T., Colin, C. & Bartout, J. D**.** 2011. As-fabricated and heat-treated micro- structures of the Ti-6Al-4V alloy processed by selective laser melting, *Metallurgical and Materials Transactions A*, 42(10), pp. 3190-3199

Xu, W., Brandt, M., Sun, S., Elambasseril, J., Liu, Q., Latham, K., Xia, K. & Qian, M., 2015. Additive manufacturing of strong and ductile Ti–6Al–4V by selective laser melting via in situ martensite decomposition. *Acta Materialia*, 85, pp.74-84.

4.3. Tensile properties and microstructure of direct metal laser sintered Ti6Al4V (ELI) alloy

4.3.1. Abstract

Direct metal laser sintering (DMLS) is an additive manufacturing technology used to melt metal powder by high laser power to produce customised parts, light-weight structures, or other complex objects. During DMLS, powder is melted and solidified track-by-track and layer-by-layer; thus, building direction can influence the mechanical properties of DMLS parts. The mechanical properties and microstructure of material produced by DMLS can depend on the powder properties, process parameters, scanning strategy, and building geometry. In this study, the microstructure, tensile properties, and porosity of DMLS Ti6Al4V (ELI) horizontal samples were analysed. Defect analysis by CT scans in pre-strained samples was used to detect the crack formation mechanism during tensile testing of as-built and heat-treated samples. The mechanical properties of the samples before and after stress relieving are discussed.

4.3.2. Introduction

Direct metal laser sintering (DMLS) can significantly influence the performance of implants from biocompatible alloys because this additive manufacturing technology is able to manufacture customised shape parts, light-weight structures, or other complex objects from metal powder by laser. The DMLS object consists of many tracks and layers having metallurgical contact with each other, and its microstructure is a result of multiple rapid heating-melting-solidification cycles. The complex microstructure of DMLS alloys, which is different from cast/wrought material, is a result of the different phases in the material, the solidification texture caused by the nature of manufacturing (track-by-track and layer-by-layer), residual stresses arising at high thermal gradients and thermocycling, and the high probability of pore formation in the case of non-stable process parameters. Mechanical properties depend not only on the material, but also on the laser's process-parameters, the building and scanning strategies, the powder layer's thickness, and the protective atmosphere.

Titanium and its alloys are widely used as biomaterial because they have low weight and high strength, good fracture toughness, and high corrosion resistance. The protective and stable oxides on the titanium surface are able to provide osseointegration, which is favourable for the structural and functional connection between bone and implant (de Viteri & Fuentes, 2013).

The mechanical properties of two-phase titanium alloys, like Ti6Al4V, strongly depend on the number, distribution and morphology of the phases (Donachie, 2013; Boyer 1994). Ti6Al4V

with lamellar structures has high strength with some decrease in ductility and demonstrates good fracture toughness. Refinement of the microstructure results in a higher yield strength.

Table 4.3.1 shows the mechanical properties of the DMLS Ti6Al4V and Ti6Al4V (ELI) samples that were built horizontally. All the indicated sources showed that the as-built samples had a fine α' martensitic microstructure. High cooling rates at DMLS result in the formation of the acicular/lamellar α′ hexagonal martensitic phase in Ti6Al4V. At cross-sections along the building direction, columnar structures are clearly visible, whilst in the transverse direction, bundles of columnar grains can be seen. A martensitic α' microstructure is less ductile than the globular microstructure formed during conventional processing (Kasperovich & Hausmann, 2015). Strongly-textured structures can lead to significant anisotropic mechanical properties, causing different mechanical responses to external loading along different sample orientations (Xu *et al.*, 2015). Even for specimens built in the same direction, a discrepancy in the data for the mechanical properties of DMLS Ti6Al4V is 1.28 times for ultimate tensile strength (UTS), 1,407 versus 1,095 MPa, 1.35 times for yield strength (YS), 990 versus 1,333 MPa, and the difference is 4.25 times (2-8.5%) for elongation (Table 4.3.1). The coefficient of variation (CV), which represents the ratio of the standard deviation to the average, was up to 48 per cent for elongation at break.

According to the standard specifications for wrought Ti6Al4V (ELI) and cast Ti6AlV alloys for surgical implant applications (ASTM F136-13 and ASTM F1108-14), the elongation of the material should be at least 8 per cent (Table 4.3.1). The content of interstitials has a substantial influence on the mechanical properties of Ti6Al4V. As indicated by Boyer *et al.* (1994) and Donachie (2000), an oxygen content higher than 0.2 wt.% leads to a higher strength and a lower ductility in the Ti6Al4V alloy. A decrease in oxygen and nitrogen content improves the ductility, fracture toughness, stress-corrosion resistance, and resistance against crack growth. As published in the literature, the UTS for DMLS Ti6Al4V (ELI) horizontal samples varied from 1,206 to 1,267 MPa, with an average YS from 1,110 to 1,137 MPa, and a Young's modulus of 105-109 GPa (Vracken *et al.*, 2012; Vilaro *et al.*, 2011). After annealing at 730 °C for two hours and air cooling, needle α' phase embedded in α+β phases was found Vilaro *et al.*, (2011). No significant microstructural changes were identified after stress-relieving heat treatment at temperatures lower than 650 °C. UTS increased by 6 per cent (Becker *et al.*,2015) or decreased by 8 per cent (Mertens *et al.*, 2014) for Ti6Al4V alloy, and decreased by 15-17 per cent for Ti6Al4V ELI alloy (Vracken *et al.*, 2012;Vilaro *et al.*, 2011). After heat treatment, elongation was increased 3.7 times for Ti6Al4V and 1.25 times for Ti6Al4V (ELI).

Table 4.3.1. Tensile properties of as-built and annealed DMLS horizontal Ti6Al4V samples

Machine/Process-parameters (if indicated)	Ultimate tensile strength, MPa	Tensile yield, MPa	Elastic modulus, GPa	Elongation at break, %	Density	Microstructure	Source
Ti6Al4V alloy							
Experimental machine built at ILT	1140±10	1040±10		8.2±0.3	99.7 ±0.1	acicular α'	Facchini *et al.*,2010
EOSINT M270 Laser power, 195 W Scanning speed, 0.225 m/s	1095±10	990±5	110±5	8.1±0.3			Facchini *et al.*,2010
EOSINT M270	1248	1043	112	8.5			Frey *et al.*,2011
EOSINT M270	1269±9	1195±19		5±0.5		α' martensitic laths	Rafi *et al.*, 2013
EOSINT M270	1407	1333		4.54		α' plates	Murr *et al.*,2009
EOSINT M280 Standard process-parameters for 30 µm powder layer thickness	1155±20			4.1±2	99.79 ±0.2	fine acicular α' martensite	Becker *et al.*,2015
After stress-relieve heat treatment	1230±20			7.0±2			
MTT SLM 250 Laser power, 175 W, 2 mm FOD Scanning speed, 0.71 m/s Layer thickness, 30 µm Hatch distance, 120 µm	1321±6	1166±6	112	2±0.7	>99.5	α', no β-phase	Mertens *et al.*, 2014
Annealed 640°C for 4 h	1225±4	1104+8		7.4±1.6		No significant microstructural change	
Ti6Al4V (ELI)							
Laser power, 250 W Spot size, 52 µm Scanning speed, 1.6 m/s Layer thickness, 30 µm Hatch distance, 60 µm	1267±5	1110±9	109.2±3.1	7.28±1.12	fully dense	acicular α' martensitic	Vrancken *et al.*, 2012
Heat treatment 3 h at 705°C, air cooling	1082±34	1026±35	114.6±2.2	9.04± 2.03			
Trumpf LF250 Laser power, 200 W Spot size, 220 µm Scanning speed, 0.5 m/s Layer thickness, 30 µm Hatch distance, 200 µm Preheating 500°C	1206±8	1137±20	105±5	7.6±2		acicular α' martensitic	Vilaro *et al.*, 2011
Annealing at 730 °C during 2 hours, air cooling	1046±6	965±16	101±4	9.5±1		needle α' phase embedded in α+β	
Annealed wrought Ti6Al4V (ELI) ASTM F136-13	Min 825	Min 760		Min 8	Area reduction: Min 14-15%		

Thus the difference in the mechanical properties of the samples and a wide scatter of the data raises an urgent issue about the repeatability of the mechanical properties of TI6Al4V alloy, and the impact of porosity and the chemical composition on the mechanical properties of the DMLS samples. The purpose of the study is to investigate the microstructure and mechanical properties in as-built and stress-relieved conditions, and to compare them with the international

standards for biomedical applications. In-situ development of porosity at tension of Ti6Al4V (ELI) samples was used to determine fracture mechanisms for as-built and heat-treated specimens.

4.3.3. Materials and methods

Powder and manufacturing of the DMLS samples

The chemical composition of the employed spherical argon-atomised Ti6Al4V (ELI) (–45 µm) powder from TLS Technik was as follows in wt.%: Ti (bal.), Al (6.44), V (3.99), O (0.12), N(<0.002), H(0.001), Fe (0.19), C(0.007), and Y (<0.001). The chemical composition corresponds to the ASTM standard for Ti grade 23. The 10th, 50th, and 90th percentiles of the equivalent diameter (weighted by volume) of the powder particles were d_{10}=11.2 µm, d_{50}=20.6 µm, and d_{90}=31.8 µm respectively. The Ti6Al4V samples were produced by the EOSINT M280 system. A back-and-forth (zig-zag) scanning by strips with a hatch distance of 100 µm was applied when manufacturing the blocks. The blocks were built without supports, directly on the substrate. The substrate and powder materials were similar in chemical composition. Argon was used as the protective atmosphere; the oxygen level in the chamber was 0.07–0.12 per cent. A first series of as-built rectangular bars were cut off from the substrate; a second series of specimens remained on the substrate and were heat-treated in Ar argon atmosphere at 650°C (three hours) for stress relieving.

Microstructural analysis

Scanning electron microscopy (SEM) was carried out with the LEO 1350 FEG-SEM operated at 20 kV, and the NeoScope JCM 5000. Cross-sections of the samples were subjected to grinding with 320 SiC paper, then polishing by 9 µm diamond suspension and with 0.05 µm Silica. Cross-sections of the samples were etched in Kroll's reagent. Transmission electron microscopy (TEM) was done with JEOL JEM 2100, equipped with a LaB6 cathode and a digital camera Gatan SC1000 Orius, and JEM-200CX. Specimens for TEM were electro-chemically prepared.

Tensile tests

Round metal specimens with threaded ends were machined from DMLS rectangular bars 10 mm × 10 mm × 60 mm in size according to the geometry recommended by ASTM E8M standard (gauge length four times the diameter). Tensile tests were performed with an Instron 1342 servo-hydraulic testing machine with a clip-on extensometer of 12.5 mm and under a constant strain rate of 1.5 mm/min.

X-ray micro computed tomography

The samples were subjected to X-ray micro-computed tomography (MicroCT) (Du Plessis *et al.,* 2014). MicroCT scans were done with a General Electric Phoenix V|Tome|X L240 system at 160 kV and 200 µA, including beam filtering of 0.5 mm copper; the resolution was 10 µm. CT image reconstruction was done with system-supplied software that included beam hardening correction. All analyses were done with Volume Graphics VGStudioMax 2.2, including the defect analysis module and the nominal/actual comparison module. 3D image processing was done using morphological image operations to select the sample sub-surface by four voxels, in order to eliminate any edge noise effects. Therefore any voids touching the sample edge would not be included in the analysis up to four voxels (40 µm). Defect analysis is run with a minimum pore detection limit of eight voxels, a maximum pore size of 10 mm, and a probability of 1–3. MicroCT was used to visualise and quantify the necking effect on the tensile samples.

Design of the experiment with pre-strained samples

As-built (AB) and stress-relieved (SR) horizontal samples were tested to investigate such strength characteristics as YS, UTS, Young's modulus, elongation, and area reduction. Some stress-relieved specimens were pre-strained, and then porosity was investigated using the CT scanner (Fig. 4.3.1).

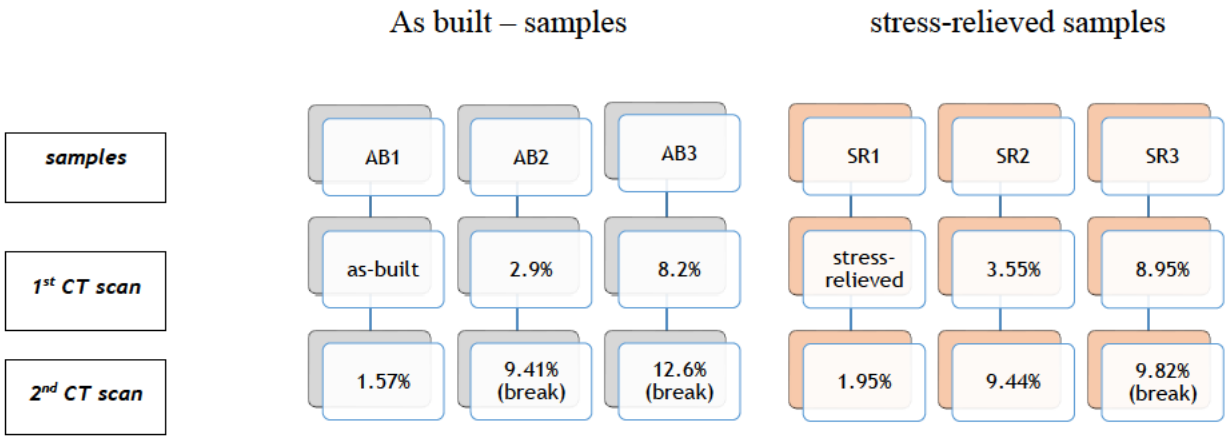

Fig. 4.3.1. Design of the experiment with the pre-strained tensile samples; resulted elongation is indicated.

4.3.4. Results and discussion

Microstructure

During DMLS, powder is melted and solidified track by track, layer by layer, thus building direction can influenced on the mechanical properties of DMLS parts. Since high thermal gradients

and thermal cycling lead to high residual stress, twinning was observed by TEM in the as-built material. The microstructure of the as-built Ti6Al4V alloy typically consists of α′ martensite. Solidification of molten alloy starts with the formation of the primary cubic beta phase. It has been shown that the as-solidified beta phase showed pronounced texture <100> (Antonysamy *et al.*, 2012). At rapid cooling below Ms temperature, beta is transformed to α′ martensite, which also has a crystallographic orientation relationship with the parental beta.

Fig.4.3.2 illustrates an EBSD orientation map of the as-built Ti6Al4V specimens. Inverse pole figure (IPS) components were used to colour the (a), (b), and (c) maps in Figure 2 so that the red, blue, or green colour corresponds to gains with <0001>, <10-10>, or <1-1-20> directions parallel to the axes *x,y , or z* respectively. Directions *x* and *y* are parallel to the laser scanning directions and form a horizontal plane, while direction *z* is the building direction. It is seen that, although the grain boundaries of the primary beta phase were easily distinguished, no obvious textures were observed in the α′ martensitic phase. Image analysis showed that the lamella thickness was in the range of 1.9-2.3 μm. Additionally, no beta phase was observed in the as-built alloy, by neither TEM nor EBSD methods. The results of the EBSD analysis carried out in the present investigations agreed well with the weak texture of α′ observed by Simonelli *et al.* (2014a), who explained weak texture observed in α′ by a high number of variants that α′ could precipitate within each prior beta grain.

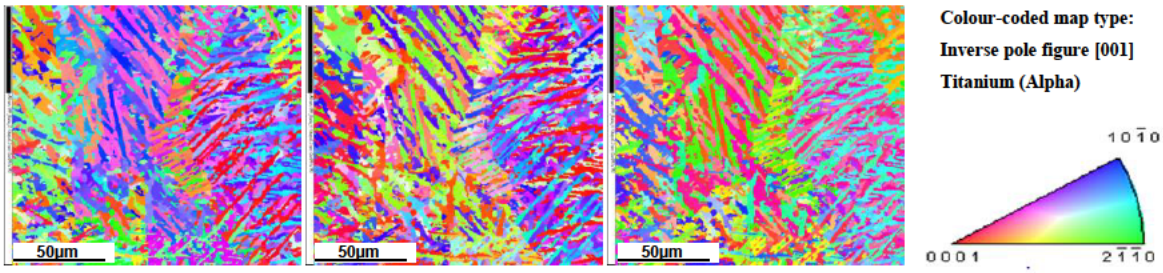

(a) (b) (c)

Fig.4.3.2. IPF EBSD orientation map ,<0001>,<10-10> or <2-1-10> directions parallel to (a) *x* direction (b) *y* direction and (c) *z* (building) direction.

Heat treatment in the α+β region commonly leads to a decomposition of the martensite. Nevertheless, stress relief of Ti6Al4V at 650°C for three hours only slightly influenced the microstructure. Although some changes in the morphology hexagonal phase were observed and a number of indexed by EBSD high-angle boundaries were detected, no remarkable increase in an average thickness of lamella was observed (see Figures 4.3.3a-c). Analysis of the results of the transmission electron microscopy of the Ti6Al4V specimens in stress-relieved conditions revealed

the presence of very small globular grains of the alpha phase formed after the heat treatment. It indicates that new grains nucleation and growth processes had already started in the microstructure after three hours at 650°C. Nevertheless, only a few globular grains were observed in the TEM in this investigation, and none of them exceeded 500 nm in size. However, TEM, EBSD, and XRD carried out in the present research did not reveal the formation of detectable amounts of beta phase in the stress-relieved specimens.

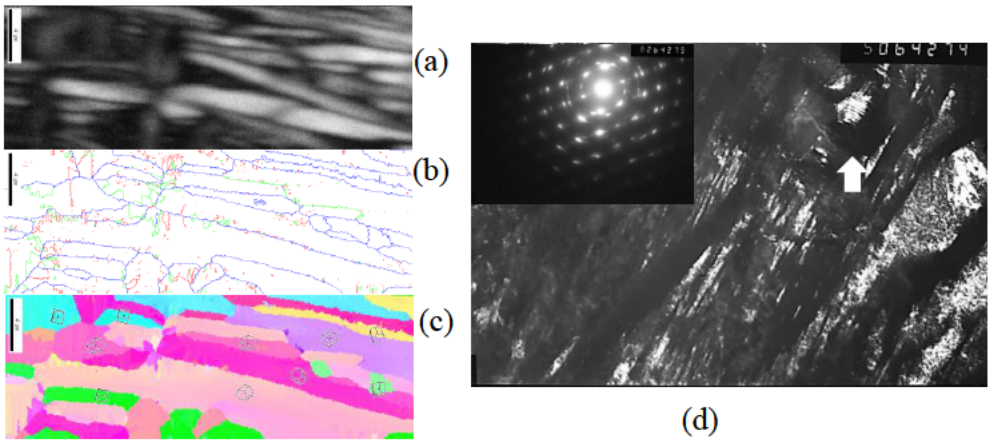

Fig.4.3.3. (a) SEM image, (b) grain boundary reconstruction, and (c) IPF EBSD orientation map of Ti6Al4V stress-relieved at 650°C for three hours; (d) the dark-field TEM image of stress-relieved Ti6Al4V made in (110) hcp reflex.

The experimental observations differed from the results presented by various authors (Vracken *et al.*, 2012; Vilaro *et al.*, 2011; Sallica-Leva *et al.*,2016; Simonelli *et al.*, 2014a), where the decomposition of martensite and formation of the beta phase started after stress-relief treatment at 730-800°C for 1-2 hours. A reason for the deviation could be that the stress-relief heat treatment was done at temperatures remarkably higher than those in the present work. It also agrees well with the DCS analysis carried out by Sallica-Leva (2016), which has shown that $\alpha' \rightarrow \alpha+\beta$ decomposition takes place in a temperature interval of 760-850°C, while the stress relief occurred between 440 and 590°C. Nevertheless, Sallica-Leva (2016) has also shown the presence of the beta phase already after treatment for 2 hours at 650°C. This contradiction could be explained by taking into account the thermal history of the material manufactured by SLM/DMLS. It has been shown that, when depending on manufacturing regimes, the final structure is subjected to different conditions of in-situ cycling reheating, which influences the microstructure of the material (Xu *et al.*, 2015; Simonelli *et al.*, 2014b).

Mechanical properties

In the present investigations, 0.19 wt.% oxygen and 0.058 wt.% nitrogen were measured in the DMLS specimens, which is slightly higher than the nominal content. The experimentally-observed mechanical properties were similar to the ones summarised in Table 4.3.1. The tensile stress–strain curves of the as-built and stress-relieved Ti6Al4V are shown in Figure 4, and are summarised in Table 4.3.2. It was found that the as-built and stress-relieved samples had higher YS and UTS than annealed wrought Ti6Al4V (ELI) (Table 4.3.1). As can be seen from Fig. 4.2.1 (a), the differences in the mechanical properties of the horizontal specimens in each series were small, and the coefficients of variation were very low (Table 4.3.2).

Table 4.3.2. Tensile properties of horizontal DMLS Ti6Al4V (ELI) samples

Specimens	YTS (Offset 0.2 %), MPa	Modulus (Chord 200 MPa – 800 MPa), GPa	UTS, MPa	Elongation, % 4.D.	Area reduction, %
As-built					
average±S.D.	1098±2	112±2	1265±5	9.4±0.46	25.6±2.41
CV	0.002	0.02	0.004	0.05	0.09
Stress-relieved					
average±S.D	1098±5	117±2*	1170±6*	10.9±0.8*	29.3±0.78*
CV	0.005	0.02	0.005	0.07	0.03

*significant differences (*t-test*,$p<0.05$)

Vickers microhardness at 300 g load was measured on the as-built and stress-relieved specimens. The microhardness for different cross-sections was similar, and the values did not show any statistically significant difference (t-test, $p<0.001$) with reference to the building direction. The average value was 389±14.8 HV300 for the as-built samples, and the microhardness was slightly lower (374±17 HV300) for the stress-relieved samples. The stress-relieving heat treatment led to an increase in the area reduction from 25.6 per cent (AB samples) to 29.3 per cent (SR samples). The elongation was 9.4 per cent for the as-built Ti6Al4V samples, and increased to 10.9 per cent after the stress relief. These ductility properties satisfied the standards for medical applications.

Analysis of fracture surfaces

After the tensile tests, the fracture surfaces in the as-built and stress-relieved samples look like a 'cup and cone', which is characteristic for ductile types of the fractures (Fig.4.3.4a –b). The central area was clearly distinguished from the shear lips on the periphery. The fractured surface

in the central zone was irregular, not horizontal, with the formation of dimples (Figs. 4.3.4c–d). Although the dimple rupture dominated, quasi-cleavage facets features of a brittle kind were observed (Figs. 4.3.4e–f).

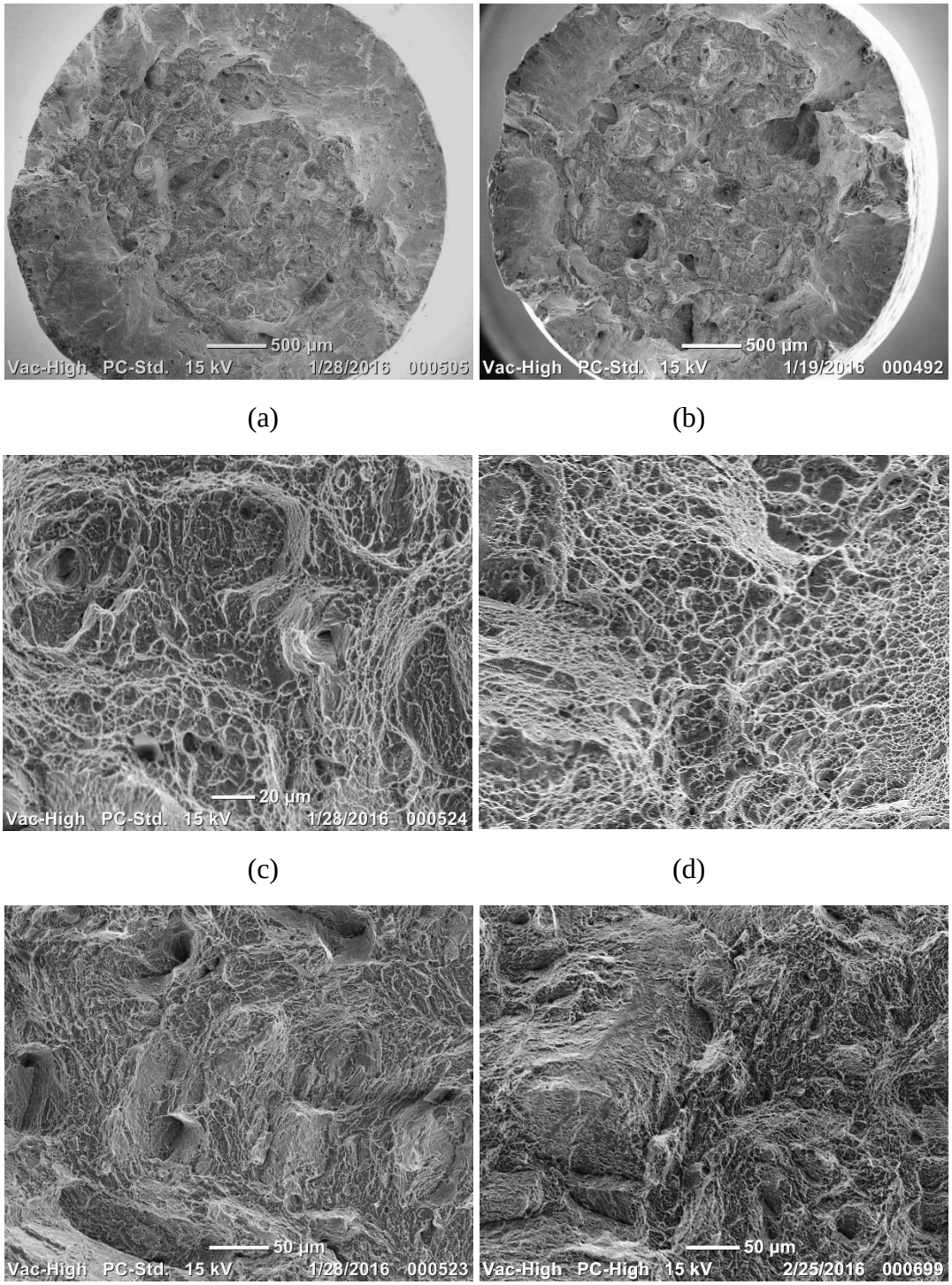

Fig.4.3.4. (a, b) Fracture surface cup-and-cone, (c, d) dimples, and (e, f) quasi-cleavage facets in as-built (a, c, e) and stress-relieved (b, d, f) samples.

High-magnification analysis showed that martensite needles are often visible on the quasi-cleavage surfaces. Therefore it is possible to confirm that these regions are formed when the crack propagates along a martensite colony. When the crack reaches a primary beta grain boundary or a fusion boundary, the growth direction is changed. The interface, therefore, acts as a crack deflector, preventing quick failure. This conclusion is in agreement with the results presented by Wen *et al.* (2014). Since the mechanisms of ductile fracture and the formation of a cup-and-cone shape in the necking region are usually associated with pore coalescence, a defect analysis by CT scans in the pre-strained samples was used to detect the crack formation mechanism.

Defect analysis and crack formation mechanisms

The process of defect analysis of the samples with a low level of porosity and small pores is a complex task in CT scans because small pores and the noise signal can be overlapped (Du Plessis *et al.*, 2015). Some pores can be missed due to contrast variations between the scans, and due to the metal type and size of the pores relative to the scan resolution. After DMLS at optimal process parameters, the Ti6Al4V (ELI) as-built and stress-relieved samples had low levels of porosity. In the as-built sample, 34 pores in total were found, which totalled 0.0022 per cent porosity. In the stress-relieved specimen, 40 pores were indicated and porosity was 0.0018 per cent. On the whole, pores were coarser, and a maximum pore size of 132 μm was measured in the as-built sample (Fig. 4.3.5). An analysis of the pore geometry showed that most estimated pores had an elongated shape (Fig. 4.3.5b); the sphericity factor for the as-built sample was 0.62±0.03 and 0.71±0.06 for the stress-relieved ones (for the ideal sphere, the sphericity factor is equal to 1.0). The biggest pores were elongated perpendicular to the building direction and can apparently be classified as interlayer pores.

To investigate the evolution of porosity, the development of pore size and morphology, and the influence of these parameters on mechanical behaviour, as-built and stress-relieved specimens were pre-strained to 1.57–9.44 per cent (Fig. 4.3.1). The morphology of the pores and their size were substantially changed after pre-strain (Fig. 4.3.5–4.3.8). In the pre-strained samples, pores look like an agglomerate of several pores. Some pores were interconnected with quite thin channels, possibly cracks (Figs. 4.3.6–4.3.7). Pore coarsening has been observed in both as-built and stress-relieved specimens. Thus the AB3 sample, pre-strained up to 8.2 per cent, had the biggest pore size of 236 μm. The maximum pore sizes in the stress-relieved specimens deformed at 8.95-9.44 per cent, but still had integrity, and were 100-160 μm (Figures 4.3.6–4.3.8).

Generally, this behaviour is described by the cumulative curves presented in Fig.4.3.8. An analysis of the cumulative frequency distribution of the equivalent diameter in the pre-strained as-

built and stress-relieved samples showed that pores became bigger with strain (Fig. 4.3.8). Notably in the as-built specimen, pore growth is already clearly visible after 1.57 per cent strain, while in the stress-relieved specimen, some growth was observed in the 9.44 per cent strained specimen. This behaviour could be associated with residual stresses in the as-built specimens.

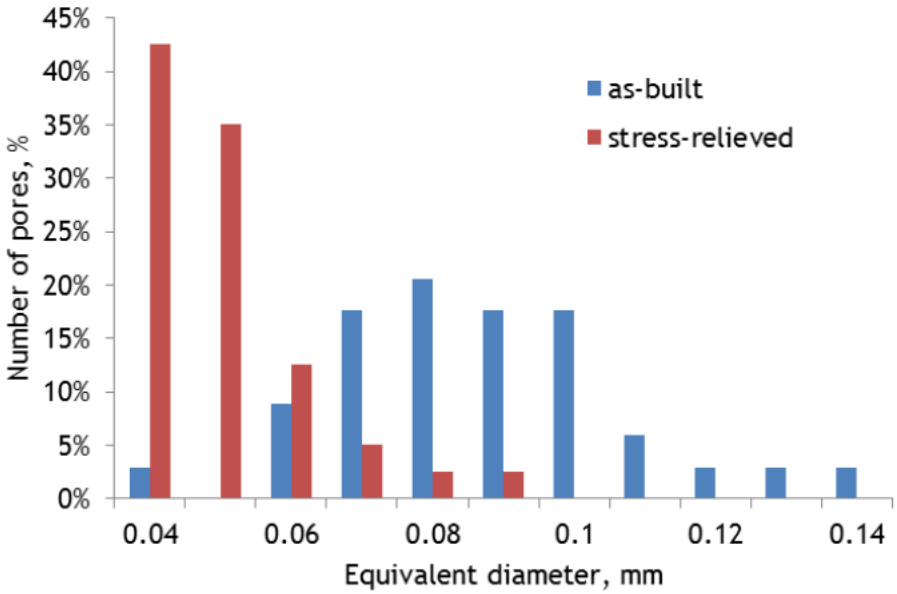

(a)

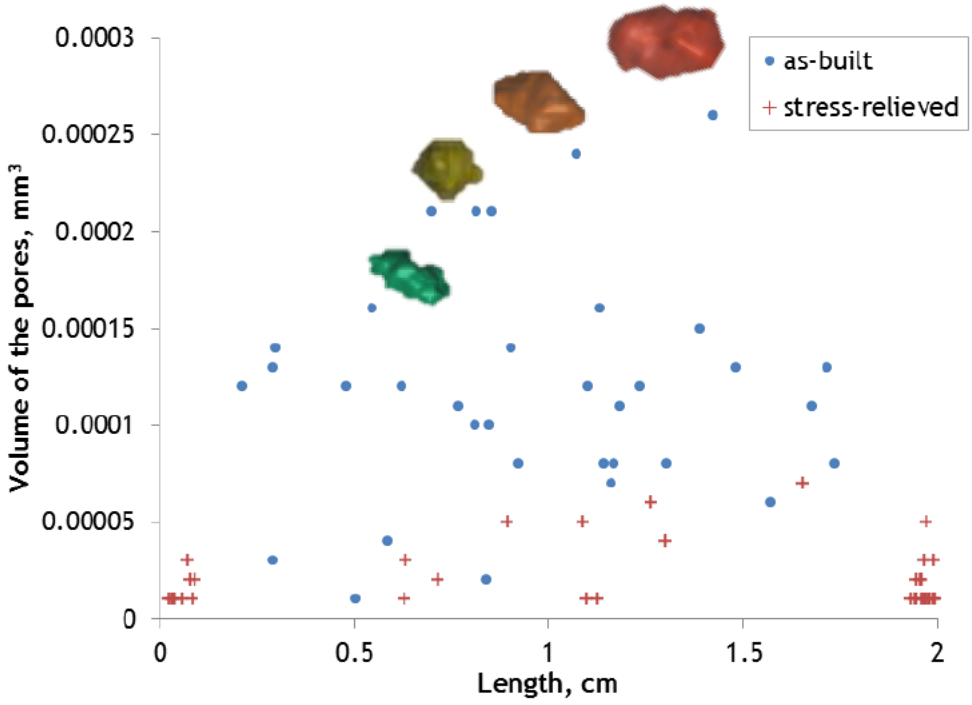

(b)

Fig.4.3.5. Histogram of frequency distribution (a) and volume of the pores with reconstruction of the biggest pores (b).

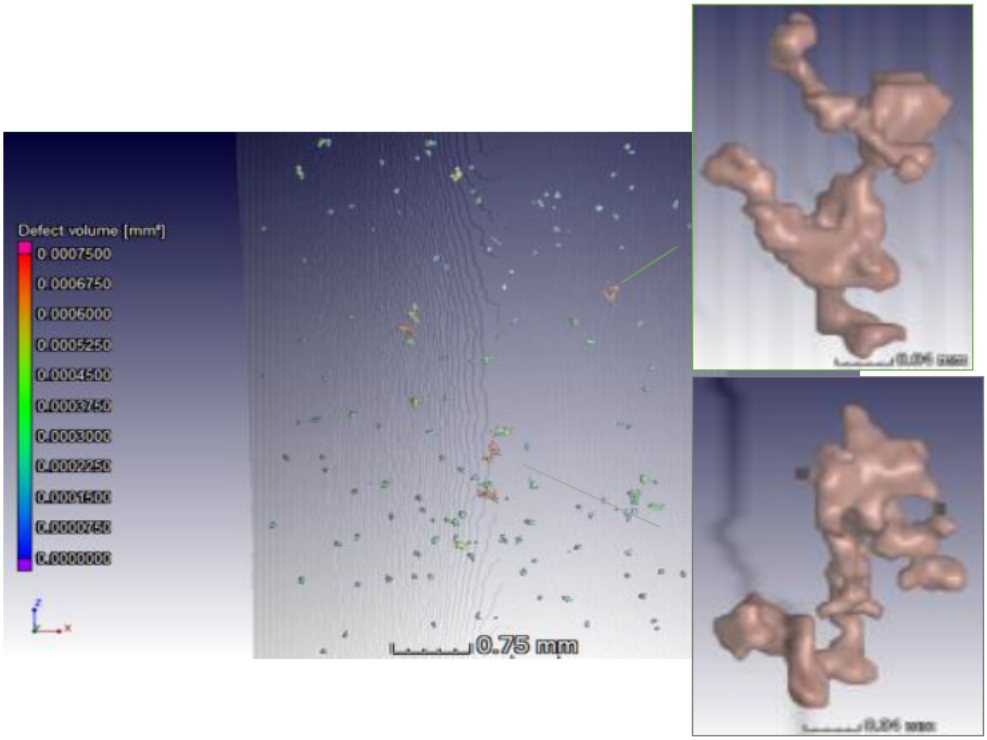

(a)

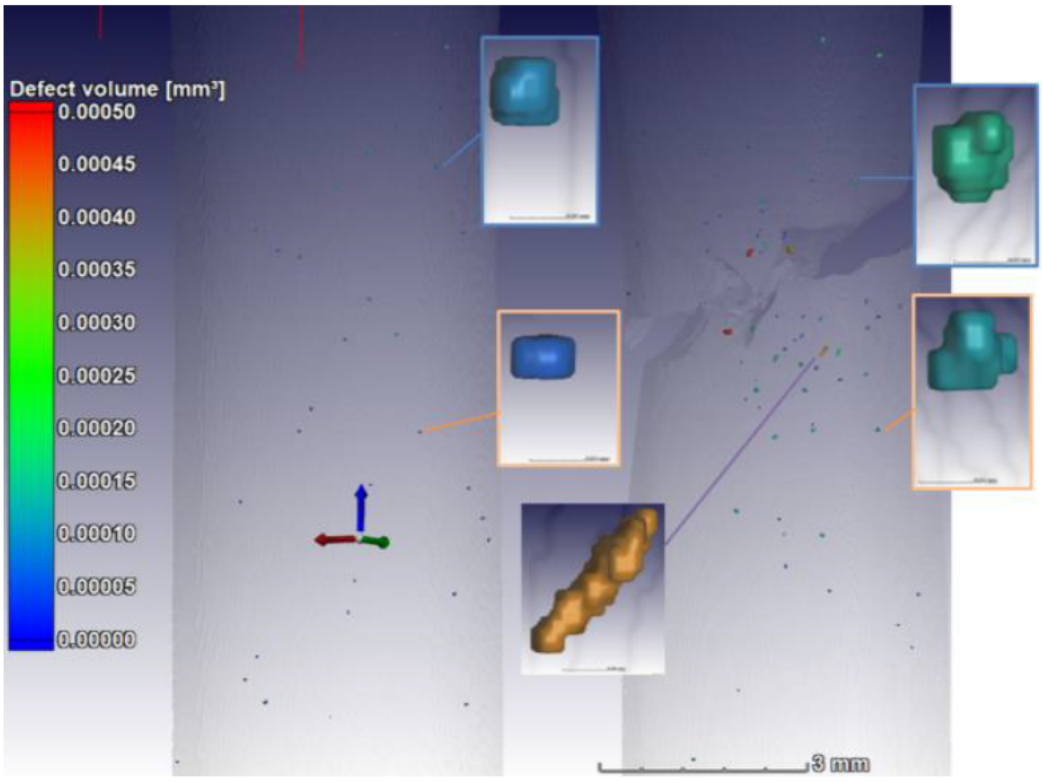

(b)

Fig. 4.3.6. Morphology of the pores in pre-strain as-built AB3 (a) and AB2 samples (b).

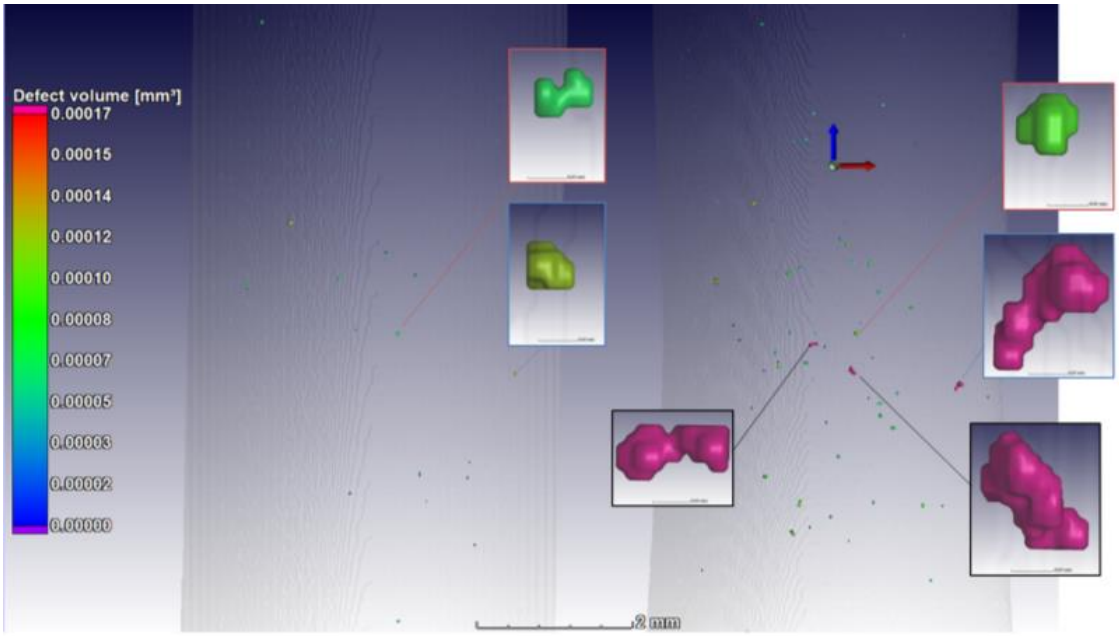

Fig. 4.3.7. The evolution of the pores in stress-relieved SR2 pre-strained sample.

After DMLS, the residual stresses are large enough and are not distributed homogeneously in the sample (Yadroitsev & Yadroitsava, 2015). Generally, in the final as-built samples, the residual stress distribution is complex and stresses are high. It was shown that near the surface, the Ti6Al4V (ELI) samples produced in similar conditions and attached to the substrate had tensile stresses (Yadroitsava *et al.*, 2015). Subsequent cutting and machining of the rectangular blocks to the shape suitable for the mechanical test also modifies the stresses. Therefore, it is difficult to conclude exactly what the stress conditions were in the interior of the tensile specimens. Nevertheless, it is clear that the superposition of stresses around a pore might result in a stress concentration above critical values, resulting in quicker pore growth.

An analysis of porosity in the necking area in specimens strained to failure showed a much larger number of pores, small and coarse, around the crack (Fig. 4.3.9).

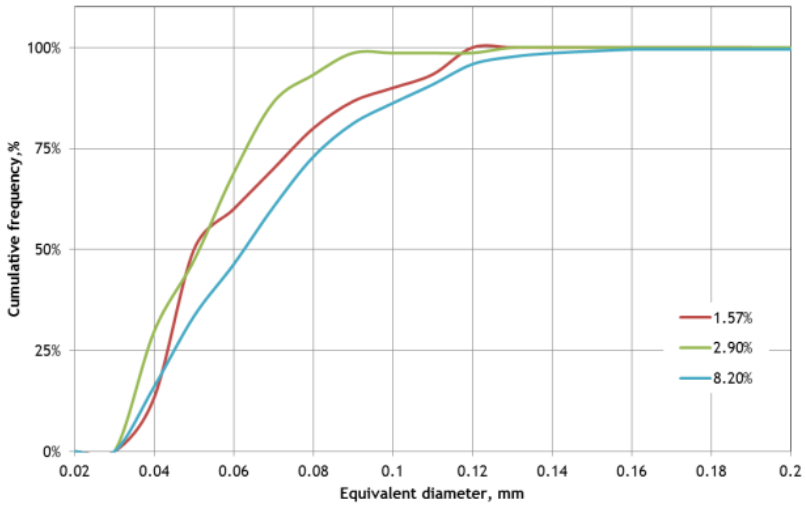

(a)

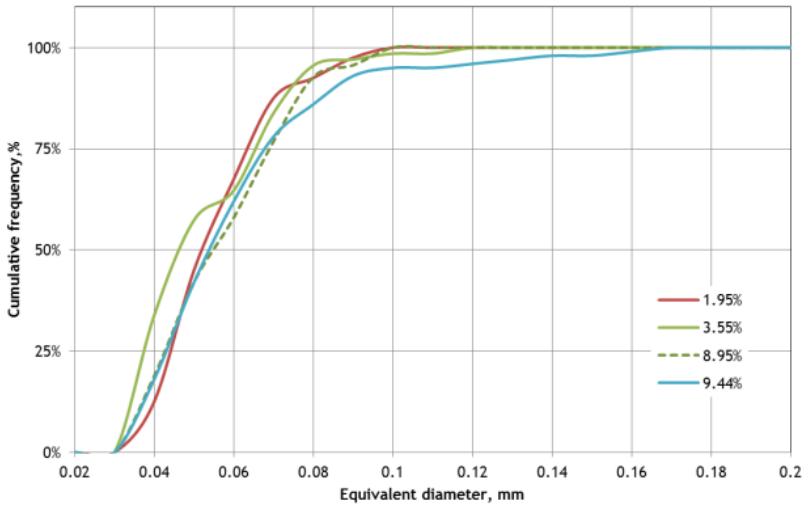

(b)

Fig. 4.3.8. Cumulative frequency distribution of pore sizes in pre-strained as-built (a) and stress-relieved (b) samples. Size of the pore was calculated as the equivalent diameter of the circumscribed sphere.

The AB3 sample, pre-strained up to 8.2 per cent, had the biggest pore size of 236 µm. But the fracture line in the as-built and stress-relieved samples did not cross the biggest pores when the samples were broken (Figures. 4.3.6 & 4.3.9). Thus localisation of plastic deformation at tension intensifies both pore growth and pore coalescence processes. From the previous discussion, one can conclude that, if porosity is higher and pores are coarser in the as-built specimen, then the pores grow and coalesce more easily. This results in the faster formation of cracks and ultimately failure. Therefore, both the initial porosity and residual stresses resulted in a lower ductility in the as-built Ti6Al4V.

AB2 sample

AB3 sample

SR2 sample

SR3 sample

Fig. 4.3.9. Coalescence of the pores and necking creation in as-built and stress-relieved samples.

Stress-relief results in the reduction of residual stresses and some changes in the microstructure, which caused an increase in elongation from 9.4 to 10.9 per cent and an area reduction from 25.6 to 29.3 per cent after heat treatment.

Conclusions

In contrast with the published data, after the stress-relief of Ti6Al4V (ELI) at 650°C for three hours in Ar argon atmosphere, no beta phase was detected by TEM, EBSD, and XRD. This heat treatment slightly influenced the microstructure: very small (500 nm) globular grains of alpha phase were found. It has been assumed that while manufacturing with different process-parameters, final structures are subjected to different conditions of in-situ cycling reheating, which influences the microstructure of the material.

Defect analysis by MicroCT showed that the DMLS Ti6A4V (ELI) samples had a high density (>99.9%). The CT scans suggested the moderately ductile fracture mechanism of the DMLS samples under tension with formation of the necking region, which was associated with pore coarsening and coalescence.

The results of this study clearly show that if the DMLS process parameters are properly selected, the properties of DMLS specimens from Ti6Al4V (ELI) fully meet the requirements of the standards, and the only post-processing that is required is stress-relieving.

The impact of process parameters on the microstructure and mechanical properties remains an open and relevant matter for future research.

Acknowledgements

This work is based on research supported by the South African Research Chairs Initiative of the Department of Science and Technology and the National Research Foundation of South Africa (Grant №97994) and the Collaborative Programme in Additive Manufacturing (Contract №CSIR-NLC-CPAM-15-MOA-CUT-01). Mechanical testing was performed in a mechanical testing laboratory at the CSIR, and the authors are grateful to Chris McDuling. The authors also thank CRPM for manufacturing the DMLS samples.

References

Antonysamy, A.A., Prangnell, P.B., Meyer, J. 2012. Effect of wall thickness transitions on texture and grain structure in additive layer manufacture (ALM) of Ti6Al4V, *Materials Science Forum*, 706-709, pp. 205-210.

Becker, T.H., Beck, M., Scheffer, C. 2015. Microstructure and mechanical properties of direct metal laser sintered Ti-6Al-4V, *South African Journal of Industrial Engineering*, 26(1), pp. 1-10.

Boyer, R., Welsch, G., Collings, E. 1994. Materials Properties Handbook: Titanium Alloys, Materials Park, Ohio: ASM International.

de Viteri, V.S. and Fuentes, E. 2013. Titanium and Titanium Alloys as Biomaterials. In: J. Gegner, ed., *Tribology - Fundamentals and Advancements*. InTech, pp. 155-181.

Donachie, M.J. 2000. Titanium: A Technical Guide, 2nd Edition, Materials Park, Ohio: ASM International.

Du Plessis, A., Seifert, T., Booysen, G., Els, J. 2014. Microfocus X-ray computed tomography (CT) analysis of laser sintered parts, *South African Journal of Industrial Engineering*, 25(1), pp. 39-49.

Du Plessis, A. & Rossouw, P. 2015. Investigation of porosity changes in cast Ti6Al4V rods after hot isostatic pressing, *Journal of Materials Engineering and Performance*, 24(8), pp. 3137-3141.

Facchini, L., Magalini, E., Robotti, P., Molinari, A., Hoges, S., Wissenbach, K. 2010. Ductility of a Ti-6Al-4V alloy produced by selective laser melting of prealloyed powders, *Rapid Prototyping Journal*, 16(6), pp. 450–459.

Frey, M., Shellabear, M., Thorsson, L. 2009. Mechanical testing of DMLS parts. *EOS whitepaper*, EOS GmbH, Munich.

Kasperovich, G. & Hausmann, J. 2015. Improvement of fatigue resistance and ductility of TiAl6V4 processed by selective laser melting, *Journal of Materials Processing Technology*, 220, pp. 202–214.

Mertens, A., Reginster, S., Paydas, H., Contrepois, Q., Dormal, T., Lemaire, O., Lecomte-Beckers, J. 2014. Mechanical properties of alloy Ti–6Al–4V and of stainless steel 316L processed by selective laser melting: influence of out-of-equilibrium microstructures, *Powder Metallurgy*, 57(3), pp. 184-189.

Murr, L.E., Quinones, S.A., Gaytan, S.M., Lopez, M.I., Rodela, A., Martinez, E.Y., Hernandez, D.H., Martinez, E., Medina, F., Wicker, R.B. 2009. Microstructure and mechanical behavior of Ti-6Al-4V produced by rapid-layer manufacturing, for biomedical applications, *Journal of the Mechanical Behavior of Biomedical Materials*, 2(1), pp. 20–32.

Rafi, H., Karthik, N.V., Gong, H., Starr, T.L., Stucker, B.E. (2013). Microstructures and mechanical properties of Ti6Al4V parts fabricated by selective laser melting and electron beam melting, *Journal of Materials Engineering and Performance*, 22(12), pp. 3872–3883.

Sallica-Leva, E., Caram, R., Jardini, A.L., Fogagnolo, J.B. 2016. Ductility improvement due to martensite α′ decomposition in porous Ti–6Al–4V parts produced by selective laser melting for orthopedic implants, *Journal of the Mechanical Behavior of Biomedical Materials*, 54, pp. 149-158.

Simonelli, M., Tse, Y.Y. and Tuck, C. 2014. On the texture formation of selective laser melted Ti-6Al-4V, *Metallurgical and Materials Transactions* A, 45(6), pp. 2863-2872.

Simonelli, M., Tse, Y.Y. and Tuck, C. 2014a. Effect of the build orientation on the mechanical properties and fracture modes of SLM Ti–6Al–4V, *Materials Science and Engineering*: A, 616, pp. 1-11.

Simonelli, M., Tse, Y.Y. and Tuck, C. 2014b. The formation of alpha plus beta microstructure in as-fabricated selective laser melting of Ti-6Al-4V, *Journal of Materials Research*, 29(17), pp.2028-2035.

Vilaro, T., Colin, C., Bartout, J. D. 2011. As-fabricated and heat-treated micro-structures of the Ti-6Al-4V alloy processed by selective laser melting, *Metallurgical and Materials Transactions* A, 42(10), pp. 3190-3199.

Vrancken, B., Thijs, L., Kruth, J.P. and Van Humbeeck, J. 2012. Heat treatment of Ti6Al4V produced by Selective Laser Melting: Microstructure and mechanical properties, *Journal of Alloys and Compounds*, 541, pp. 177–185.

Wen, S., Li, S., Wei, Q., Yan, C., Zhang, S., Shi, Y. 2014. Effect of molten pool boundaries on the mechanical properties of selective laser melting parts, *Journal of Materials Processing Technology*, 214, pp. 2660-2667.

Xu, W., Brandt, M., Sun, S., Elambasseril, J., Liu, Q., Latham, K., Xia, K., Qian M. 2015. Additive manufacturing of strong and ductile Ti–6Al–4V by selective laser melting via in situ martensite decomposition, *Acta Materialia*, 85, pp. 74–84.

Yadroitsava I., Grewar S., Hattingh D., Yadroitsev I. 2015. Residual stress in SLM Ti6Al4V alloy specimens, *Materials Science Forum*, 828-829, pp. 305-310.

Yadroitsev, I. & Yadroitsava, I. 2015. Evaluation of residual stress in stainless steel 316L and Ti6Al4V samples produced by selective laser melting, *Virtual and Physical Prototyping*, 10(2), pp. 67-76.

4.4. Validation of miniaturised tensile testing on DMLS TI6AL4V (ELI) specimens

4.4.1. Abstract

Direct metal laser sintering (DMLS) is a relatively new technology that is developing rapidly. Since DMLS material is created by melting/solidifying tracks and layers from powder, even building geometry can influence the mechanical properties. To certify a material, the testing specimens must be designed and manufactured according to the appropriate standards. Miniaturised tensile DMLS samples could be a good alternative for express quality control, and could reduce the cost of DMLS-specific testing. In this study, as-built and stress-relieved miniaturised tensile DMLS Ti6Al4V (ELI) specimens with different surface qualities were investigated. The fracture surfaces and mechanical properties of the mini-tensile specimens were analysed and compared with standard full-sized specimens also manufactured by DMLS. The obtained data showed the applicability of mini-tensile tests for the express analysis of DMLS objects if a correction factor is applied for the calculation of the load-bearing cross-section of the specimen.

4.4.2. Introduction

Direct metal laser sintering (DMLS) is a powder bed fusion process used to make metal parts directly from metal powders. It is an automated process that provides a platform for the production of complex three-dimensional geometries. Three-dimensional scans or CAD data are sliced into multiple layers via software. Using this data, the machine parameters are calculated and/or chosen for the building process. First a thin layer of powder is deposited onto the building platform, after which it is scanned by the electronically-controlled laser, and the exposed area is melted by the laser beam, matching the contour area of the sliced 2D data. The next layer is deposited and exposed, which fuses with the previous sintered area and, in so doing, a 3D part is built up.

During DMLS, a very small molten pool is formed that results in a large thermal gradient at high scan speeds. The microstructure and mechanical properties obtained in DMLS are unique, and are influenced by different process parameters. Machine-based input parameters are also crucial to the stability of the building process, such as the laser type and its mode and spot size, protective atmosphere and its flows, delivering system, and even the substrate surface prior to exposure (Yadroitsev, 2009).

As-built DMLS samples can have anisotropy in mechanical properties, since DMLS is a layer-by-layer powder technology. Along with the defects inherent to non-optimal process parameters, there is a second important aspect that strongly influences the quality of the SLM material: internal stresses resulting from rapid solidification during the process. The mechanical properties of DMLS material depend on the specimen geometry, build orientation, and surface finish (Frey *et al.*, 2009). The DMLS surfaces are very rough, especially those that are not parallel to the building platform where powder attaches with sintered material.

Titanium alloys have two main benefits for biomedical applications: good corrosion resistance, and a high strength-to-weight ratio. Medical implants made of titanium alloys are strong, lightweight, corrosion-resistant, long-lasting, and non-ferromagnetic; and they accommodate the possibility of osseointegration. The development of biocompatible materials and new processes, such as DMLS, have resulted in significant progress in customised design and a reduction in the production time of implants and prostheses, without compromising functionality.

The capacity of DMLS to manufacture medical devices with complex shapes, in combination with the unique properties of titanium alloys, holds great promise for the medical industry. Ti6Al4V components, produced by DMLS, have to comply with international standards for biomedical applications. Different process parameters, the orientation of the object, and its design features can influence the mechanical properties (Table 4.4.1). It is therefore of paramount importance that designers know the mechanical properties of every part produced in order to ensure a safe and appropriate application. Ti6Al4V, being a heat-treatable alloy, makes it attractive for the DMLS application because post-processing can produce a variety of different properties for specific applications (Rafi *et al.*, 2013; Vrancken *et al.*, 2012; Yadroitsev *et al.*, 2014). Due to very fine martensitic α' microstructure with the texture in the build direction, the DMLS object should also be heat-treated differently from wrought alloy parts.

Table 4.4.1. Mechanical properties of Ti6Al4V vertical samples produced by DMLS

	Specimen labels	*YS, MPa*	*Young's Modulus, GPa*	*UTS, MPa*	*Elongation, %*
Frey *et al.*, 2009.	As-built	1070±50	110±10	1200±50	11±2
	Annealed*	1000±20	114±10	1060±20	15±1
Rafi *et al.*, 2013	As-built	1143±30		1219±20	4.89±0.6
Vilaro *et al.*, 2011	As-built	962±47	102±7	1166±25	1.7±0.3
Kasperovich, & Hausmann, 2015.	As-built	664-802	99-121.6	1040-1062	11.3-12.7
Standard specification for Ti6Al4V alloy castings for surgical implants – ASTM F1108-14		Min 758		Min 860	Min 8

4.4.3. Tensile mechanical tests

Standard tensile specimens

Tension tests provide information about certain material properties of test specimens: ultimate tensile strength (UTS), the yield stress (YS), and elongation. With the use of an extensometer, it can also provide the Young's modulus and strain rate of the material being tested. For manufacturing, uniaxial tensile stresses can be used in alloy development, quality control, and design under certain circumstances. Standard Test Methods for Tension Testing of Metallic Materials E8/E8M [8] describes the tension testing of metallic materials at room temperature; specifically, the methods of determination of YTS, UTS, elongation, and reduction of area. As indicated, ASTM E8 specimens smaller than 6 mm diameter can be used when tested material is too small or "when all parties agree to their use for acceptance testing" (ASTM E8/E8M-16a).

Mini specimens

The grips used were wedge-type grips in the case of the miniature samples. This can result in small inconsistencies in the stress measurement, although it has a more significant effect on the YS and an even greater effect on the Young's modulus (Jia &Kagan, 1999); as a result, the data provided UTS and elongation, as these remain relatively unaffected.

Roughness, notches, or any impurities in the samples can affect the results. Kashaev *et al*. (2013) have shown that micro-fatigue specimens have a fatigue life similar to that of standard specimens if the cross-sections of the mini-specimens are corrected for roughness.

The aim of the present study is to determine the possibility of using as-built and polished miniaturised samples for defining the basic properties of DMLS Ti6Al4V (ELI) alloy before and after stress relieving.

4.4.4. Materials and methods

The Ti6Al4V (ELI) powder used was pre-alloyed gas atomised powder. The chemical composition was as follows: Ti – balance, Al – 6.34%, V –3.94%, O – 0.058%, N – 0.006%, H – 0.001%, Fe – 0.25%, C – 0.006%, and Y and Zn less than 0.001% (weight %). The equivalent diameters (weighted by volume) of the powder particles were d_{10} = 13 µm, d_{50} = 23 µm, and d_{90} = 37 µm.

Ti6Al4V samples were produced by the EOSINT M280 system (EOS GmbH). A back-and-forth scanning by strips (5 mm width) with the hatch distance of 100 µm was applied to manufacturing specimens with 30 µm layer thickness. The substrate and powder materials were

similar in chemical composition. Argon was used as the protective atmosphere; the oxygen level in the chamber was 0.05–0.09 per cent.

Ten vertical standard round samples with threaded ends were machined from SLM rectangular bars with dimensions of 11 mm x 11 mm x 62 mm according to the recommendations of ASTM E8, with a gauge length four to five times the diameter; the specimen's diameter was 4.3 - 4.5 mm. Surface roughness for the standard round machined samples was 4.8±0.63 µm (Rz), and Ra was 0.8±0.13 µm. Five bars were subjected to a stress-relieving procedure (Figure 1a). Tensile tests were performed with an Instron 1342 servo-hydraulic testing machine with circular locked grips and a clip-on extensometer of 12.5 mm under a constant strain rate of 1.5 mm/min.

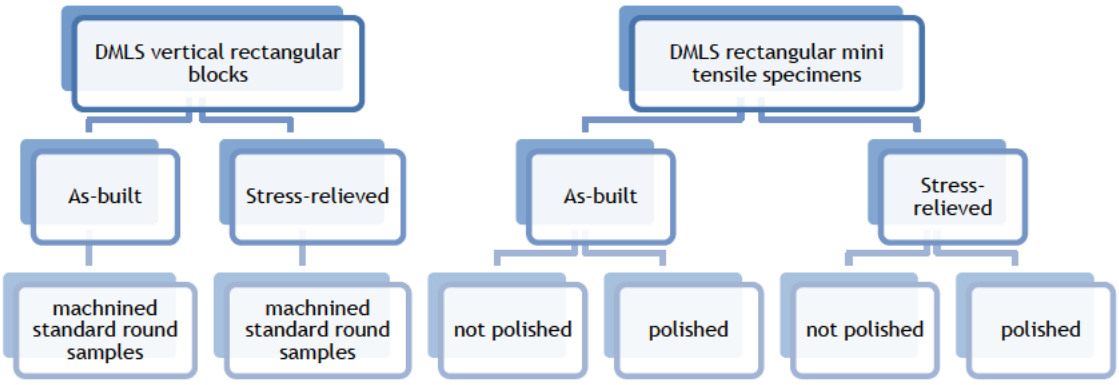

Fig. 4.4.1. Design of the experiment.

Sixteen rectangular pin-loaded mini-samples of 10 mm gauge length, 2 mm width, and 1 mm thickness were built directly at the same process-parameters by the EOSINT M280 system (Fig. 3.4.3). The dimensions of the tensile mini-samples are shown in Figs. 3.4.3. Tensile tests were performed with an MTS Criterion Model 43 electric testing machine with wedge grips and without extensometer under a constant strain rate of 0.25 mm/min. Clamping of the miniature samples for the purpose of tensile testing was done via customised inserts, as seen in Figs. 4.4.2a-e.

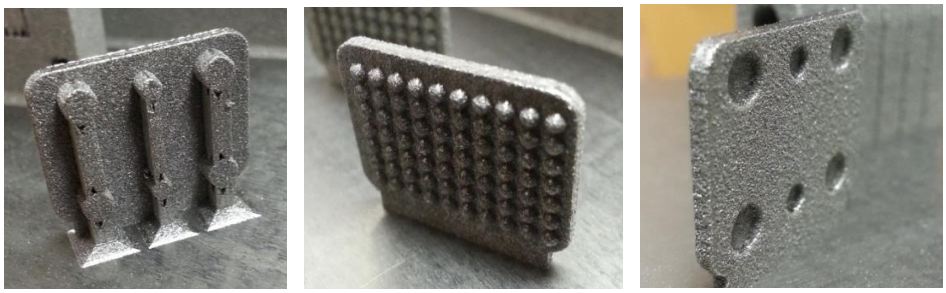

(a) (b) (c)

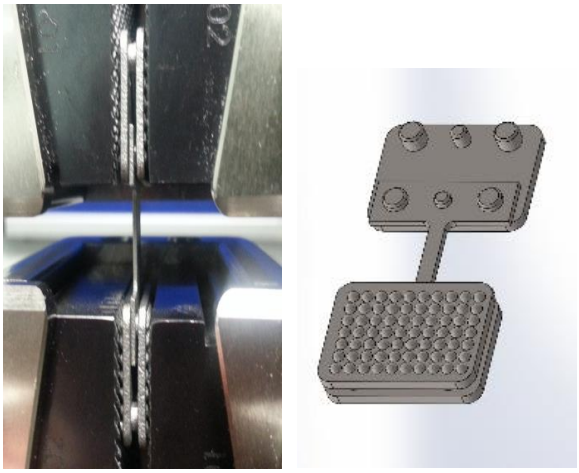

(d) (e)

Fig 4.4.2. Insert with pins (a); grip surface (b); insert with cavity (c); mini-specimen setup with inserts and wedge grips tightened (d); and computer model of specimen and inserts (e).

Heat treatment for stress relieving of all specimens were done in an Argon atmosphere at 650°C for 3 hours.

4.4.5. Results and discussions

The mechanical properties of standard samples manufactured vertically, show excellent mechanical properties (Table 4.4.2). For standard round specimens, Young's modulus was defined as a chord between 200 MPa and 800 MPa, tensile stress at Yield was defined at offset 0.2% of the Young's Modulus. As was indicated by Frey *et al.* (2009), round machined samples give relatively consistent and reliable data for DMLS specimens.

Table 4.4.2: Tensile properties of standard round specimens of Ti6Al4V ELI of as-built DMLS parts at EOS prescribed process parameters

Specimen labels		*YS, MPa*	*Young's modulus, GPa*	*UTS, MPa*	*Elongation, %*
Standard round specimens	As-built	1105±9.1	109±1.5	1238±8.9	10.74±0.7
	Stress-relieved	1098±8.1	115.8±1	1171.6±6	11.89±1

The analysis of the fracture surfaces of standard machined vertical samples showed that a cup-and-cone shape of the necking region was observed in the as-built and stress-relieved samples. The region of fibrous fracture was in the central area of the neck (Fig. 4.4.3a). The fibrous zone was irregular, with dimple rupture fracture; quasi-cleavage facets were also visible with SEM (Fig. 4.4.3b). The mechanism of ductile fracture and the formation of a cup-and-cone shape in the necking region are usually associated with pore coalescence.

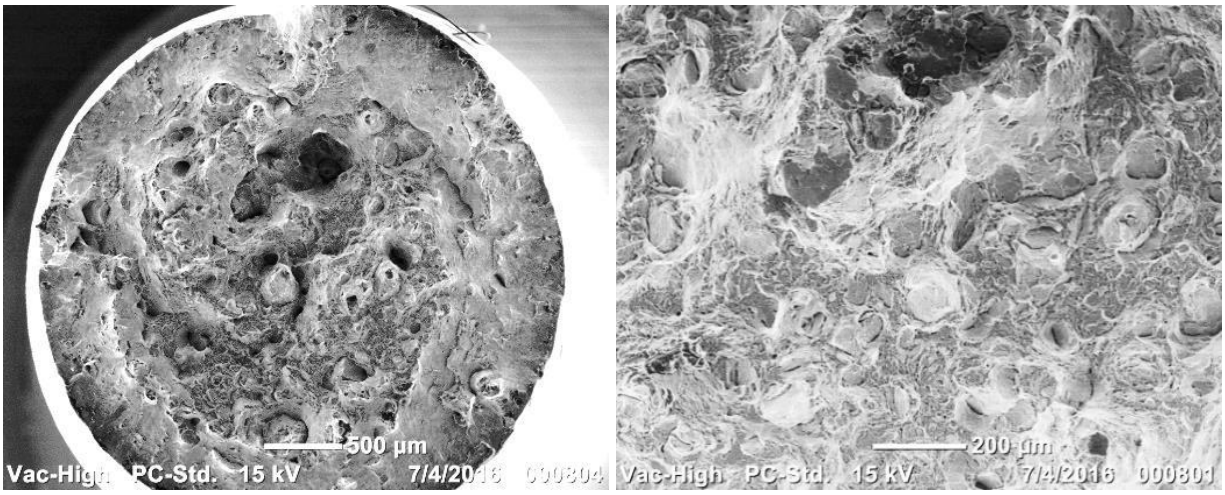

(a) (b)

Fig.4.4.3. Fracture surface of standard vertical samples: (a) cup-and-cone shape; and fracture surface at higher magnification (b).

According to the building strategy, all the specimens were built vertically, which meant that the columnar primary β grains also grew nearly parallel to the building direction (Simonelli, 2014). With respect to the specimen geometry and test arrangement, the columnar primary beta grains were oriented parallel to the load application direction. Under these conditions, a crack formed due to pore coalescence propagates perpendicular to the columnar primary ß grains. In Fig. 4.4.3b it is seen that when the crack reaches primary ß grain boundaries or pores, the growth direction is changed. Therefore, the interface acts as a crack deflector that prevents quick failure. This conclusion is in agreement with the results presented by Wen *et al.* (2014).

An examination of the tensile fracture surfaces and a comparison of the polished cross-sections of the mini-specimens by SEM revealed the specific role of macro- and micro-structure caused by the nature of the layer-by-layer DMLS. For the mini-samples, primary ß grains were oriented along the building direction (Fig. 4.4.4) and had a smaller size than in the standard samples produced from bars. Representative fractographs of the tensile fracture surfaces for the mini-samples are shown in Fig. 4.4.5. On the whole, the rectangular mini-samples showed surface fractures similar to those in the standard specimens. The finer scale topography of the fracture

surface and shallower dimples were observed in the fibre zones in comparison with the standard samples (Figs. 4.4.3, 4.4.5c and 4.4.5d). A clearly observed quasi-cleavage fracture mode indicates a brittle component of fracture. Unlike in the standard specimens, a columnar microstructure is not obvious at the fracture surface. It could be associated with the finer microstructure of the mini-specimens. An estimation of the column width done by an intercept method showed that the standard specimen columns had 120 µm average width, while in the mini-specimens this value was about 100 µm.

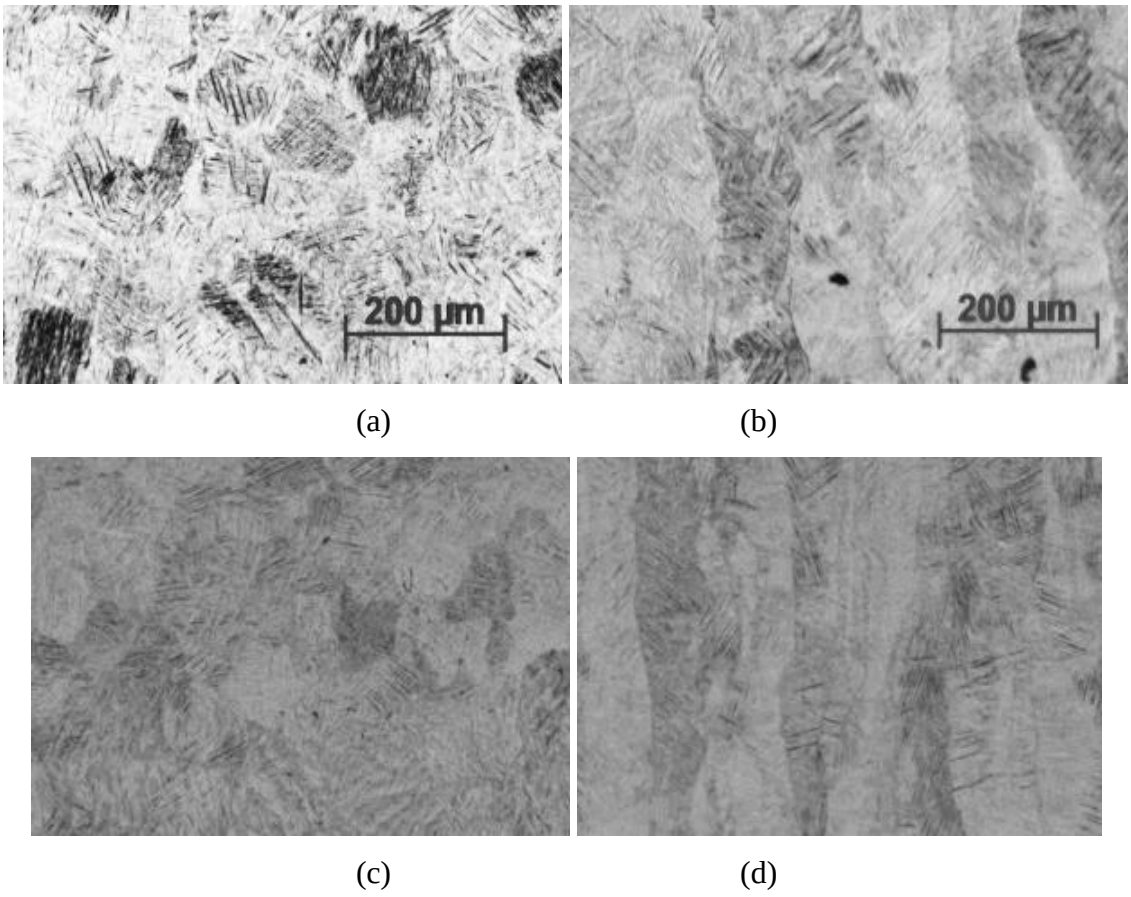

Fig.4.4.4. Cross-section of the stress-relieved standard (a, b) and mini samples (c, d) perpendicular to the building direction (a, c) and along the building direction (b, d).

To investigate the influence of surface finish on the tensile properties of the mini-samples, both as-built and stress-relieved specimens were tested, with non-polished and polished surfaces. The mini-samples after polishing showed lower values for UTS than did the standard samples (Figure 4.4.6a). The UTS for the non-polished as-built specimens was 50 per cent lower than in the standard specimens. After stress-relieving, the UTS of the un-polished specimens was 45 per cent lower. After polishing, UTS increased (Table 4.4.3), but was still six per cent and three per

cent lower (for the as-built and the stress-relieved specimens respectively) than for the standard samples.

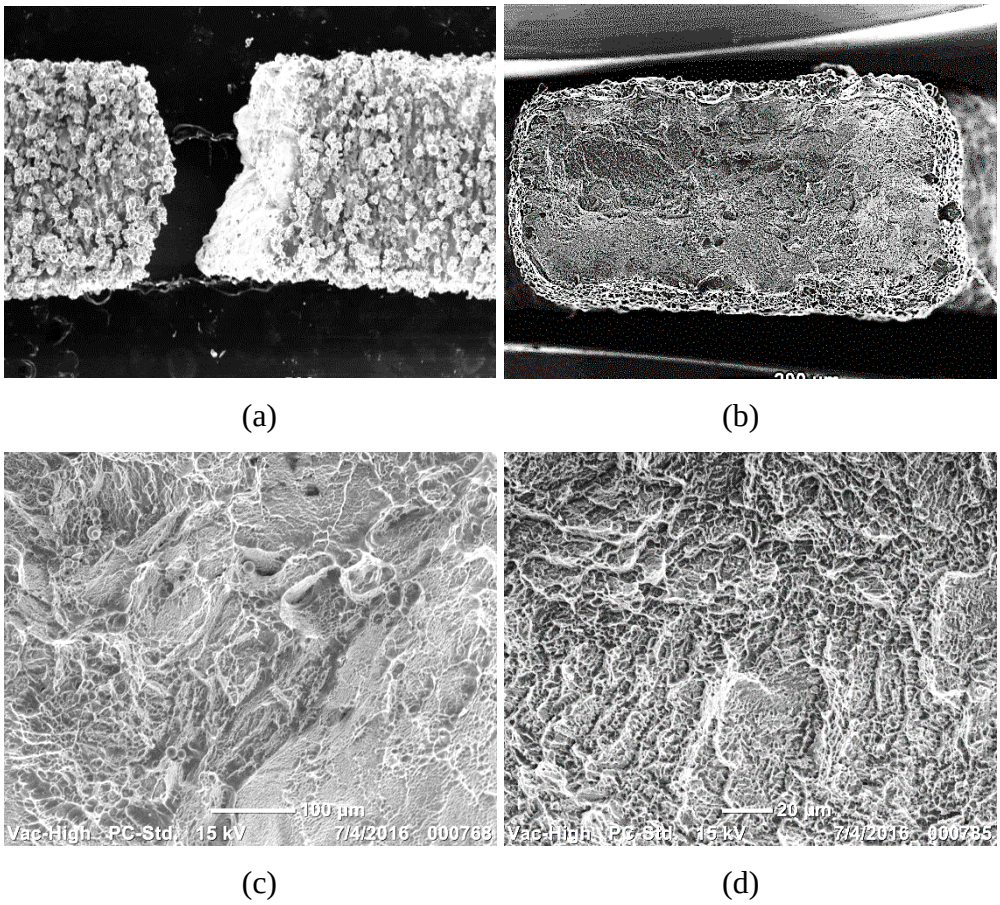

(a) (b)

(c) (d)

Fig.4.4.5. Fracture of as-built mini samples (a, c) and after stress-relieving heat treatment (b, d).

For the mini samples, high roughness could be a crucial factor in the load-bearing cross-section. Attached partially melted powder particles were found at the surfaces of non-polished samples and formed an irregular surface layer. The thickness of this layer was about 100 µm and could be estimated in terms of surface roughness characteristics as a mean roughness depth R_z. As was shown by Kashaev *et al.* (2013) it is possible to introduce a correction factor to estimate effective load-bearing cross-section, A_{eff},:

$$A_{eff} = (S - 2R_z) \cdot (W - 2R_z)$$

where S is the thickness and W is the width of the mini specimen.

Applying the effective load-bearing cross-section to the experimental data obtained for the mini-specimens showed results closer to UTS values received for the standard round samples (Table 4.3.3). It is also seen that this approach is effective for the polished specimens, as some residual surface roughness remains after polishing (Fig. 4.4.7). Differences between the obtained

elongations at breakpoint for the standard and mini-samples are attributed to the shape of the samples and size effects, and are not related to surface quality. It is seen that ductility characteristics are about the same for the polished and the non-polished specimens.

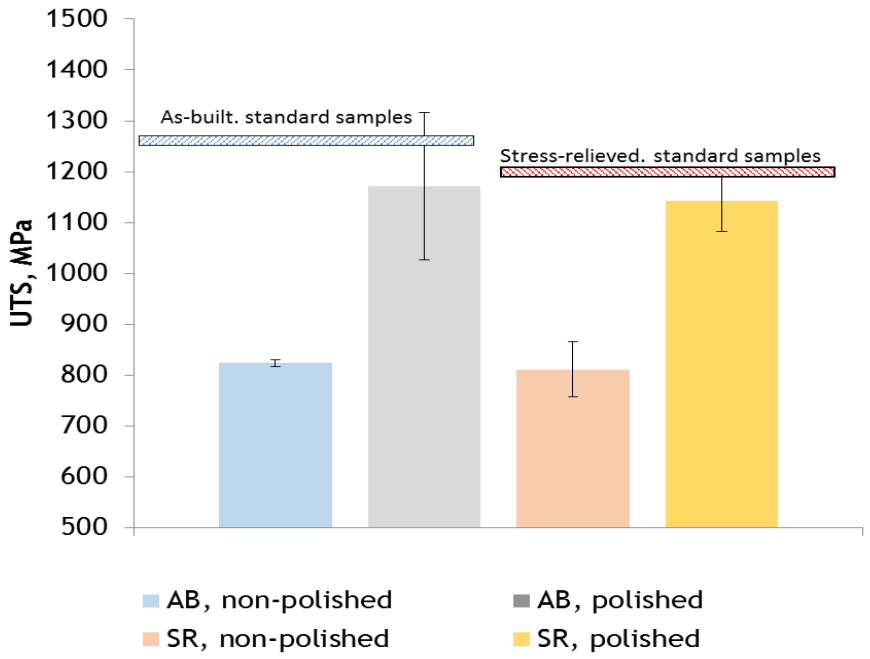

(a)

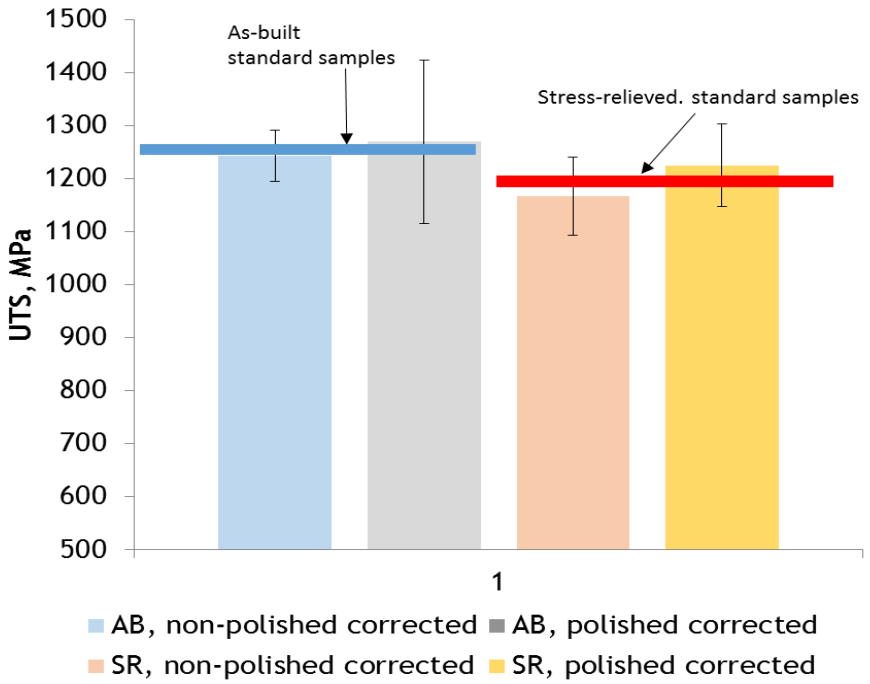

(b)

Fig.4.4.6. Average UTS for mini samples before and after polishing (a) and corrected UTS (b).

Table 4.4.3: Tensile properties of standard round specimens and mini samples of Ti6Al4V ELI of as-built DMLS parts at EOS prescribed process parameters

Specimen labels		*Roughness*		*UTS, MPa*	*Elongation, %*
		Ra, µm	*Rz, µm*		
Standard round specimens	As-built	0.76±0.13	4.8±0.6	1238±9	10.74±0.7
	Stress-relieved			1172±6	11.89±1
Non-polished mini samples	As-built	21.7±4.37	125.2+20.49	823±8	6.6±0.4
	Cross-section corrected			1243±49	
	Stress-relieved	18.3±3.79	109.2±24.1	811±54	6.4±1.4
	Cross-section corrected			1167±74	
Polished mini samples	As-built	3.5±1.11	21.9±7.16	1172±144	6±0.9
	Cross-section corrected			1270±154	
	Stress-relieved	3.3±0.91	19.2±7.75	1143±60	5.5±0.4
	Cross-section corrected			1230±78	

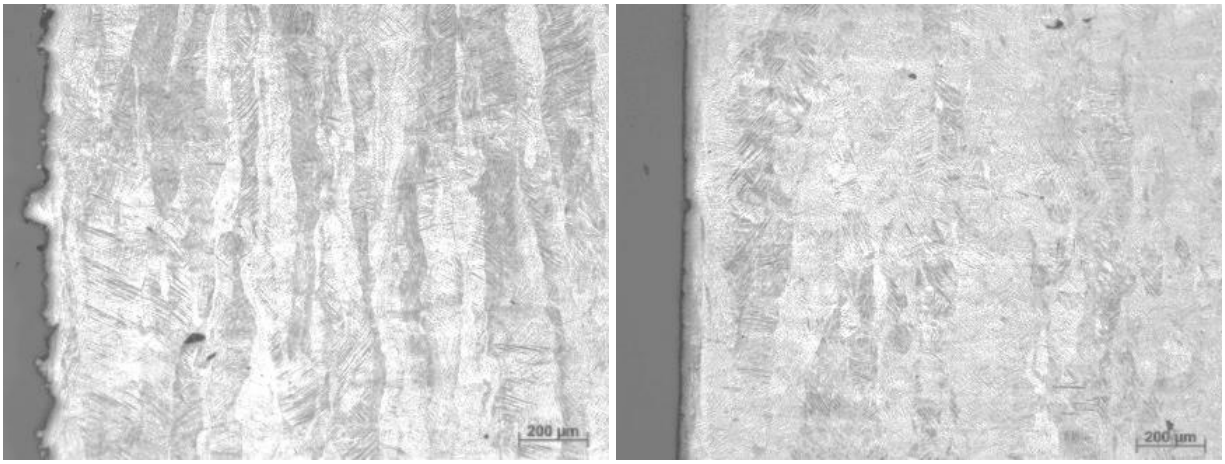

(a) (b)

Fig.4.4.7. Cross-section of mini samples before (a) and after polishing (b) along building direction.

Besides surface roughness, a microstructural factor could also influence mechanical testing results. It has been shown by Antonysamy *et al.* (2013) that the microstructure of Ti6Al4V in the regions near side surfaces differs from the regular bulk regions. In regions close to the side surface, the primary beta phase does not form regular vertical grains. Instead, some deviations from the vertical crystallization direction have been observed. This could be related to a change of solidification conditions and the direction of the thermal gradient. In the present investigation, this

effect was not observed. Probably due to other manufacturing parameters, primary β also formed almost vertical columnar structures in regions very close to the irregular side surfaces; in the near-surface region, however, the grains are finer.

Fig.4.4.7 shows that surface polishing did not remove the material deeply enough to eliminate the influences of the side microstructure. Nevertheless, according to the experimentally-obtained mechanical properties, the differences in microstructure observed in this region apparently have a negligible influence on the mechanical properties of the mini-samples. To confirm this, a comparative analysis of mini-specimens with and without obvious differences in microstructure in the side surface region is necessary.

Conclusions

The tests done show that, even on a small scale (with a width of about 10 single tracks), the construction of DMLS components is strong and reliable. This testifies to the sound process parameters.

The mini-samples are effective for the determination of the basic properties of DMLS material. The samples were found to be relatively consistent with all the failures occurring within the gauge length. Nevertheless, due to the attached partially-melted powder layer on the side surfaces of the vertically-built samples, a correction of data is required.

Surface polishing was not found to be sufficient for improving the reliability of the measured mechanical data (deviation from standard 15-20%) due to possible residual surface roughness. The results corrected with respect to the effective load-bearing cross-section A_{eff} were found to be closest to the values obtained with reference standard tensile specimens (deviation from standard 5-7 per cent).

Further microstructural analysis has to be done to investigate the effect of the orientation of primary β grains and texture in the mini-samples from Ti6Al4V. This data will be helpful for micro-manufacturing by DMLS.

Acknowledgements

This work is based on the research supported by the South African Research Chairs Initiative of the Department of Science and Technology and National Research Foundation of South Africa (Grant №97994) and the Collaborative Program in Additive Manufacturing (Contract №CSIR-NLC-CPAM-15-MOA-CUT-01). The authors express their gratitude to Chris McDuling at the CSIR for mechanical testing and technical input.

References

Antonysamy, A.A., Meyer, J., Prangnell, P.B., 2013. Effect of build geometry on the –grain structure and texture in additve manufacture of Ti6Al4V by selective electron beam melting, *Materials Characterization 84*, pp. 153-168.

ASTM E8 / E8M-16a, 2016, *Standard Test Methods for Tension Testing of Metallic Materials*, ASTM International, West Conshohocken, PA, www.astm.org

Frey, M., Shellabear, M., Thorsson, L. 2009. *Mechanical testing of DMLS parts. EOS whitepaper*, EOS GmbH Electro Optical Systems, Munich.

Jia, N. & Kagan, V. A., 1999, Interpretations of tensile properties of polyamide 6 and PET based thermoplastics using ASTM and ISO procedures, *Limitations of test methods for plastics, ASTM STP 1369*, Ed. J. S. Peraro, American Society for Testing and Materials, West Conshohocken, PA.

Kashaev, N., Horstmann, M., Ventzke, V. & Riekehr, S. H. N., 2013. Comparative study of mechanical properties using standard and micro-specimens of base materials Inconel 625, Inconel 718 and Ti-6Al-4V. *Journal of Materials Research and Technology*, 2(1), pp. 43-47.

Kasperovich, G., Hausmann, J. 2015. Improvement of fatigue resistance and ductility of TiAl6V4 processed by selective laser melting, *Journal of Materials Processing Technology* 220, pp. 202–214.

Rafi, H. Karthik, N.V. Gong, H. Starr, Th.L. Stucker B. E., 2013. Microstructures and mechanical properties of Ti6Al4V parts fabricated by selective laser melting and electron beam melting. *Journal of Materials Engineering and Performance, 22*, pp. 3873–3883.

Simonelli, M., 2014. *Microstructure evolution and mechanical properties of selective laser melted Ti-6Al-4V.* PhD thesis, Loughborough University, UK.

Vilaro, T., Colin, C., Bartout J.D. 2011. As-fabricated and heat-treated microstructures of the Ti-6Al-4V alloy processed by selective laser melting. *Metallurgical and materials transactions A* 42, pp. 3190-3199.

Vrancken, B., Thijs, L., Kruth, J.P., Van Humbeeck, J., 2012. Heat treatment of Ti6Al4V produced by Selective Laser Melting. *Journal of Alloys and Compounds* 541, pp. 177–185.

Wen, S., Li, S., Wei, Q., Yan, C., Zhang, S., Shi, Y., 2014. Effect of molten pool boundaries on the mechanical properties of selective laser melting parts. *Journal of Materials Processing Technology*, 214, pp. 2660-2667.

Yadroitsev I. (2009). Selective laser melting: direct manufacturing of 3D-objects by selective laser melting of metal powders. Saarbrucken: *LAP Lambert Academic Publishing* AG & Co. KG; 307 p.

Yadroitsev, I., Krakhmalev, P., Yadroitsava, I., 2014 Selective laser melting of Ti6Al4V alloy for biomedical applications: Temperature monitoring and microstructural evolution, *Journal of Alloys and Compounds*, 583, pp. 404-409.

Chapter 5. CONCLUSION AND FUTURE WORK

DMLS process, mechanical testing of materials, features of conventional (wrought and cast) and additive manufactured samples were described in literature review. It was shown that since DMLS material consists of single tracks and layers, porosity, microstructure and tensile properties of DMLS samples at different scanning strategies and process-parameters differ from conventional material. In this work it was found that under optimal process parameters (laser power, scanning speed, layer thickness, laser spot size, *etc.*) in Ar atmosphere with control of oxygen level and optimal scanning strategy, as-built Ti6Al4V (ELI) samples showed excellent density. MicroCT scans found that DMLS Ti6A4V (ELI) samples produced at optimal and stable process-parameters had porosity lower than 0.003% .

The residual stresses measured by XRD near the surface of the as-built DMLS parts were tensile and very high (220–800 MPa). The direction of the maximal principal stress is coincided with the direction of the laser scanning. No significant correlation was found between the number of powder layers, the surface roughness and value of the maximum principal residual stresses. Measured minor principal stresses which is perpendicular to the scanning direction, correlated with roughness of the top layers. Residual stresses near the surface of the cube 10 mm ×10 mm ×10 mm produced without support were close to the values of 40-layers Ti6Al4V (ELI) sample.

Analysis of literature data show that process parameters play a major role in the quality of 3D objects manufactured by DMLS. From literature data, vertical Ti6Al4V samples had Yield Strength ranged from 664 MPa to 1443 MPa, Young's Modulus was varied from 99 GPa to 114 GPa, and elongation was changed from 1.7% to 12.7%. DMLS ELI samples with lower per cent of oxygen in processed powder (<0.13%) show Yield Strength from 736 MPa to 1106 MPa and elongation of brake of 11%.

In present work was shown that under chosen parameters repeatability of the mechanical properties in each series of the experiments was very high, coefficient of variations were less than 0.1%. The build direction has negligible effect on the tensile properties of DMLS Ti6Al4V (ELI) samples. Vertical samples has UTS of 1238±9 MPa, YS of 1105±9 MPa, Young's modulus of 109±2 GPa. Horizontally produced DMLS Ti6Al4V ELI samples had YS of 1097±2 MPa, UTS of 1264±5 MPa, and Young's modulus 111±2 GPa. Only vertical samples were slightly more ductile as compared with horizontal samples: elongation at brake was 10.7±0.7% *versus* 9.4±0.4% respectively.

A fractographic study confirmed the moderately ductile fracture mechanism of the DMLS Ti6Al4V ELI samples under tension with formation of the necking region, which was associated with pore coarsening and coalescence.

Cooling rates influence phases and their morphology in Ti6Al4V alloy. High cooling rates at laser processing (10^5–10^6 K/s) result in high residual stress and formation of the α´ martensitic phase. In as-built samples, β-phase was not detected by TEM, EBSD, and XRD under chosen process-parameters. After stress-relief of Ti6Al4V (ELI) at 650°C for 3 hours in Argon atmosphere β-phase again was not detected. Very small (0.5 μm) globular grains of α-phase were found after this heat treatment.

The stress relieving heat treatment improved the ductility of the DMLS Ti6Al4V ELI alloy. The initial porosity and high residual stresses resulted in a lower ductility in the as-built Ti6Al4V in comparison with heat treated samples. The study shows that tensile properties of stress-relieved DMLS Ti6Al4V (ELI) samples fully meet the requirements of the standards for Ti6Al4V implants:

- ASTM F136 – 13. Standard Specification for Wrought Titanium-6Aluminum-4Vanadium ELI (Extra Low Interstitial) Alloy for Surgical Implant Applications;
- ASTM F1472 – 08. Standard Specification for Wrought Titanium-6Aluminum-4Vanadium Alloy for Surgical Implant Applications;
- ASTM F1108–14. Standard Specification for Titanium-6Aluminum-4Vanadium Alloy Castings for Surgical Implants.

Tensile properties of standard (ASTM E8 / E8M-16a) and mini-tensile DMLS specimens were compared. After the correction of surface bearing area, taking into account roughness of the DMLS samples, the resulted mechanical properties correlated with standard samples with deviation of 5-7%. Low coefficient of variation in the measured data and consistency in all the failures occurring within the gauge length confirmed the applicability of mini-tensile tests for the express analysis of DMLS samples.

In this work mechanical properties, microstructure and porosity of Ti6Al4V (ELI) samples produced by DMLS at standard EOSINT M280 (200 W) process parameters were investigated. Influence of the building strategy on microstructure and mechanical properties of DMLS as-built and heat treated specimens was studied. A comparison of mechanical properties of standard and mini-tensile DMLS specimens was done. Track-by- track, layer-by-layer DMLS method allows manufacturing 3D parts that previously weren't possible with conventional manufacturing. The ability to produce complex structures from predetermined CAD data makes DMLS ideal for biomedical applications. Thermal stresses, shrinkage and phase transformation lead to high

residual stresses in DMLS objects. In-situ heat treatment relieving residual stress during DMLS is a promising direction for future work with this alloy. Further microstructural analysis has to be done for investigation of the effect of orientation of primary β grains and texture in Ti6Al4V samples on mechanical properties. Fatigue properties of DMLS Ti6Al4V samples produced at similar process-parameters in vertical and horizontal directions are of great interest for future work for full qualification of DMLS Ti6Al4V (ELI) alloy.